# THE DEVELOPMENT AND EVALUATION OF SMALL MOLECULE-PEPTIDE CONJUGATES AS PROBES OF PROKARYOTIC RIBOSOME EXIT TUNNEL-NASCENT PEPTIDE INTERACTION

A Dissertation

Presented to

The Academic Faculty

by

Arren Zachary Washington

In Partial Fulfillment

of the Requirements for the Degree

Doctor of Philosophy in the

School of Chemistry and Biochemistry

Georgia Institute of Technology

August 2016

# THE DEVELOPMENT AND EVALUATION OF SMALL MOLECULE-PEPTIDE CONJUGATES AS PROBES OF PROKARYOTIC RIBOSOME EXIT TUNNEL-NASCENT PEPTIDE INTERACTION

Approved by:


Dr. Adegboyega K. Oyelere, Advisor
School of Chemistry and Biochemistry
*Georgia Institute of Technology*

Dr. Stefan France
School of Chemistry and Biochemistry
*Georgia Institute of Technology*

Dr. Charles Liotta
School of Chemistry and Biochemistry
*Georgia Institute of Technology*

Dr. Steven Harvey
Department of Biochemistry and Biophysics
*University of Pennsylvania*

Dr. Loren Williams
School of Chemistry and Biochemistry
*Georgia Institute of Technology*



Date Approved: December 1, 2016

# ACKNOWLEDGEMENTS

First and foremost, I must express my gratitude to Dr. Adegboyega Oyelere. Without him and his guidance, the work presented here would not have been possible. I am very grateful to have had an advisor with as much passion and insight to offer on a project such as this. He not only taught me the laboratory skill set needed to achieve the goals, but also a way of thinking that will be beneficial in addressing any project in my future.

To my committee members: Drs. Loren Williams, Charles Liotta, Stefan France, and Steven Harvey. I knew that I could always come to you should I need guidance or perspective. My interactions with RiboEvo and its extended family helped shape the way I viewed aspects of this project on a larger scale.

To my lab members: Thank you for the support, guidance, and encouragement throughout my time here.

To those people that impacted my life while here: Dr. Anthony Baldridge, Dr. Josh Canzoneri, Dr. James Black, Dr. Pamela Pollet, Dean John Stein, Vice Provost Susan Cozzens, Associate Vice Provost Leslie Sharp, Robbie Brawner Ouzts, Dr. Subhasish Tapadar, and Yogi Patel. In no small measure, each and every one of you helped me to either strive or survive, and sometimes both.

Next, I would like to thank my parents, Charlene and Jim Washington. They have helped and supported me through countless struggles. Some minor, others major. Their faith in me never wavered. Without their guidance and love over the years, I would

never have entered this phase of my life. I love you both beyond words. Thank you for everything you've taught me.

To my beautiful wife, Amanda, thank you for the patience, for the support and understanding, for loving me unconditionally. I cannot wait for the next chapter of our life together to begin. I love you, Angel.

Lastly, I would like to offer my truest thanks to all who were involved to make this work a reality and offer a sincere apology to those whom I failed to mention.

# TABLE OF CONTENTS

# LIST OF TABLES

# LIST OF FIGURES

# LIST OF SYMBOLS AND ABBREVIATIONS

| | |
|---|---|
| aa-tRNA | Aminoacyl-tRNA |
| CCA-pcb | CCA-phenylalanine-caproic acid-biotin |
| CMCT | 1- Cyclohexyl-(2-morpholinoethyl)carbodiimide metho-p-toluene sulfonate |
| ddNTP | Dideoxynucleotide triphosphate |
| DEPC | Diethyl pyrocarbonate |
| DMS | Dimethyl sulfate |
| DNA | Deoxyribonucleic acid |
| dNTP | Deoxynucleotide triphosphate |
| DTT | Dithiothreitol |
| EDCI | *N*-(3-dimethylaminopropyl)-*N'*-ethylcarbodiimide |
| EDTA | Ethylenediaminetetraacetic acid |
| EF-G | Elongation Factor – G |
| EF-Tu | Elongation Factor – Tu |
| fMet | Formyl methionine |
| GTP | Guanosine Triphosphate |
| HEPES | 2-[4-(2-hydroxyethyl)piperazin-1-yl]ethanesulfonic acid |
| HOBT | Hydroxybenzotriazole |
| IF1/2/3 | Initiation Factor 1/2/3 |
| LB | Luria Bertani Broth |
| LSU | Large Subunit, Ribomal |

| | |
|---|---|
| MDa | MegaDalton |
| $MLS_B$ | Macrolide-lincosamide-streptogramin B |
| mRNA | Messenger RNA |
| MRSA | Methicillin-resistant *Staphloccus aureus* |
| NMIA | N-Methyl isatoic anhydride |
| OD600 | Optical Density, 600nm |
| ORF | Open reading frame |
| PDB | Protein Databank |
| PrAMPs | Proline-rich antimicrobial peptides |
| PTC | Peptidyl Transferase Center |
| RAP | Ribosome arrest peptide |
| RNA | Ribonucleic acid |
| rProtein | Ribosomal Protein |
| RRF | Ribosomal Recycling Factor |
| RRL | Rabbit reticulocyte |
| rRNA | Ribosomal RNA |
| RT | Reverse Transcription |
| SD Sequence | Shine Delgarno Sequence |
| SDS | Sodium dodecyl sulfate |
| SHAPE | Selective 2'-Hydroxyl Acylation analyzed by Primer Extension |
| SSU | Small Subunit, Ribosomal |
| TBE | Tris Borate EDTA buffer |
| tRNA | Transfer RNA |

| | |
|---|---|
| TSB | Tryptic Soy Broth |
| VRE | Vancomycin-resistant *enterocci* |

## SUMMARY

As the knowledge base grows in regard to peptide synthesis and ribosomal actions, one facet of this is the extent and selectivity of interactions between the ribosomal exit tunnel and the nascent peptide. Small molecule probing techniques have provided insight from binding locations of ribosomal targeting therapeutics as well as potential downstream conformational changes to regions of dynamic flexibility with more solvent exposure aiding in the determination of complex higher-order structures. Crystallography provided a means to explore atomic-level interactions. This not only offered insight into potential questions and controversies posed by previous biochemical data, but also aided in the exploration and design of translation inhibiting antibiotics. However a means of more broadly probing the exit tunnel interactions without relying on mRNA and artificially stalling translation remained elusive. The methodology presented within this document provides an approach to introduce a broad range of customizable peptide probes to discrete regions of the exit tunnel in a manner independent on translation. Through the use of ribosomal large subunit targeting molecules (either clinically relevant or widely used mechanistic probes) as both delivery platforms as well as anchors, a means of presenting peptide sequences of various lengths and amino acid composition became possible. Covalent modification of various anchor types offered the possibility of interaction scanning windows within the peptidyl transferase center and well into the ribosomal exit tunnel. The successful presentation and evaluation of these small molecule-peptide conjugates provides an opportunity to identify regions of interaction within the exit tunnel while potentially displaying preference to amino acid types within these windows. Through the use of four major anchor types, two clearly

rose to be viable while a third is continuing to show promise. Probe-dependent interactions within the ribosome have been shown both biochemically and crystallographically strongly indicating that the methodology is not only viable, but a very attractive route of exploration for a region once thought to have little, if any, interaction with nascent peptides. Biochemically, probes **14a**-**14h** all show an orientation that projects the peptide moiety toward the peptidyl transferase center. This is indicated through small molecule probing of the *Escherichia coli* ribosome and probe-dependent protection of U1963 of the large subunit 23S rRNA. Crystallographic data collected of probe **14c** within the *Thermus thermophilus* further confirmed this by providing atomic level detail of the peptide realigning over the macrolactone ring to project back toward the PTC. This marks the first use of a translation-independent peptide probe resulting in substantial conformational change of multiple residues lining the exit tunnel. Subsequent generations improved upon the design by seeking to project the peptide portion in a specific manner to expand the probing window. Probes **19**-**28** sought to exploit a strong pi stack interaction existing within the SecM peptide sequence. Within the SecM peptide sequence, tryptophan-155 engages in a pi stack with adenine-751, a 23S nucleotide that lines the wall of the prokaryotic ribosome exit tunnel further down the tunnel away from the PTC and macrolide binding site. Successful engagement of this interaction would serve as a directional handle to encourage threading of the probe peptide selectively down the tunnel. The collective observations taken from all probe classes as well as experimental opportunities therein spurred a new conjugate series. Seeking to improve cell membrane activity in a step to improve whole cell activity of the conjugate probes,

the peptide moiety was redesigned to incorporate membrane-active peptidomimetics that resulted in large increases in whole-cell antibiotic activity.

# CHAPTER 1 INTRODUCTION

## 1.1 Prokaryotic Protein Translation

All cells, both prokaryotic and eukaryotic, are reliant on ribosomes for the synthesis of protein through the process of translation. Prokaryotic ribosomes (70S) are made up of two subunits: the small subunit (30S) consists of a 16S ribosomal RNA (rRNA) sequence and over 20 ribo-proteins (rProteins) whereas the large subunit (50S) contains two rRNA sequences (23S and 5S) in addition to 30-40 rProteins.[1-5] Translation is initiated upon complexation of the small subunit with the Shine-Delgarno sequence of messenger RNA (mRNA). Initiation factors 1 and 3 (IF1, IF3) aid in proper codon-anticodon pairing of fMet-tRNA (the initiator tRNA most seen in bacterial systems), while IF2-GTP coordinate the positioning of the charged end of fMET-tRNA in the ribosomal P-site. Finally, the 50S large subunit caps this complex creating a functional 70S ribosome.[6-12] This complexation happens on the order of seconds whereas once in Elongation, the prokaryotic ribosome is capable of catalyzing the peptide bond formation at a rate of approximately 20 amino acids per second.[7] Progression to the elongation phase is thought to be gated by IF2-bound GTP hydrolysis.[6] Successful hydrolysis makes available the A-site for the first non-initiator tRNA shuttled by GTP-elongation factor Tu (EF-Tu). Elongation continues through iterative rounds of tRNAs delivering appropriate amino acids as determined by codon:anticodon pairing between the mRNA and the stem loop of the tRNA, nucleophilic attack transferring the nascent chain to the A-site, and translocation of tRNAs in a ratcheting motion that is catalyzed by EF-G and GTP. This translocation has been described as either a 2-3-2 (whereby the A-site vacancy is filled before E-site ejection) or a 2-1-2 (E-site ejection precedes A-site occupancy).[13] Translation is terminated once a stop codon is encountered. This triggers hydrolysis and release of the nascent peptide as well as recycling of the ribosome subunits.

Peptide elongation occurs within the peptidyl transferase center (PTC). It is within the PTC that the charged end of the aminoacyl-tRNA nucleophilically attacks the peptide chain bound to the P-site tRNA through an ester bond. This ester bond is broken as the peptide transfers to the A-site tRNA, extending the protein by one amino acid. Translocation as described above shifts the A-site tRNA/protein complex to the P-site. As the protein continues to grow, it exits the PTC through the ribosomal exit tunnel. This channel, approximately 80 Å long and 20 Å wide, cuts through the large subunit (LSU) and provides a pathway to extrude the nascent peptide.[14,15] Once thought to be a passive conduit, there is growing support to suggest that the exit tunnel not only forms interactions but even regulates rates of translation of specific leader sequences thereby situationally stalling translation to allow the mRNA to adopt a secondary fold with another Shine-Delgarno sequence. Examples of this, such as Erm class methyltransferases, are discussed in later sections.[16-18]

### 1.1.1 Biochemical Techniques: Small Molecule Probing

The current understanding of the process of translation has further revealed the versatility of the RNA in biology. RNA is responsible for much of the architecture of the ribosome and aids in the decoding as seen with rRNA, carries genetic information through mRNA, and shuttles the necessary building blocks with tRNA. Through all of these various functions, structural relationships and higher-level interactions are both complex and ordered. Taking the ribosome as an example, the secondary and tertiary interactions of both RNA-RNA as well as RNA-protein maintain the complex structural fidelity.

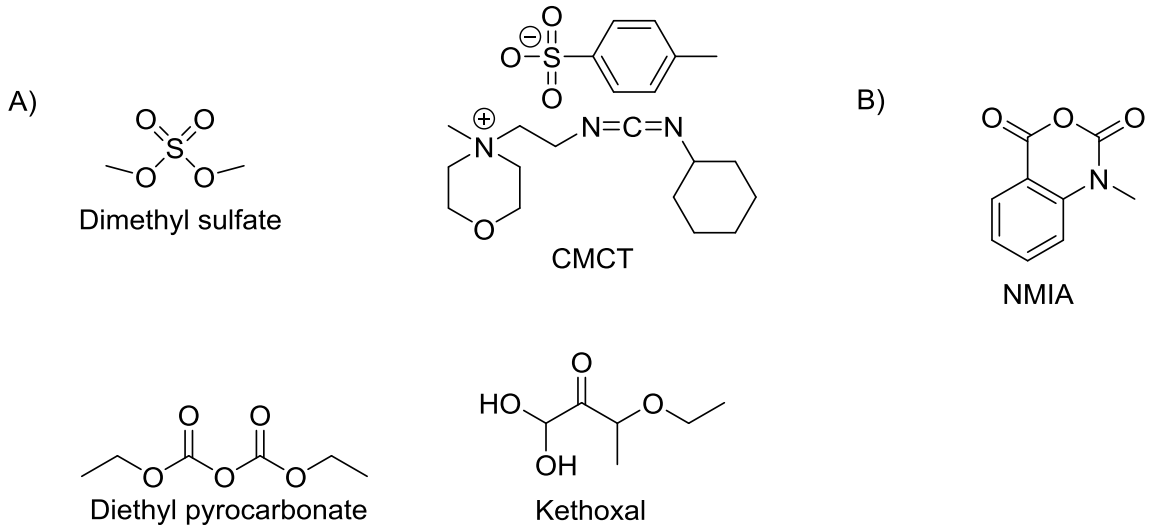


**Figure 1: Small molecule probes. A) Traditional, base-specific probing molecules. B) N-methyl isatoic anhydride (NMIA); reagent commonly used for SHAPE reactions.**

Toward understanding the complexity of these interactions, RNA probing became a highly practiced and refined field going back four decades with methods established to very broadly understand secondary structures to the very specific atomic level detail provided by chemical probes.[19-21] Small molecules such as dimethyl sulfate (DMS), 1-cyclohexyl-(2-morpholinoethyl)carbodiimide metho-p-toluene sulfonate (CMCT), diethyl pyrocarbonate (DEPC), and kethoxal all generate adducts in a base-specific manner providing local structural information like base pairing and stacking (Fig. 1). These modifications are predominately about the Watson-Crick face, allowing for adduct formation to be viewed as a function of solvent exposure at the hydrogen bonding face. Hydroxyl probing, alternatively, cleaves the phosphate backbone of solvent-exposed regions. Newer generations of probing such as in-line probing and Selective 2'-Hydroxyl Acylation analyzed by Primer Extension (SHAPE) shine a light on regions of dynamic flexibility that are either ligand-induced or simply sites of low rigidity (Fig. 2).[22,23] N-methylisatoic anhydride (NMIA), a SHAPE reagent, is capable of being nucleophilically

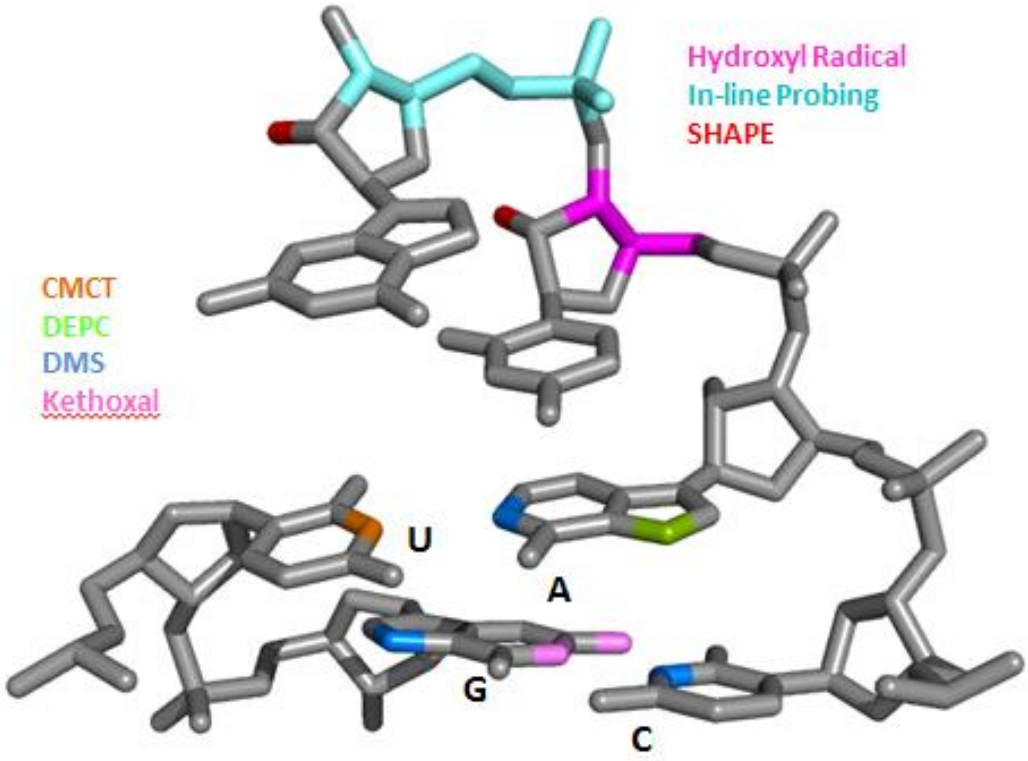


**Figure 2: Base-specific (left) and sequence-independent (right) chemical probes.**

attacked by the 2'-OH of RNA ribose generating a modified adduct. All small molecule adducts or fragments can then be visualized via electrophoretically separated cDNA products resulting from primer extension with reverse transcriptase (RT). Orientation is achieved through Sanger sequencing where in-tandem RT experiments incorporating one of four chain-terminating dideoxynucleotide triphosphates (ddNTPs) lead to sequence data. With the adduct formation at the ribose 3'-OH, progression by RT is halted resulting in a banding accumulation at the site of that specific ddNTP (Fig. 3).[24]

While all of these probing techniques are powerful in their own right, a larger benefit comes from their combination and coupling with secondary structure folding predictions.[25,26] By incorporating experimental data, confidence in the folding prediction increases greatly. As demonstrated by Weeks, *et al.*, the inclusion of traditional, base-specific probes boosted predictive folding to approximately 65% accuracy over an

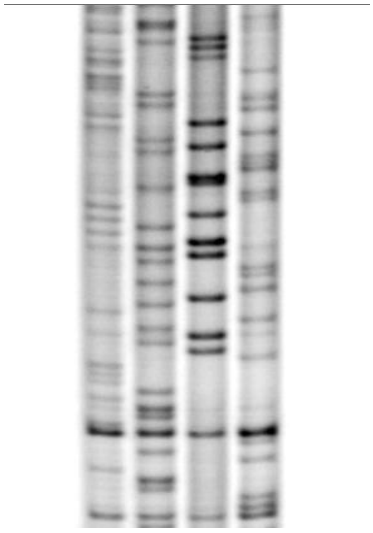

**Figure 3: Example of Sanger Sequencing.**

unconstrained 46% predictive accuracy when looking at *E. coli* 16S rRNA. They, then, showed an additional increase to 95% using SHAPE reactivity to constrain other key regions. This marriage of wet lab results and *in silico* predictions has changed the way nucleic acid probing is performed. However, another method of visualizing higher order interactions has a different series of benefits.

### 1.1.2 Crystallography

Nearly concurrent with these strides in nucleic acid probing, ribosomal crystallography was advancing as fast as modern software, analytics, and technology would allow. Initially plagued by poor crystals, the selection of a more suitably robust organism increased the possibility of crystal growth and improved imaging through increased tolerance of the harsh conditions required for crystal formation. These heartier ribosomes allowed for increased crystal populations permitting more successful diffraction. Preliminary low resolution success with *Bacillus stearothermophilus*[28] improved by selecting the heartier *Haloarcula marismortui*[29] which resulted in high resolution

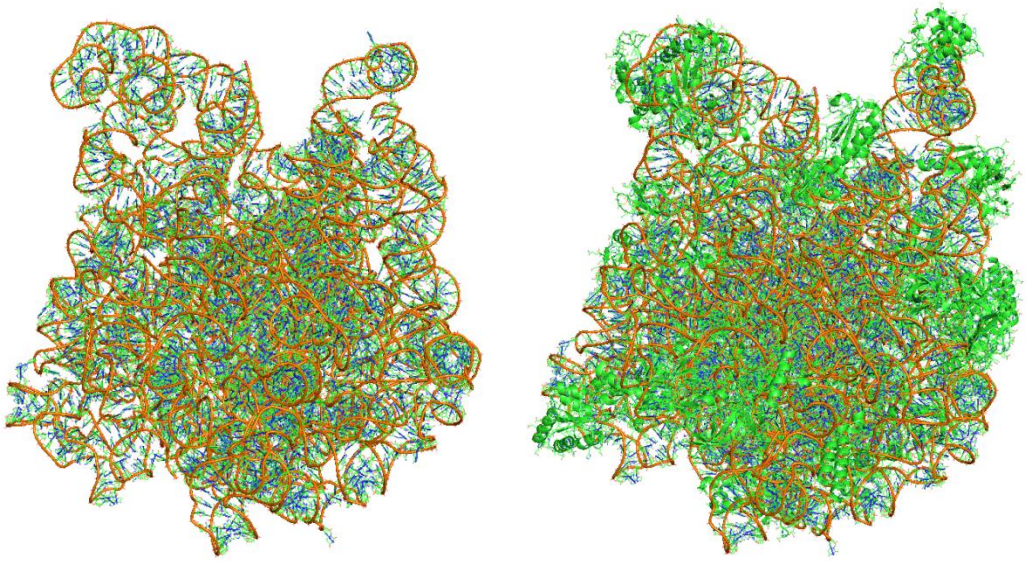

**Figure 4: *Haloarcula marismortui* 50S: Improvements in data collection and analysis allowed for increased resolution in ribosomal crystallography. *Left:* PDB 1FFK. One of the first electron density maps, however many regions of high variability did not resolve. *Right:* PDB 3I56. Use of additional techniques provide more complete pictures of LSU, especially protein incorporation.**

diffraction in 1991. Improved organism selection along with continued refinement finally allowed diffraction patterns to be solved below 3 Å resolution for 30S, and even past 6 Å for the whole 70S ribosome.[30-32]

Iterative experimental improvements moved in tandem with data collection and interpretation. A daunting complication demonstrating this was finding a way to prevent the deterioration of this 2.8 MDa biomolecule believed to be a result of the harsh conditions inherent to synchrotron irradiation.[33] Major methodology advances in the mid to late 1980s helped preserve the integrity of crystalized ribosomes through cryogenic temperatures during data collection.[34,35] Continued advancement in data generation and collection exposed the next major technical problem of data interpretation. The complex diffraction patterns generated could not be interpreted without better ways to solve the

phasing issue. These diffraction patterns started to take form in 1998 as the use of molecular replacement and heavy atom clusters[36] provided footholds to a 9 Å electron density map of *H. marismortui* 50S (Fig. 4).[32] Continuing to improve on past results, electron density maps became more refined at resolutions better than 3.5 Å with more complexity. The community was getting ever clearer glimpses of mRNA and various tRNAs bound to complete 70S.[37] The culmination of these collective advances resulted in not just a tremendous foundation for future generations of researchers across multiple fields, but also in the awarding of the 2009 Nobel Prize in Chemistry to Vankatraman Ramakrishnan, Thomas A. Steitz, and Ada E. Yonath for the pioneering work that brought about the field of ribosomal crystallography.[38-40]

Utilizing these new techniques finally provided for the opportunity to solve high resolution structures of ribosomes at an accelerated pace. The proverbial flood gate had opened and outstanding questions now had methodology in place to be answered. Among these were establishing a better understanding for the mechanism of action for both clinically relevant and probing small molecules. Within a year of those seminal crystal structure publications, crystals containing antibiotics became of utmost importance with each group listed above and others worldwide solving multiple structures with synthetic variants of biologically relevant factors or varied ribosome-targeting classes of antibiotics.

## 1.2 Targeting the Prokaryotic Ribosome

### 1.2.1 Antibiotics

Antibiotics are collectively a broad category of small molecules that are either naturally synthesized for defense by various organisms or modified in a laboratory to increase clinical viability. The bactericidal activity comes from the molecules' abilities to inhibit many biological properties such as cell wall synthesis, DNA replication, or translation. As this thesis revolves around ribosomal activity and interactions, emphasis will be placed on translation inhibitors with further emphasis on the large subunit (LSU) binders. While biochemical information collected since the 1960s utilizing the probing techniques discussed previously was able to suggest targets, validation through crystallography was lacking.[41] A great undertaking changed this as multiple research groups dedicated efforts to cocrystalizing various ribosomes with a vast array of antibiotics. This new information provided a level of understanding that not only afforded interaction mapping, but brought about the possibility to improve upon drug design for progressive generations of compound classes.

Within the small subunit, aminoglycosides bind to the key structural element helix 44 (h44) (Fig. 5). They inhibit translation by interfering with decoding leading to aberrant proteins including the potential to slip past the stop codon.[42-44] By stabilizing the nucleotides that monitor codon:anticodon interactions, near-cognate tRNAs become accepted with incorrect amino acid incorporation resulting. Recently, the Arya lab has developed methods for rapid synthesis and a multi-assay screening of a vast library neomycin-amino acid conjugates to evaluate the effects of charge and sterics on optimal binding and activity.[45] Tetracycline, a planar fused-ring system with a hydrophobic face

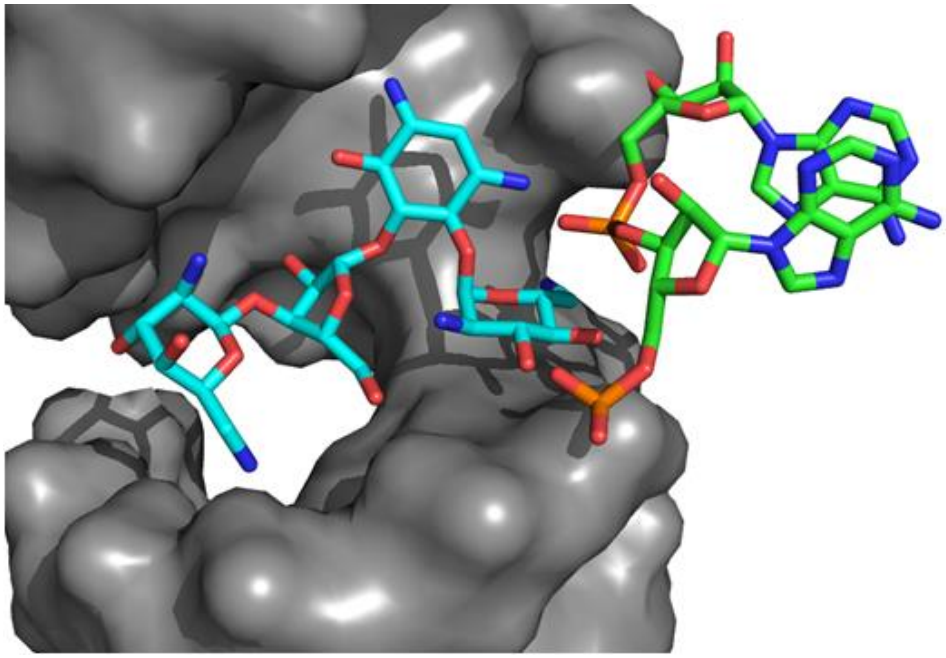

**Figure 5: Neomycin bound to h44 analog with universally conserved A1492/3 bumped out (PDB 2A04).**

opposite a hydrophilic edge, is a widely prescribed broad-spectrum antibiotic that acts primarily by sterically hindering the entrance of the A-site tRNA.[46-48] A third target within small subunit binders prevents the initiation complex from forming. Examples of these include potent universal translation inhibitors edeine and pactamycin that both lead to mRNA displacement which decreases movement capability as well as start codon:anti-codon interactions.[41,46-48]

The large subunit also contains regions of high conservation that are targets of therapeutic targets. The small molecules that target the 50S bind between the ribosome's catalytic core, the PTC, and the threshold of the ribosomal exit tunnel. While many LSU-targeting classes exist and there are a plethora of outstanding reviews dedicated to a more comprehensive list, this section will only focus on a handful demonstrating parent scaffold variation. Collectively, they fall into two generalized mechanisms of action:

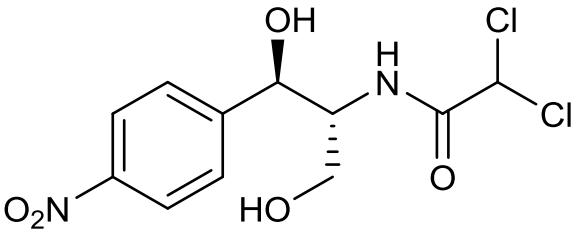


Chloramphenicol

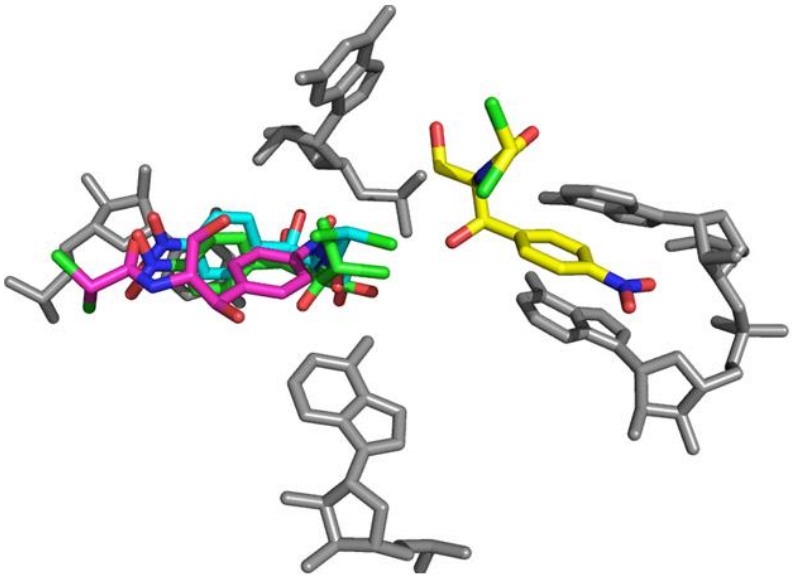

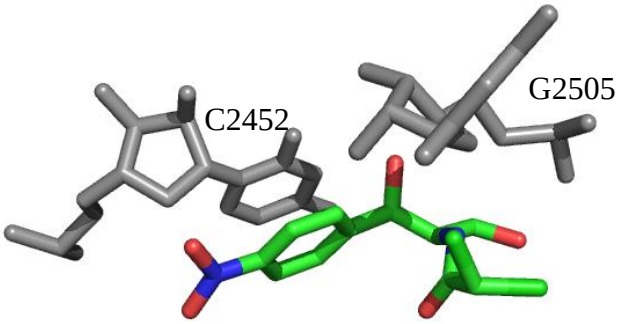


**Figure 6: Chloramphenicol Binding.** ***Top*** **Structure of chloramphenicol.** ***Middle*** **Various binding motifs of chloramphenicol: Green –** ***E. coli*** **(PDB 3OFC), Cyan –** ***T. thermophilus*** **(PDB 3OH5), Magenta –** ***D. radiodurans*** **(PDB 1KO1), Yellow –** ***H. marismortui*** **(PDB 1NJI).** ***Bottom*** **Stacking of the p-nitrophenyl can be seen with the pyrimidine C2452 as well as H-bonding with the phosphate backbone of G2505.**

Steric prevention 1) of tRNA binding; or 2) that either creates a cascade event shifting key residues or the tRNA charged end resulting in loss of elongation.

Chloramphenicol (Fig. 6) has been shown to have varied binding in a species dependent manner. In both *E. coli*[49] and *T. thermophilus*[50], it binds distinctly within the A-site crevice displacing the charged end of aa-tRNA. Major binding stability in both systems comes about from the p-nitrophenyl moiety being stabilized through a π stack with C2452 of the 23S rRNA and the amide seemingly engaged in hydrogen bonding with a nonbridging phosphate oxygen of G2505. Within *E. coli*, N6 of A2062 appears to interact with one of the chlorine atoms. Interestingly, the primary hydroxyl reaches toward a verified potassium ion in *T. thermophilus*, however it is aligned toward the alternate nonbridging phosphate oxygen of G2505 in *E. coli*. A secondary binding site has been shown both biochemically and crystallographically in archaeal *H. marismortui* further down the tunnel where there is competitive binding with macrolide class antibiotics.[51] This alternate (and exclusive to archaea) binding site results from the loss of PTC binding due to a C2055A mutation that drastically disrupts the local orientation and the formation of another hydrophobic pocket formed by G2099 and A2100 (A2058/A2059 in eubacteria). While the binding of chloramphenicol in *D. radiodurans*[52] shows similarities to that of *E. coli* and *T. thermophilus*, it appears to adopt a reversed orientation. This is presumed to be the result of nearby metal ions since regional rRNA sequences are conserved. *D. radiodurans* crystals show stability afforded by two nearby magnesium ions, however they are not observed in *T. thermophilus* or *E. coli* systems. While evidence suggests the mechanism of inhibition for chloramphenicol to be A-site binding interference[53,54], there is also precedent showing accumulation of oligopeptides

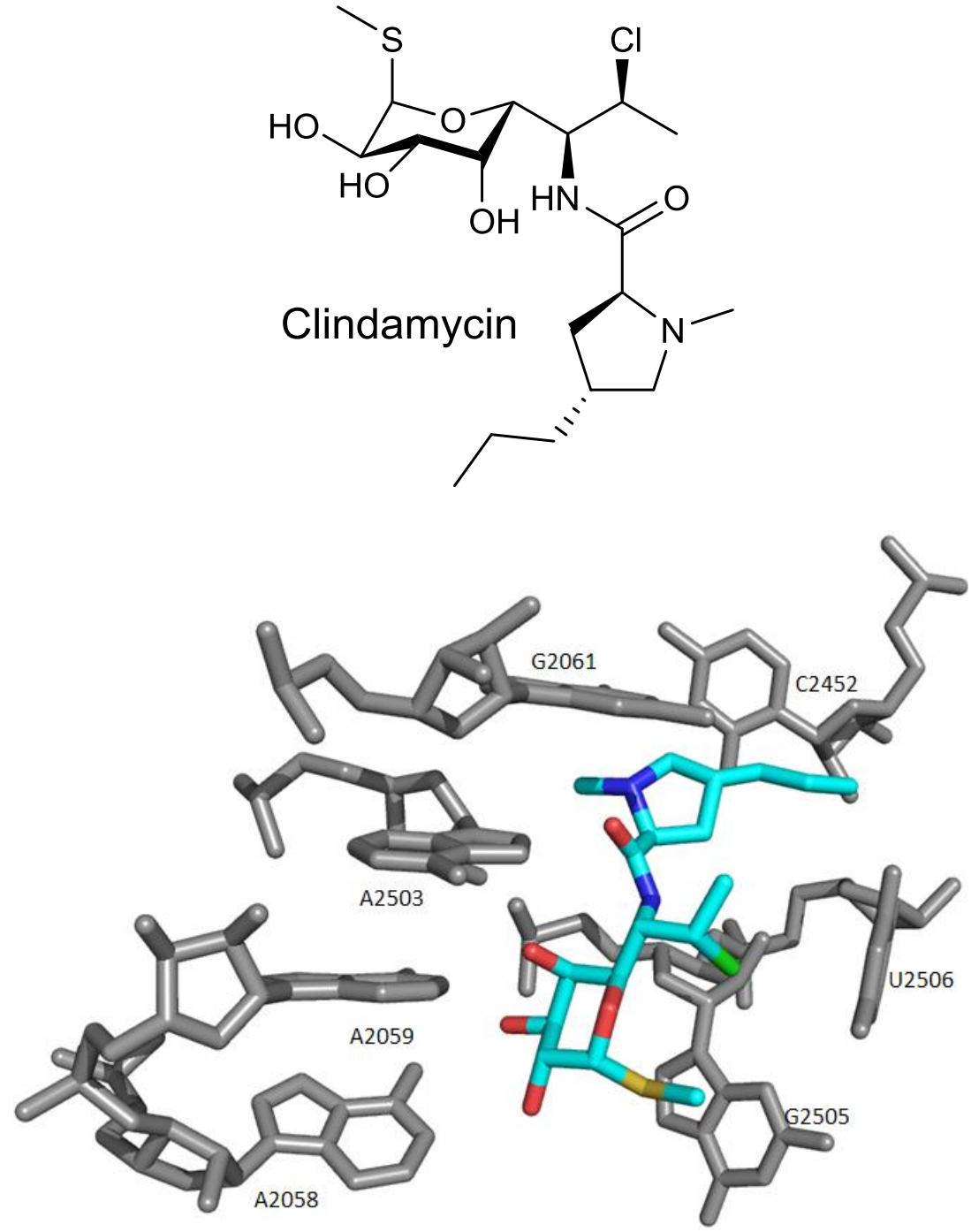


**Figure 7: Clindamycin Binding. *Top* Structure of clindamycin. *Bottom* Extended local contacts by clindamycin in E. coli (PDB 3OFZ).**

which is reminiscent of macrolide-like inhibition whereby sterics promote premature tRNA dropoff.[55-57] Interestingly, this latter understanding shows less inhibition toward bulky aromatic amino acids, but sees greater inhibition in the presence of charged or smaller amino acids.[58,59]

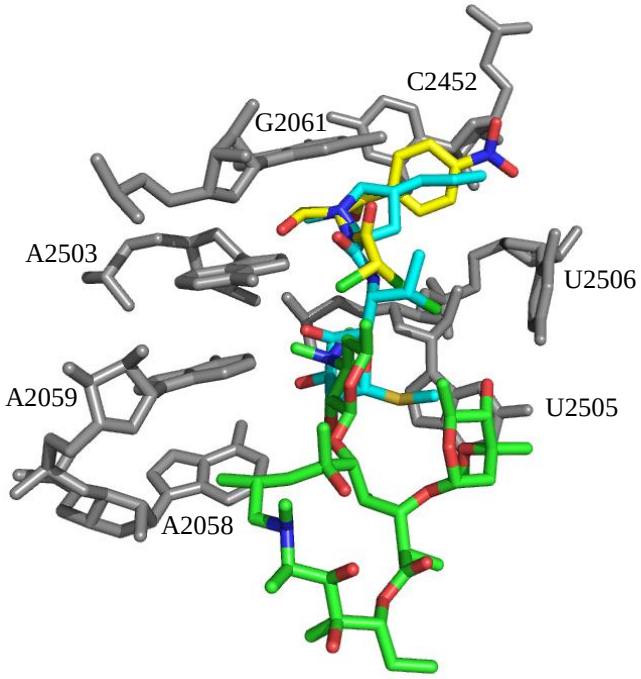


**Figure 8: Shared binding sites. Clindamycin (cyan, PDB 3OFZ); Chloramphenicol (yellow, PDB 3OFC); Azithromycin (green, PDB3OI1). Significant hydrogen bonding with A2058 and A2059 for both clindamycin and azithromycin. Chloramphenicol and clindamycin share the site with bonding interactions with C2452 and G2505.**

Lincosamides such as clindamycin (Fig. 7) bind to eubacterial 50S in a similar fashion to chloramphenicol inasmuch as they prevent proper positioning of aminoacyl-tRNA through sterics while overlapping the binding domain of both chloramphenicol as well as erythromycin.[52,60] The major binding stability is found with the galactose moiety of lincosamides. It is here where hydrogen bonding between the three galactose hydroxyls interact with A2058, A2059, A2503, and G2505; an observation further

substantiated with $MLS_B$-targeting resistance mechanisms. While these interactions provide the stability, the hydrophobic packing of the distal pyrrolidinyl propyl moiety has been shown to be responsible for the loss of translation through prevention of peptide bond formation.[46,49-52,60,61]

While not clinically viable due to lack of kingdom specificity, puromycin is used extensively as a tool in gaining a mechanistic understanding of peptide bond formation. Resembling the charged end of a tyrosine-like tRNA including an N6 dimethyl adenine, peptide bond formation halts as a result of a nonhydrolyzable amide bond replacing the ester linkage. As a mechanistic probe, puromycin has been used in the fragment assay, a tool allowing for understanding PTC activity in the absence of everything save the 50S large subunit and a P-site tRNA mimic.[62-64] However, early iterations of this assay relied heavily on high concentrations of alcohol to improve binding affinity of first generation P-site substrates. These nonphysiological conditions were addressed by improvement of the substrate through a transition from CCA-fMet to the higher molecular weight CCA-phenylalanine-caproic acid-biotin (CCA-pcb).[65] This alteration, along with an extended C-puromycin (Fig. 9), was capable of producing the same assay results without the inclusion of any alcohol.

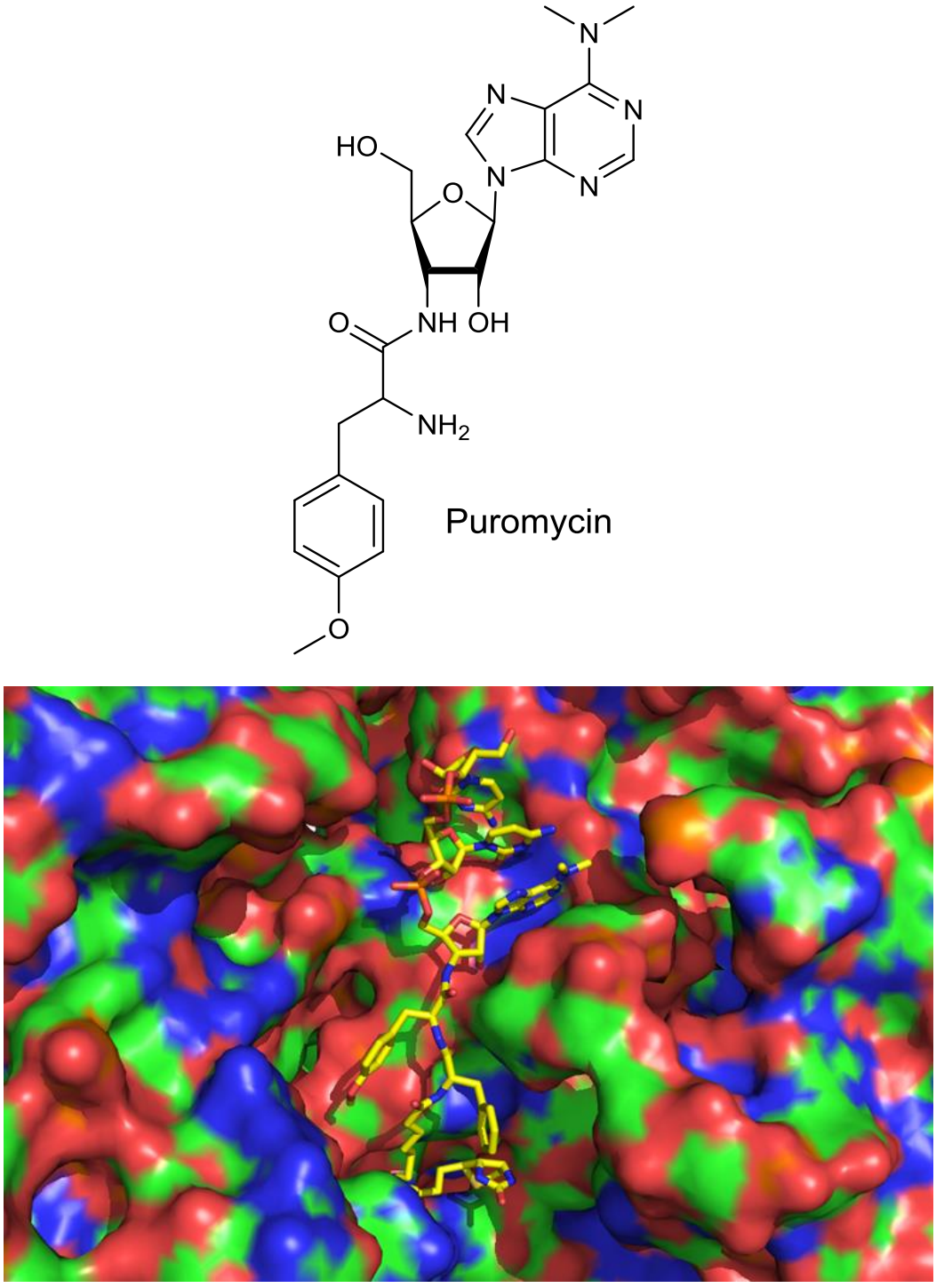


**Figure 9: Puromycin structure (Top); Structure of the puromycin analog CCA-pcb bound in the PTC of *H. marismortui* (PDB 1KQS) (Bottom).**

Streptogramin classes of antibiotics are divided into A and B types that work synergistically to inhibit translation (Fig. 10).[66] While both types are capable of independent function as bacteriostatics, the combined effect is profound and bactericidal.[67] A-type streptogramins bind near the entrance of the exit tunnel by stacking its conjugated C9-C12 alkenyl stretch with G2061 and the oxazole moiety with A2451. This orientation allows the conjugated amide spanning C4-N7 to displace A2062 with a $90^{o}$ rotation from its native position. B-type streptogramins bind slightly further down the exit tunnel from their A counterparts. The induced rotation of A2062 creates both a π-stack interaction with the 3-pyridinol portion of B types as well as two hydrogen bonds with the N16 amide and C14 carbonyl. The importance of this interaction is seen with an A2062C mutation that results in a loss of activity for both streptogramins and macrolides. Another crucial stack between the dimethyl aminophenyl moiety and A2058 is shown as modification of this residue through *erm* methylation or mutation provides streptogramin B resistance.[68,69] Additional interactions are seen with hydrophobic packing of nearby backbone C17-C19 with U2586 as well as the C3 phenyl stacking below U2609 ribose.[46]

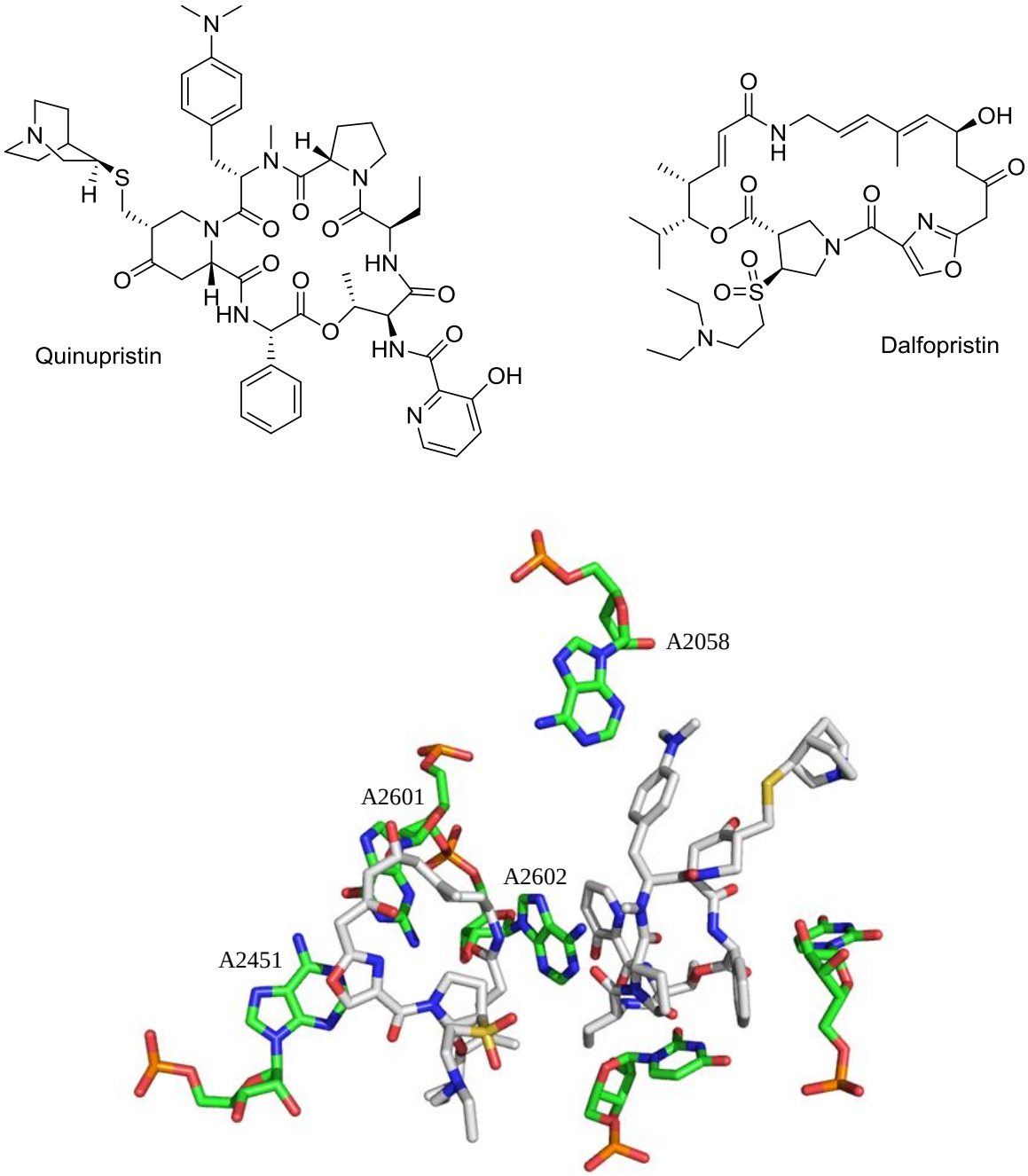


**Figure 10: Streptogramin A/B components Quinupristin and Dalfopristin (Synercid) bound to E. coli (PDB 4TP9). A2062 can be seen stacking with the pyridinol of Quinupristin.**

Linezolid, an oxazolidinone antibiotic, became clinically available in 2000 with much anticipation. It marked the first truly novel antibiotic design that was not a synthetically modified variant of existing scaffolds (Fig. 11).[70] It showed success against existing Gram-positive strains, including vancomycin-resistant *enterocci* (VRE) as well as methicillin-resistant *Staphlococcus aureus* (MRSA), however does not perform well against Gram-negative bacterium due to intrinsic efflux pumps.[71] There was some mystery as to where linezolid bound within the ribosome until initial mutational studies in 1999 suggesting it as a PTC binder.[72,73] Follow up studies continued to support this, however use of footprinting with small molecule probes was unable to elucidate the region better. Cross-linking studies finally identified close association with both A2602 and ribosome-bound tRNA.[74,75] Crystal structures of linezolid within the 50S of both *H. marismortui* and *D. radiodurans* solved in 2008 show it as an A-site binder with many regional contacts.[76,77] Interestingly, what was once thought to be a distinctly different target based on initial studies and inhibitory profile is staggeringly close, even competitively overlapping, the binding sites of many other A-site inhibitors such as chloramphenicol and streptogramin A. More so, the rRNA mutations conferring resistance is very extensive, including residues over 15 Å away from the believed active binding site.[78] However, despite this growing body of data and understanding, there is still not a consensus as to the full mode of action of this class. One belief involves the ribosomal translation factor, LepA, binding to the PTC in which the oxazolidinone compound prevents A-site tRNA from fully accommodating, thus leading to infidelity of translation.[79] However, even with this as a perceived possibility, MIC values within *ΔlepA* are unchanged.[74]

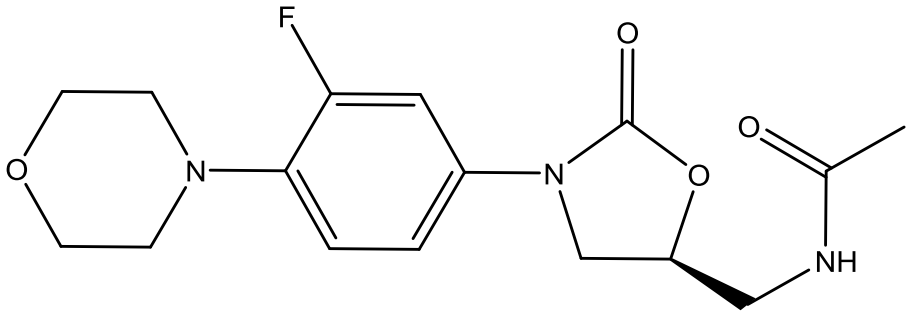


Linezolid

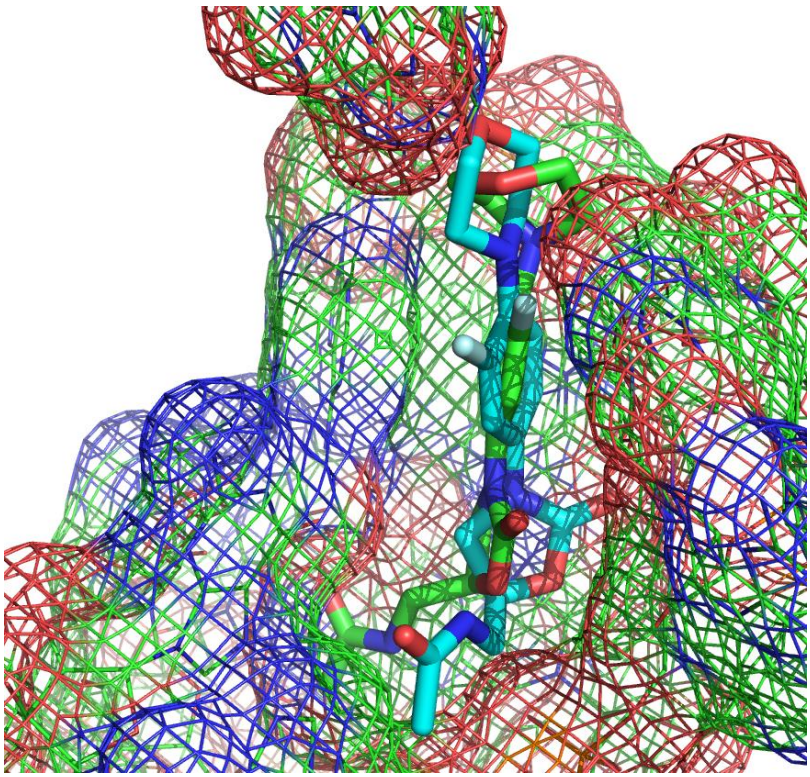

**Figure 11: Linezolid Binding.** ***Top*** **Structure of linezolid.** ***Bottom*** **Two orientations of linezolid overlaid. Green:** ***S. aureus*** **(PDB 4WFA), Cyan:** ***D. radiodurans*** **(PDB 3DLL).**

As translation progresses, the nascent peptide exits the PTC and the ribosome through the exit tunnel that was once thought to provide a passive chute of travel. Within the architecture of the exit tunnel, approximately 10 Å from the PTC, is a natural choke point where rProteins L4 and L22 protrude into the tunnel resulting in a halving of the diameter.[14,15,17] Between the PTC and this narrowing exists the macrolide binding site. Macrolides, while one of the most diverse and widely used classes clinically, all share a similar binding modality and work to stall translation by creating congestion within the tunnel. This is thought to relay back to the PTC and prevent elongation through various mechanisms. Once believed to simply serve as a wall that disallows progression of the nascent peptide, it has been shown that peptides ranging from two to ten amino acids long accumulate during macrolide-induced translational arrest. This coupled with the understanding that the distance of 10 Å equates to three or four amino acids suggests that certain sequences are capable of bypassing the "wall".[80-91]

Collectively, this clinically relevant class is generalized as a 14-16 member macrolactone ring that is decorated with various sugars. Erythromycin, the first generation macrolide antibiotic dating back to the 1950s, has a desosamine sugar attached at C5 as well as a cladinose sugar at C3 (Fig. 12). One of the most vital interactions comes from the 2' OH on the desosamine forming a hydrogen bond with A2058 of the 23S rRNA.[49,50,52,93] The relevance of this binding if further highlighted in recognizing that a major macrolide resistance pathway disrupts this interaction through steric modification of that critical residue.[60] Furthermore, corresponding residues in archaeal and eukaryotic systems are guanidine, and binding does not occur.[94] While it has been shown that a bacterial system with an A2058G mutation becomes resistant to macrolides,

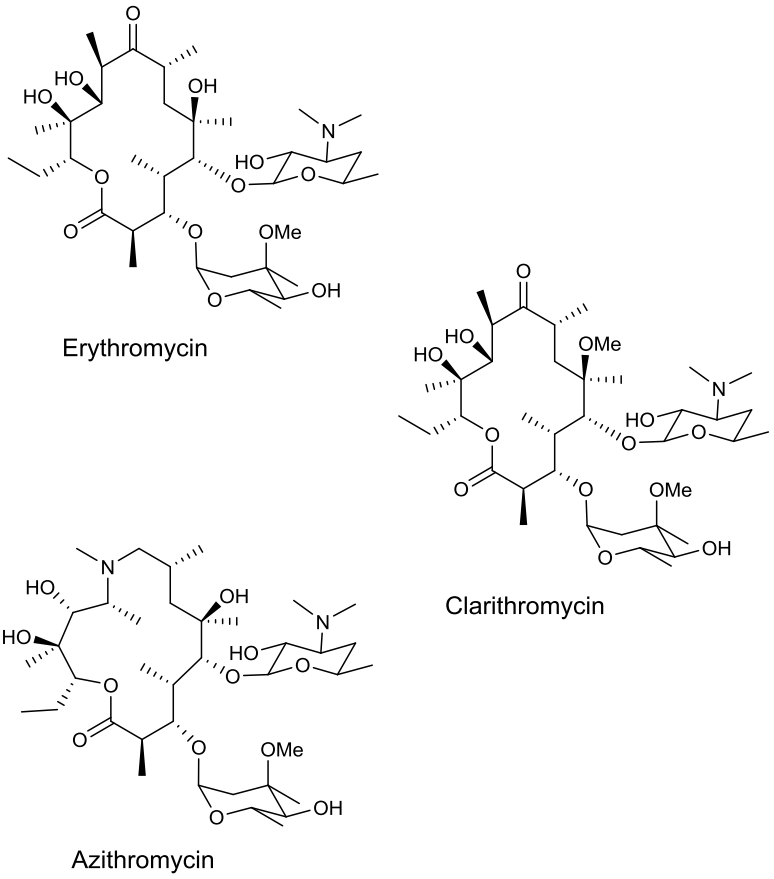


**Figure 12: Structures of representative examples of clinically useful macrolides.**

it has similarly been shown yeast carrying a G2058A mutation does not gain sensitivity.[95] These last two experiments suggest that, while the presence of A is important, there is likely a neighboring influence as well. Other common interactions involve hydrophobic packing of the lactone near A2058 and A2059 along with hydrogen bonding between O4 of U2609 with the hydroxyl at either C11 or C12.

In light of growing resistance, newer generations of macrolides were developed through semi-synthetic means. Clarithromycin, differing from erythromycin through C6 hydroxy methylation, served as a major advancement by reducing acid sensitivity. Other variations included the insertion of a methylated amine between C9 and C10

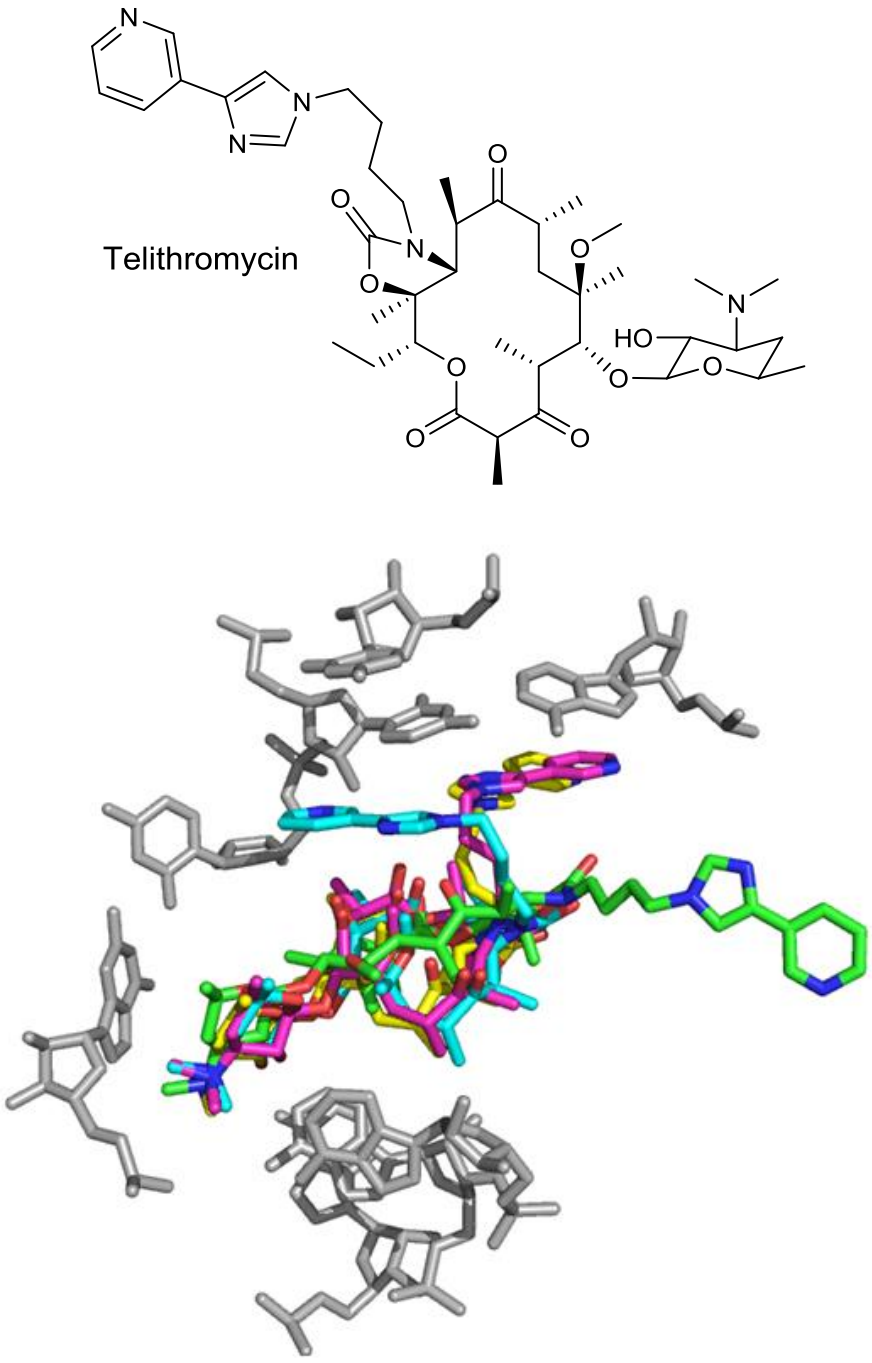


**Figure 13: Telithromycin Binding.** ***Top*** **Structure of telithromycin.** ***Bottom*** **An overlay of telithromycin adopting differed positioning of the alkyl-aryl arm bound to** ***T. thermophilus*** **(yellow, PDB 3OI3),** ***E. coli*** **(magenta, PDB 3OAT),** ***D. radiodurans*** **(green, PDB 1P9X), and** ***H. marismortui*** **(cyan PDB 1YIJ).**

(azithromycin), or replacement of the C9 ketone with an extended oxime (roxithromycin).[96-98] Clarithromycin was further modified to afford the ketolide subclass by hydrolyzing the C3 cladinose sugar followed by oxidation of the alcohol to the ketone.[99-101] Telithromycin, a clinically used ketolide, also has an alkyl-aryl arm extending off of a cyclic carbamate spanning C11 and C12 of the macrolactone (Fig. 13). This aryl region displays varied binding based on the presence or absence of

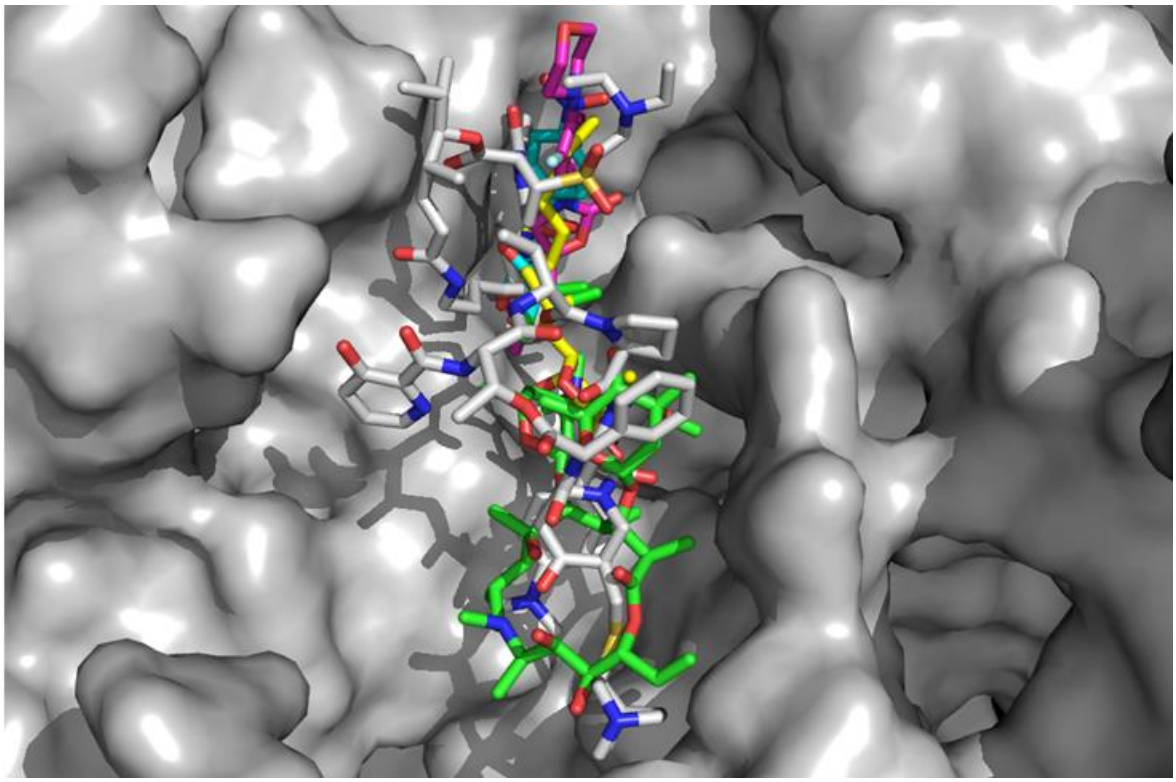

**Figure 14: An overlay of major LSU-binding drug classes. Azithromycin (green, PDB 3OI1), Synercid (white, PDB 4TP9), Clindamycin (yellow, PDB 3OFZ), Linezolid (purple, PDB 4WFA), Chloramphenicol (cyan, PDB 3OFC).**

A752:U2609 base pair. When present as in *E. coli* or *T. thermophilus*, this aryl moiety projects across the tunnel to engage in a π stack. However, in the absence of this base

pair the extension either projects further down the tunnel as seen in *D. radiodurans* or flips back over itself towards the PTC as in *H. marismortui*.[49,50,60,102]

As shown above, the structural complexity of the various classes is extreme. In overlaying these binding locations, it becomes abundantly clear, however, that there are a substantial number of clinically relevant classes that bind within a very narrow window (Figs. 8 and 14). While certain structural elements are mandatory for clinical application, portions of the scaffold are capable of synthetic modification. These regions may be modified for improved activity, circumventing resistance mechanisms, or transformation from therapeutic to probe. This last option is desirable for the prospect of being capable of enabling analysis of potential interactions between the tunnel and a peptide without a reliance mRNA or stalling translation. This could expand upon the knowledge base of situationally gated open reading frames (ORFs) sequestered by leader sequence-dependent translational stalling.

### 1.2.2 Known Exit Tunnel Interacting Peptides

There exist multiple examples where leader sequences of functional peptides serve the purpose of regulating the expression of their downstream partner. These ribosome arrest peptides (RAPs) are able to gate the rate of both transcription and translation through varying interactions within the exit tunnel as well as the PTC.[16-18,103]

As a mechanism of control for intracellular levels of tryptophan, there exist two proteins specific to tryptophan whose translation are gated by the leader sequence TnaC. The ORF of this leader is regulated by free levels of Trp. Under high concentrations of Trp, TnaC stalling gives way to TnaA (tryptophanase, a protein responsible for metabolic degradation of Trp) and TnaB (a Trp-specific permease) having exposed Shine-Delgarno sequences.[104-106] This regulation has been shown to be a result of free L-Trp binding to an unknown site near the PTC or narrowly into the exit tunnel. Initial data suggested the binding location to be firmly within the PTC and preventing nascent chain-tRNA

hydrolysis, however the interactions between TnaC-I19 and 23S rRNA A2058/9, situated well within the exit tunnel, appear to be crucial for Trp-mediated regulation. When Trp levels are low, translation of TnaC completes without issue, hydrolysis of the peptide from tRNA occurs, and ribosomal dissociation results. Upon dissociation, Rho-termination factors are able to bind and prevent RNA polymerase transcription of TnaA/B. This Rho-dependent termination occurs before functional transcripts are polymerized, thus negating the possibility of these Trp-specific housekeeping proteins.[107]

While various crystallographic, computational, and biochemical techniques have shone light on multiple possible interactions, three conserved amino acids within the 24-mer leader sequence are thought to be responsible for stalling while the previously mentioned I19 is strongly implicated in the recognition of free L-Trp. Interactions between TnaC-W12 with K90 and R92 of rProtein L22 are consistently shown to be vital to translational arrest. This interaction dictates the spacing for a feedback relay to the PTC and P24.[108] Cryo-EM data show the neighborhood near P-site tRNA bound P24 of A2602 and U2585 repositioned in such a way that would encroach on the binding domain of release factor 2. Between the two exists the third conserved site, D16, which seemingly interacts with the 23S A752:U2609 base pair. As expected, TnaC-mediated stalling is abolished when those sites are mutated.[109] This observation extends to ribosomal manipulation, as well, where insertions or mutations to the relevant regions of 23S and L22 prevent Trp induced stalling.

Another class of RAPs confers macrolide-induced macrolide resistance through polymethylation of A2058, a critical residue of the 23S sequence described above. Within the Erm class, there are four distinct leader sequences that are believed to activate under two various feedbacks: A2062-initiated cascades (ErmAL1 and ErmAL2/CL) or U2585 corruption (ErmBL and ErmDL).[110]

*ErmAL1*, the first of two leader sequences for *ermA*, gates the Shine-Delgarno (SD) sequence for *ermAL2*. Drug-dependent stalling is required for both leader

sequences in order for the translation of ErmA. *ErmAL1* encodes for a 15 amino acid protein where stalling has been shown to occur before the nucleophilic attack by E9 on to V8. *ErmAL2/CL* are highly homologous inasmuch as they are 19 amino acid peptides stalling between I9 and N10, again in a drug-dependent manner, thus allowing for the *ermA/C* ORF to become available. Ala scanning within *ermAL1* identified I5, A6, V7, and V8 as critical for stalling, while *ermAL2/CL* requires I6, F7, V8, and I9.[112,113] Furthermore, the identities of *ermAL1*-A6 and *ermAL2/CL*-F7 appear to have additional implications. These amino acids modulate the reactivity of the A-site tRNA in a manner independent of the aminoacyl-tRNA. This collection of Ala scanning suggests that the size of the N-2 position (A6 for ErmAL1 and F7 for ErmAL2/CL) is capable of modulating the stalling of these sequences. If there is a large, bulky side chain, more A-site inactivation is observed.[111]

For the above mentioned Erm types, there is seemingly little involvement of the N-terminus amino acids preceding the stalling window of four amino acids other than their being included in the leader sequences. Additionally, recognizing that there is insufficient distance between the PTC and the site of drug binding (approximately 10 Å)

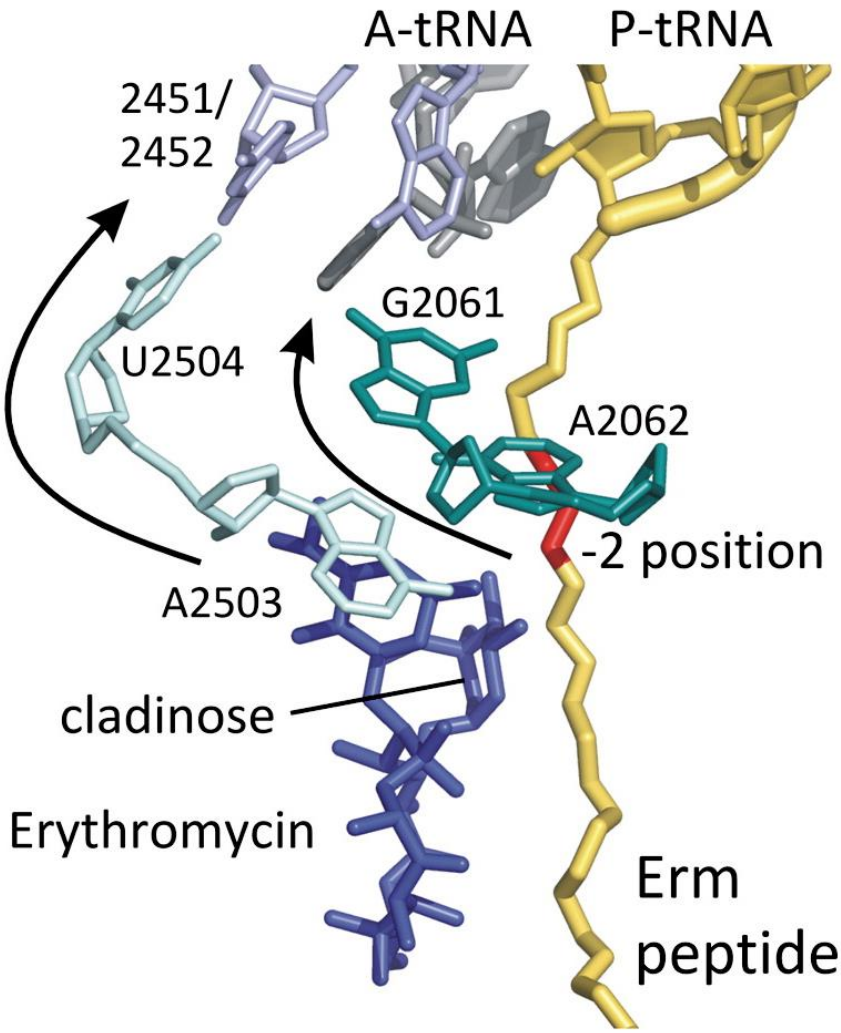


**Figure 15: Possible signal-relay pathways of Erm stalling. Both relay systems are dependent on the cladinose sugar repositioning the nascent Erm peptide. Figure adapted from [16].**

to accommodate a peptide of that length, the long held belief that macrolides stalling through simple steric congestion must be reevaluated. As part of understanding the molecular components involved in ErmCL stalling, Vazquez-Laslop *et al.* performed a range of experiments that mutated both rRNA and L22, as well as identified the critical moieties of macrolides.[112] They were able to show that a constriction between the C3 cladinose sugar and A2062 are vital for stalling (Figure 15). In the macrolide subclass

where the C3 cladinose is replaced with a ketone (ketolides) or under A2062N conditions, stalling is not observed. When a three amino acid deletion is performed on L22 within the hairpin protruding into the exit tunnel beyond the drug binding site, a substantial reduction in stalling was also observed. These combined results clearly suggest that it is not merely sterics that generate the stalled ribosomal complex. The proposed stalling mechanism, as evidenced by crystallographic and biochemical techniques, indicates a relay starting with the peptide sensor, A2062, being knocked out of place. This repositioning ripples through nearest neighbors to perturb A2451/C2453 within the A-site crevice.

Other leader sequences within the *erm* class stall through substantially different means. ErmBL, consistent with the others, is a relatively short leader that stalls between P-site bound D10 and A-site A11.[114] It has been recently shown that the stall occurs before nucleophilic attack as A11 does not become incorporated into the peptide product. It is believed that this results from drug-dependent locking of an uninduced state. Peptide bond formation is predicated on the proper alignment between the aminoacyl tRNA and the P-site ester-linked peptide. For the A-site CCA conserved tail to appropriately place itself for nucleophilic attack, 23S residues U2584 and U2585 must shift out of place into an "induced fit" state. As is the case with previously discussed Erm leaders, ErmBL is capable of navigating the restricted aperture of the drug-containing exit tunnel; however the resulting deviation off of its native path brings the critical R7 into very close proximity with U2586 as well as V9/D10 to U2585. The resulting downstream effect of these newfound interactions is a stabilization of the uninduced state where proper positioning and alignment of aminoacyl-K11 is incapable of nucleophilic attack.

The final Erm leader to be discussed here is ErmDL, and it is by far the most unusual within the class.[115] It has been shown to stall at the necessary "RLR" sequence, however, and rather surprisingly, the relative codon placement within a given transcript is seemingly irrelevant. While the wild type peptide is 14 amino acids, this R6-L7-R8 motif

was shown to be possible of stalling with truncations of the N-terminus to the point where R2-L3-R4 showed near identical levels of drug-dependent stalling. Moreover, it was determined that the stall occurs before the peptide translocates onto R4. It is important to note that this stalling still occurred with R4K mutants, however translation returned with R4L variants thereby suggesting the extended cationic side chain plays a role. By use of SHAPE probing followed by corroborating molecular dynamics simulations, evidence supports the hypothesis that macrolide binding allosterically repositions U2585 within the PTC. It is believed that this corruption provides suitable repositioning of A-site R-tRNA to disallow catalysis.

The final sequence, known as SecM, is a protein secretion monitor where upon complete translation, it is transported to the periplasm followed by rapid protease degradation. Its stalled translation allows for the synthesis of SecA, a translocation ATPase.[116-120] Of those sequences discussed in this review, SecM is by far the longest at 170 amino acids, however the all critical interactions occur between the PTC and the L4/L22 choke point within the exit tunnel. Experimentally, the minimum sequence required for ribosomal stalling is 150FXXXXWIXXXXGIRAGP166 with stalling occurring prior to nucleophilic attack by P166. In fact, Nakatogawa and Ito were successful in showing that the truncated SecM sequence of F150-P166 fused to LacZα is capable of producing stalling nearly as efficiently as the full sequence.[116,117] It has been shown that there are two mandatory interactions where modifications to either the nascent chain or the ribosomal counterpart lead to full abolishment of stalling. These take place with W155/A751 as well as R163/A2062. Mutational studies that altered any of these, either through identity changes or insertion as is the case with A751, resulted in a full transcript.[118,119] The reported pi stack between W155 and A751 creates a substantial compaction of the C-term end of SecM where the relaxed extension is shortened by nearly 7 Å, or almost 23%, of the maximum regional length. This compaction facilitates the positioning of R163 where it is believed to force A2062 out of position causing a

cascade through A2503 ultimately leading to a 2 Å shift of the P-site tRNA away from A-site, thus preventing nucleophilic attack and elongation.[120] Additionally, mutations of the β hairpin of L22, namely G91A and A93S, affect interactions with A751 leading to the same compromised stalling. Understandably, the A-site-bound P166 is highly conserved. Mutations such as P166A/F/azetidine result in recovery of translation suggesting the local changes in the PTC are not solely sufficient in stalling translation.[117] Instead, use of a sterically hindered amino acid with reduced nucleophilicity is also required. Additional sites of significance are F150, G161, and I162 where Ala mutations resulted in partial recovery of translation.

## 1.3 Discussion

The ribosomal exit tunnel is clearly much more dynamic than was first believed. This is demonstrated by the robust structures of antibiotics that are accommodated and capable of specific local interactions. It is also seen in the capability of various naturally existing peptide sequences to modulate the rate of translation in response to various intracellular triggers. However these isolated cases are very specific and a more universal understanding of the capabilities within the tunnel is lacking. This is in part due to an inability to deliver an extensive array of probes to parse out a greater scope of the extent of interactions. In an effort to develop methodology to achieve this larger network of interactions between the exit tunnel and a nascent peptide, we first recognized that we must remove the reliance on a stalled ribosomal complex as they are too specialized and limited.[121] By systematically delivering a diverse set of translation-independent peptides of known sequence to shifting but discrete windows within the PTC and exit tunnel, probing may be accomplished to observe situational interactions. To accomplish this, LSU-binding antibiotics were covalently modified to accommodate attachment of peptide or peptide-like moieties. Following successful synthesis and characterization, conjugate viability was first assessed using a cell-free assay utilizing a luciferase reporter. Provided the conjugates are still showing activity, small molecule probing (footprinting) experiments followed to both validate anchor binding location and peptide-exit tunnel interactions. Additionally, whole cell growth inhibition was performed on all derivatives to understand potential therapeutic viability of certain modifications. The modularity of this approach offered convergence of full conjugate probes differing at the antibiotic "anchor" as well as the peptide sequence of the "probe" moiety.

## 1.4 References


1. Schuwirth, B. S., Borovinskaya, M. A., Hau, C. W., Zhang, W., Vila-Sanjurjo, A., Holton, J. M. and Cate, J. H. (2005) Structures of the bacterial ribosome at 3.5 Å resolution. *Science 310*, 827-834.
2. Wimberly, B. T., Brodersen, D. E., Clemons, W. M. Jr., Morgan-Warren, R. J., Carter, A. P., Vonrhein, C., Hartsch, T. and Ramakrishnan, V. (2000) Structure of the 30S ribosomal subunit. *Nature 407*, 327-339.
3. Selmer, M., Dunham, C. M., Murphy, F. V., Weixlbaumer, A., Petry, S., Kelley, A. C., Weir, J. R. and Ramakrishnan, V. (2006) Structure of the 70S ribosome complexed with mRNA and tRNA. *Science 313*, 1935-1942.
4. Schluenzen, F., Tocilj, A., Zarivach, R., Gluehmann, M., Janell, D., Bashan, A., Bartels, H., Agmon, I., Franceschi, F. and Yonath, A. (2000) Structure of functionally activated small ribosomal subunit at 3.3 angstroms resolution. *Cell 102*, 615-623.
5. Ban, N., Nissen, P., Hansen, J., Moore, P. B. and Steitz, T. A. (2000) The complete atomic structure of the large ribosomal subunit at 2.4 Å resolution. *Science 289*, 905-920.
6. Simonetti, A., Marzi, S., Jenner, L., Myasnikov, A., Romby, P., Yusupova, G.; Klaholz, B. P. and Yusupov, M. (2009) A structural view of translation initiation in bacteria. *Cell Mol Life Sci 66*, 423-436.
7. Lovmar, M. and Ehrenberg, M. (2006) Rate, accuracy and cost of ribosomes in bacterial cells. *Biochemie 88*, 951-961.

8. Rodnina, M. V., Beringer, M. and Wintermeyer, W. (2007) How ribosomes make peptide bonds. *TRENDS Biochem Sci 32*, 20-26.
9. Nissen, P., Hansen, J., Ban, N., Moore, P. B. and Steitz, T. A. (2000) The structural basis of ribosome activity in peptide bond formation. *Science 289*, 920-930.
10. Robinson, A. and van Oijen, A. M. (2013) Bacterial replication, transcription and translation: mechanistic insights from single-molecule biochemical studies. *Nat Rev Microbiol 11*, 303-315.
11. Milon, P., Carotti, M., Konevega, A. L., Wintermeyer, W., Rodnina, M. V. and Gualerzi, C. O. (2010) The ribosome-bound initiation factor 2 recruits initiator tRNA to the 30S initiation complex. *EMBO Rep. 11*, 312-316.
12. Milon, P., Maracci, C., Filonava, L., Gualerzi, C. O. and Rodnina, M. V. (2012) Real-time assembly landscape of bacterial 30S translation initiation complex. *Nat Struct Mol Biol 19*, 609-615.
13. Chen, C., Stevens, B., Kaur, J., Smilansky, Z., Cooperman, B. S. and Goldman, Y. E. (2011) Allosteric vs. spontaneous exit-site (E-site) tRNA dissociation early in protein synthesis. *Proc Natl Acad Sci USA 10*8, 16985-16985.
14. Voss, N. R., Gerstein, M., Steitz, T. A. and Moore, P. B. (2006) The geometry of the ribosomal exit tunnel. *J Mol Biol 360*, 893-906.
15. Jenni, S. and Ban, N. (2003) The chemistry of protein synthesis and voyage through the ribosomal exit tunnel. *Curr Opin Struct Biol 13*, 212-219.
16. Wilson, D. ( 2011) Peptides in the Ribosomal Tunnel Talk Back. *Mol Cell 41*, 247-248.

17. Mankin, A. (2006) Nascent peptide in the 'birth canal' of the ribosome. *TRENDS Biochem Sci 31*, 11-13.
18. Tenson, T. and Ehrenberg, M. (2002) Regulatory Nascent Peptides in the Ribosomal Tunnel. *Cell 108*, 591-594.
19. Peattie, D. A. and Gilbert, W. (1980) Chemical probes for higher-order structure in RNA. *Proc Natl Acad Sci USA 77*, 4679-4682.
20. Peattie, D. A. (1979) Direct chemical method for sequencing RNA. *Proc Natl Acad Sci USA 76*, 1760-1764.
21. Ehresmann, C., Baudin, F., Mougel, M., Romby, P., Ebel, J.-P. and Ehresmann, B. (1987) Probing the structure of RNAs in solution. *Nucleic Acids Res 15*, 9109-9128.
22. Stern, S., Moazed, D. and Noller, H. F. (1988) Structural analysis of RNA using chemical and enzymatic probing monitored by primer extension. *Method Enzymol 164*, 481-489.
23. Regulski, E. E. and Breaker, R. R. (2008) In-line probing analysis of riboswitches. *Method MolBiol 419*, 53-67.
24. Merino, E. J., Wilkinson, K. A., Coughlan, J. L. and Weeks, K. M. (2005) RNA Structure analysis at single nucleotide resolution by selective 2'-hydroxyl acylation and primer extension (SHAPE). *J Am Chem Soc 127*, 4223-4231.
25. Sanger, F., Nicklen, S. and Coulson, A. R. (1977) DNA sequencing with chain-terminating inhibitors. *Proc Natl Acad Sci USA 74*, 5463-5467.
26. Mathews, D. H., Disney, M. D., Childs, J. L, Schroeder, S. J, Zuker, M. and Turner D. H. (2004) Incorporating chemical modification constraints into a

dynamic programming algorithm for prediction of RNA secondary structure. *Proc Natl Acad Sci USA 101*, 7287-7292.

27. Deigan, K. E., Li, T. W., Mathews, D. H. and Weeks, K. M. (2009) Accurate SHAPE-directed RNA structure determination. *Proc Natl Acad Sci USA 106*, 97-102.
28. Yonath, A., Muessig, J., Tesche, B., Lorenz, S., Erdmann, V. A. and Wittman, H. G. (1980) Crystallization of the large ribosomal subunits from *Bacillus stearothermophilus*. *Biochem Int 1*, 315-428.
29. von Bohlen, K., Makowski, I., Hansen, H. A., Bartels, H., Berkovitch-Yellin, Z., Zaytzev-Bashan, A., Meyer, S., Paulke, C., Franceschi, F. and Yonath, A. (1991) Characterization and preliminart attempts for derivatization of crystals of large ribosomal subunits from Haloarcula marismortui diffracting to 3 Å resolution. *J Mol Biol 222*, 11-15.
30. Volkmann, N., Hottentrager, S., Hansen, H. A. S., Zayzsev-Bashman, A., Sharon, R., Berkovitch-Yellin, Z., Yonath, A. and Wittman, H. G. (1990) Characterization and preliminary crystallographic studies on large ribosomal subunits from *Thermus thermophilus*. *J Mol Biol 216*, 239-241.
31. Trakhanov, S. D., Yusupov, M. M., Agalarov, S. C., Garber, M. B., Ryazantsev, S. N., Tischenko, S. V. and Shirokov, V. A. (1987) Crystallization of 70 S ribosomes and 30 S ribosomal subunits from *Thermus thermophilus*. *FEBS Lett 220*, 319-322.

32. Ban, N., Freeborn, B., Nissen, P., Penczek, P., Grassucci, R. A., Sweet, R., Frank, J., Moore, P. B. and Steitz, T. A. (1998) A 9 Å resolution X-ray crystallographic map of the large ribosomal subunit. *Cell 93*, 1105-1115.
33. Phillips, J. C., Wlodawer, A., Goodfellow, J. M.; Watenpaugh, K. D., Sieker, L. C., Jensen, L. H. and Hodgson, K. O. (1977) Applications of synchrotron radiation to protein crystallography. II. Anomalous scattering, absolute intensity and polarization. *Acta Crystallogr A33*, 445-455.
34. Yonath, A., Leonard, K. R., Weinstein, S. and Wittmann, H. G. (1987). *Cold Spring Harb Symp Quant Biol 52*, 729-741.
35. Hope, H., Frolow, F. von Bohlen, K., Makowski, I., Kratky, C., Halfon, Y., Danz, H., Webster, P., Bartels, K. S., Wittman, H. G. and Yonath, A. (1989) Cryocrystallography of ribosomal particles. *Acta Crystallogr B45*, 190-199.
36. O'Hallooran, T. V., Lippard, S. J., Richmond, T. J. and Klug, A. (1987) Multiple heavy-atom reagents for macromolecular X-ray structure determination. Applications to the nucleosome core particle. *J Mol Biol 194*, 705-712.
37. Cate, J. H., Yusupov, M. M., Yusupova, G. Z., Earnest, T. N. and Noller, H. F. (1999) X-ray crystal structures of 70S ribosome functional complexes. *Science 285*, 2095-2104.
38. Wimberly, B. T., Brodersen, D. E., Clemons, W. M. J., Morgan-Warren, R., von Rhein, C., Hartsch, T. and Ramakrishnan, V. (2000) Structure of the 30S ribosomal subunit. *Nature 407*, 327-339.
39. Schluenzen, F., Tocilj, A., Zarivach, R., Harms, J., Gluehmann, M., Janell, D., Bashan, A., Bartels, H., Agmon, I., Franceschi, F. and Yonath, A. (2000)

Structure of functionally activated small ribosomal subunit at 3.3 angstroms resolution. *Cell 102*, 615-623.

40. Ban, N., Nissen, P., Hansen, J., Moore, P. B. and Steitz, T. A. (2000) The complete atomic structure of the large ribosomal subunit at 2.4 Å resolution. *Science 289*, 905-920.
41. Bashan, A., Zarivach, R., Schluenzen, F., Agmon, I., Harms, J., Auerbach, T., Baram, D., Berisio, R., Bartels, H., Hansen, H. A. S., Fucini, P., Wilson, D., Peretz, M., Kessler, M. and Yonath, A. (2003) Ribosome Crystallography: Peptide bond formation and its inhibition. *Biopolymers 70*, 19-41.
42. Yang, L. and Ye, X. (2010) Development of aminoglycoside antibiotics effective against resistant bacterial strains. *Curr Top Med Chem 10*, 1898-1826.
43. Moazed, D. and Noller, H. F. (1987) Interactions of antibiotics with functional sites in 16S ribosomal RNA. *Nature 327*, 389-394.
44. Fourmy, D., Recht, M. I., Blanchard, S. C. and Puglisi, J. C. (1996) Structure of the A site Escherichia coli 16S ribosomal RNA complexed with an aminoglycoside antibiotic. *Science 274*, 1367-1371.
45. Jiang, L., Watkins, D., Jin, Y., Gong, C., King, A., Washington, A. Z., Green, K. D., Garneau-Tsodikova, S., Oyelere, A. K. and Arya, D. P. (2015) Rapid synthesis, RNA binding, and antibacterial screening of a peptidic-aminosugar (PA) library. *ACS Chem Biol 10*, 1278-1289.
46. Wilson, D. N. (2009) The A-Z of bacterial translation inhibitors. *Crit Rev Biochem Mol 44*, 393-433.

47. Brodersen, D. E., Clemons, W. M., Carter, A. P., Morgan-Warren, R. J., Wimberly, B. T. and Ramakrishnan, V. (2000) The structural basis for the action of the antibiotics tetracycline, pactamycin, and hygromycin B on the 30S ribosomal subunit. *Cell 103*, 1143-1154.
48. Pioletti, M., Schlunzen, F., Harms, J., Zarivach, R., Gluhmann, M., Avila, H., Bashan, A., Bartels, H. Auerbach, T., Jacobi, C., Hartsch, T., Yonath, A. and Franceschi, F. (2001) Crystal structures of complexes of the small ribosomal subunit with tetracycline, edeine, and IF3. *EMBO J 20*, 1829-1839.
49. Dunkle, J. A., Xiong, L., Mankin, A. S. and Cate, J. H. D. (2010) Structures of the Escherichia coli ribosome with antibiotics bound near the peptidyl transferase center explain spectra of drug action. *Proc Natl Acad Sci USA 107*, 17152-17157.
50. Bulkley, D., Axel Innis, C., Blaha, G. and Steitz, T. A. (2010) Revisiting the structures of several antibiotics bound to the bacterial ribosome. *Proc Natl Acad Sci USA 107*, 17158-17163.
51. Hansen, J. L., Moore, P. B. and Steitz, T. A. (2003) Structures of five antibiotics bound at the peptidyl transferase center of the large ribosomal subunit. *J Mol Biol 330*, 1061-1075.
52. Schlunzen, F., Zarivach, R., Harms, J., Bashan, A., Tocilj, A., Albrecht, R., Yonath, A. and Franceschi, F. (2001) Structural basis for the interaction of antibiotics with the peptidyl transferase centre in eubacteria. *Nature 413*, 814-821.
53. Rodriguez-Fonseca, C., Amis, R. and Garrett, R. A. (1995) Fine structure of the peptidyl transferase centre on 23S-like rRNAs deduced from chemical probing of antibiotic-ribosome complexes. *J Mol Biol 247*, 224-235.

54. Miazed, D. and Noller, H. F. (1987) Chloramphenicol, erythromycin, carbomycin, and vernamycin B protect overlapping sites in the peptidyl transferase region of 23S ribosomal RNA. *Biochemie 69*, 879-884.

55. Rheinberger, H. J. and Neirhaus K. H. (1990) Partial release of AcPhe-Phe-transfer RNA from ribosomes during Poly(U)-dependent Poly(Phe) synthesis and the effects of chloramphenicol. *Eur J Biochem 193*, 643-650.

56. Mao, J. C. H. and Robishaw, E. E. (1971) Effects of macrolides on peptide-bond formation and translocation. *Biochemistry 10*, 2054-2061.

57. Poulsen, S. M., Kofoed, C. and Vester, B. (2000) Inhibition of the ribosomal peptidyl transferase reaction by the mycarose moiety of the antibiotics carbomycin, spiramycin, and tylosin. *J Mol Biol 304*, 471-481.

58. Pestka, S. (1969) Studies on the formation of transfer ribonucleic acid-ribosome complexes. X. Phenylalanyl-oligionucleotide binding to the ribosome and the mechanism of chloramphenicol action. *Biochem Bioph Res Co 36*, 589-595.

59. Pestka, S. (1969) Studies on the formation of transfer ribonucleic acid-ribosome complexes. XI. Antibiotic effects on phenylalanyl-ologionucleotide binding to ribosomes. *Proc Natl Acad Sci USA 64*, 709-714.

60. Tu, D., Blaha, G., Moore, P. B. and Steitz, T. A. (2005) Structures of $MLS_BK$ antibiotics bound to mutated large ribosomal subunits provide structural explanation for resistance. *Cell 121*, 257-270.

61. Fernandez-Munoz, R., Monro, R. E., Torres-Pinedo, R. and Vazquez, D. (1971) Substrate- and antibiotic-binding sites at the peptidyl transferase centre of E coli

ribosomes. Studies on the chloramphenicol, lincomycin, and erythromycin sites. *Eur J Biochem 23*, 185-193.

62. Hansen, J. L., Schmeing, T. M., Moore, P. B. and Steitz, T. A. (2002) Structural insights into peptide bond formation. *Proc Natl Acad Sci USA 99*, 11670-11675.
63. Simonovic, M. and Steitz, T. A. (2009) A structural view on the mechanism of the ribosome-catalyzed peptide bond formation. *Biochim Biophys Acta. 1789*, 612-623.
64. Polacek, B. T. and Mankin, A. S. (2005) The ribosomal peptidyl transferase center: structure, function, evolution, inhibition. *Crit Rev Biochem Mol 40*, 285-311.
65. Schmeing, T. M., Seila, A. C., Hansen, J. L., Freeborn, B., Soukup, J. K., Scaringe, S. A., Strobel, C. A., Moore, P. B. and Steitz, T. A. (2002) A pre-translational intermediate in protein synthesis observed in crystals of enzymatically active 50S subunits. *Nat Struct Biol 9*, 225-230.
66. Noeske, J., Huang, J., Olivier, N. B., Giacobbe, R. A., Zambrowski, M. and Cate, J. H. D. (2014) Synergy of streptogramin antibiotics occurs independently of their effects of translation. *Antimicrob Agents Ch 58*, 5269-5279.
67. Vazquez, D. (1966) Studies on the mode of action of the streptogramin antibiotics. *J Gen Microbiol 42*, 93-106.
68. Depardieu, F. and Courvalin, P. (2001) Mutations in 23S rRNA responsible for resistance to 16-membered macrolides and streptogramins in Streptococcus pneumoniae. *Antimicrob Agents Ch 45*, 319-323.

69. Sigmund, C. D., Ettayebi, M. and Morgan, E. A. (1984) Antibiotic resistance mutations in 16S and 23S ribosomal RNA genes of Escherichia coli. *Nucleic Acids Res 12*, 4653-4663.

70. Brickner, S. J., Barbachyn, M. R., Hutchinson, D. K. and Manninen, P. R. (2008) Linezolid (ZYVOX), the first member of a completely new class of antibacterial agents for treatment of serious gram-positive infections. *J Med Chem 51*, 1981-1990.

71. Schumacher, A., Trittler, R., Bohnert, J. A., Kummerer, K., Pages, J.-M. and Kern, W. V. (2007) Intracellular accumulation of linezolid in Escherichia coli, Citrobacter freundii and Enterobacter aerogenes: role of enhanced efflux pump activity and inactivation. *J Antimicrob Chemoth 59*, 1261-1264.

72. Kloss, P., Xiong, L., Shinabarger, D. L. and Mankin, A. S. (1999) Resistance mutations in 23S rRNA identify the site of action of the protein synthesis inhibitor linezolid in the ribosomal peptidyl transferase center. *J Mol Biol 294*, 93-101.

73. Long, K. S., Munck, C., Andersen, T. M., Schaub, M. A., Hobbie, S. N., Bottger, E. C. and Vester, B. (2010) Mutations in 23S rRNA at the peptidyl transferase center and their relationship to linezolid and cross-resisitance. *Antimicrob Agents Ch 54*, 4705-4713.

74. Colca, J. R., McDonald, W.G., Waldon, D. J., Thomasco, L. M., Gadwood, R. C., Lund, E. T., Cavey, G. S., Mathews, W. R., Adams, L. D., Cecil, E. T., Pearson, J. D., Bock, J. H., Mott, J. E., Shinabarger, D. L., Xiong, L. and Mankin, A. S. (2003) Crosslinking in the living cells locates the site of action of oxazolidinone antibiotics. *J Biol Chem 278*, 21972-21979.

75. Wilson, D. N., Schluenzen, F., Harms, J. M., Starosta, A. L., Connell, S. R. and Fucini, P. (2008) The oxazolidinone antibiotics perturb the ribosomal peptidyl-transferase center and effect tRNA positioning. *Proc Natl Adac Sci USA 105*, 13339-13344.

76. Ippolito, J. A., Kanyo, Z. F., Wang, D., Franceschi, F. J., Moore, P. B., Steitz, T. A. and Duffy, E. M. (2008) Crystal structure of the oxazolidinone antibiotic linezolid bound to the 50S ribosomal subunit. *J Med Chem 51*, 3353-3356.

77. Lin, A. H., Murray, R. W., Vidmar, T. J. and Marotti, K. R. (1997) The oxazolidinone eperzolid binds to the 50S ribosomal subunit and competes with binding of chloramphenicol and lincomycin. *Antimicrob Agents Ch 41*, 2127-2131.

78. Long, K. S. and Vester, B. (2012) Resistance to linezolid caused by modifications at its binding site on the ribosome. *Antimicrob Agents Ch 56*, 603-612.

79. Thompson, J., O'Connor, M., Mills, J. A. and Dahlberg, A. E. (2002) The protein synthesis inhibitors, oxazolidinones and chloramphenicol, cause extensive translational inaccuracy *in vivo*. *J Mol Biol 322*, 273-279.

80. Gaynor, M. and Mankin, A. S. (2003) Macrolide antibiotics: Binding site, mechanism of action, resistance. *Curr Top Med Chem 3*, 949-961.

81. Katz, L. and Ashley, G. W. (2005) Translation and protein synthesis: macrolides. *Chem Rev 105*, 499-528.

82. Poehlsgaard, J. and Douthwaite, S. (2003) Macrolide antibiotic interaction and resistance on the bacterial ribosome. *Curr Opin Invest Dr 4*, 140-148.

83. Takashima, H. (2003) Structural consideration of macrolide antibiotics in relation to the ribosomal interaction and drug design. *Curr Top Med Chem 3*, 991-999.

84. Tenson, T., Lovmar, M. and Ehrenberg, M. (2003) The mechanism of action of macrolides, lincosamides and streptogramin B reveals the nascent peptide exit path in the ribosome. *J Mol Biol 330*, 1005-1014.

85. Mayford, M. and Weisblum, B. (1989) ermC leader peptide. Amino acid sequence critical for induction by translational attenuation. *J Mol Biol 206*, 69-79.

86. Vazquez-Laslop, N., Thum, C. and Mankin, A. S. (2008) Molecular mechanism of drug-dependent ribosome stalling. *Mol Cell 30*, 190-202.

87. Mankin, A .S. (2008) Macrolide Myths. *Curr Opin Microbiol 11*, 414-421.

88. Kannan, K., Vazquez-Laslop, N. and Mankin, A. S. (2012) Selective protein synthesis by ribosomes with a drug-obstructed exit tunnel. *Cell 151*, 508-520.

89. Hardesty, B., Picking, W. D., Odom, O. W. (1990) The extension of polyphenylalanine and polylysine peptides on Escherichia coli ribosomes. *Biochim Biophys Acta 1050*, 197-202.

90. Wilson, D. N. (2014) Ribosome-targeting antibiotics and mechanisms of bacterial resistance. *Nat Rev Microbiol 12*, 35-48.

91. Kannan, K., Kanabar, P., Schryer, D., Florin, T., Oh, E., Bahroos, N., Tenson, T., Weissman, J. S. and Mankin, A. S. (2014) The general mode of translation inhibition by macrolide antibiotics. *Proc Natl Acad Sci USA 111*, 15958-15963.

92. Kannan, K. and Mankin, A. S. (2011) Macrolide antibiotics in the ribosome exit tunnel: Species-specific binding and action. *Ann NY Acad Sci 1241*, 33-47.

93. Hansen, J. L., Ippolito, J. A., Ban, N., Nissen, P., Moore, P. B. and Steitz, T. A. (2002) The structures of four macrolide antibiotics bound to the large ribosomal subunit. *Mol Cell 10*, 117-128.

94. Sanz, J. L., Marin, I., Urena, D. and Amils, R. (1993) Functional-analysis of 7 ribosomal systems from extremely halophilic archaea. *Can J Microbiol 39*, 311-317.

95. Bommakanti, A. S., Lindahl, L. and Zengel, J.M. (2008) Mutation from guanine to adenine in 25S rRNA at the position equivalent to E. coli A2058 does not confer erythromycin sensitivity in Sacchromyces cerevisae. *RNA 14*, 460-464.

96. Hardy, D. J., Hensey, D. M., Beyer, J. M., Vojtko, C., McDonald, E., and Fernandes, P. B. (1988) Comparative in vitro activities of new 14-, 15- and 16-membered macrolides. *Antimicrob Agents Ch 32*, 1710-1719.

97. LeTourneau, N., Vimal, P., Klepacki, D., Mankin, A. S. and Melman, A. (2012) Synthesis and antibacterial activity of desosamine-modified macrolide derivatives. *Bioorgan Med Chem Lett 22*, 4575-4578.

98. Wilson, D. N., Harms, J. M, Nierhaus, K. H., Schlunzen, F. and Fucini, P. (2005) Species-specific antibiotic-ribosome interactions: Implications for drug development. *Biol Chem 386*, 1239-1252.

99. Denis, A., Agouridas, C., Auger, J.-M., Benedetti, Y., Bonnefoy, A., Bretin, F., Chantot, J.-F., Dussarat, A., Fromentin, C., D'Ambrieres, S. G., Lachaud, S., Laurin, P., Le Martret, O., Loyau, V., Tessot, N., Pejac, J.-M. and Perron, S. (1999) Synthesis and antibacterial activity of HMR 3647 a new ketolide highly

potent against erythromycin-resistant and susceptible pathogens. *Bioorgan Med Chem Lett 9*, 3075-3080.

100. Bryskier, A. (2000) Ketolides – telithromycin, an example of a new class of antibacterial agents. *Clin Microbiol Infec 6*, 661-669.

101. Xiong, Y. Q. and Le, T. P. (2001) Telithromycin (HMR 3647): The first ketolide antibiotic. *Drugs Today (Barc.) 37*, 617-628.

102. Berisio, R., Harms, J., Schluenzen, F., Zarivach, R., Hansen, H. A., Fucini, P. and Yonath, A. (2003) Structural insight into the antibiotic action of telithromycin against resistant mutants. *J Bacteriol 185*, 4276-7279.

103. Ito, K., Chiba, S. and Pogliano, K. (2010) Divergent stalling sequences sense and control cellular physiology. *Biochemi Biophys Res Comm 393*, 1-5.

104. Cruz-Vera, L. R., Rajagopal, S., Squires, C. and Yanofsky, C. (2005) Features of ribosome-peptidyl-tRNA interactions essential for tryptophan induction of tna operon expression. *Mol Cell 19*, 333-343.

105. Gong, F., Ito, K., Nakamura, Y. and Yanofsky, C. (2001) The mechanism of tryptophan induction of tryptophanase operon expression: tryptophan inhibits release factor-mediated cleavage of TnaC-peptidyl-tRNA(Pro). *Proc Natl Acad Sci USA 98*, 8997-9001.

106. Cruz-Vera, L. R. and Yanofsky, C. (2008) Conserved residues Asp16 and Pro24 of TnaC-$tRNA^{Pro}$ participate in tryptophan induction of *tna* operon expression. *J Bacteriology 190*, 4971-4797.

107. Gong, F. and Yanofsky, C. (2002) Analysis of tryptophanase operon expression in vitro: accumulation of TnaC-peptidyl-tRNA$^{Pro}$. *J Biol Chem 277*, 17095-17100.

108. Martinez, A. K., Gordon, E., Sengupta, A., Shirole, N., Klepacki, D., Martinez-Garriga, B., Brown, L. M., Benedik, M. J., Yanofsky, C., Mankin, A. S., Vazquez-Laslop, N., Sachs, M. S. and Cruz-Vera, L. R. (2014) Interactions of the TnaC nascent peptide with rRNA in the exit tunnel enable the ribosome to respond to free tryptophan. *Nucleic Acids Res 42*, 1245-1256.

109. Seidelt, B., Innis, C. A., Wilson, D. N., Gartmann, M., Armache, J.-P., Villa, E., Trabuco, L. G., Becker, T., Mielke, T., Schulten, K., Steitz, T. A. and Beckmann, R. (2009) Structural insight into nascent polypeptide chain-mediated translational stalling. *Science 326*, 1412-1415.

110. Gupta, P., Liu, B., Klepacki, D., Gupta, V., Schulten, K., Mankin, A. S. and Vazquez-Laslop, N. (2016) Nascent peptide assists the ribosome in recognizing chemically distinct small molecules. *Nature Chem Biol 12*, 153-158.

111. Ramu, H., Vazquez-Laslop, N., Klepacki, D., Dai, Q., Piccirilli, J., Micura, R. and Mankin, A. S. (2011) Nascent peptide in the ribosome exit tunnel affects functional properties of the A-site of the peptidyl transferase center. *Mole Cell 41*, 321-330.

112. Vazquez-Laslop, N., Thum, C. and Mankin, A. S. (2008) Molecular mechanism of drug-dependent ribosome stalling. *Mole Cell 30*, 190-202.

113. Vazquez-Laslop, N., Ramu, H., Klepacki, D., Kannan, K. and Mankin, A. S. (2010) The key function of a conserved and modified rRNA residue in the ribosomal response to the nascent peptide. *EMBO J 29*, 3108-3117.

114. Arenz, S., Ramu, H., Gupta, P., Berninghausen, O., Reckmann, R., Vazquez-Laslop, N., Mankin, A. S. and Wilson, D. N. (2014) Molecular basis for erythromycin-dependent ribosome stalling during translation of the ErmBL leader peptide. *Nature Comm 5*, 3501; doi:10.1038/ncomms4501.

115. Sothiselvam, S., Liu, B., Han, W., Ramu, H., Klepacki, D., Atkinson, G. C., Brauer, A., Remm, M., Tenson, T., Schulten, K., Vazquez-Laslop, N. and Mankin, A. S. (2014) Macrolide antibiotics allosterically predispose the ribosome for translation arrest. *Proc Natl Acad Sci USA 111*, 9804-9809.

116. Nakatogawa, H. and Ito, K. (2001) Secretion monitor, SecM, undergoes self-translation arrest in the cytosol. *Mole Cell 7*, 185-192.

117. Nakatogawa, H. and Ito, K. (2002) The ribosomal exit tunnel functions as a discriminating gate. *Cell 108*, 629-636.

118. Yap, M.-N. and Bernstein, H. D. (2009) The plasticity of a translation arrest motif yields insights into nascent polypeptide recognition inside the ribosomal tunnel. *Mole Cell 34*, 201-211.

119. Bhushan, S., Hoffmann, T., Seidelt, B., Frauenfeld, J., Mielke, T., Berninghausen, O., Wilson, D. N. and Beckmann, R. (2011) SecM-stalled ribosomes adopt an altered geometry at the peptidyl transferase center. *PLoS Biol 9*, e1000581, doi:10.1371/journal.pbio.1000581.

120. Gumbart, J., Schreiner, E., Wilson, D. N., Beckmann, R. and Schulten, K. (2012) Mechanisms of SecM-mediated stalling in the ribosome. *Biophys J 103,* 331-341.

# CHAPTER 2 Design and Development of Small Molecule Probes to Analyze Ribosome Exit Tunnel-Nascent Peptide Interaction

## 2.1 Introduction

The understanding of how a ribosome functions has grown tremendously over the last six decades. One of the last remaining untold frontiers within the ribosome is the exit tunnel and the extent of interactions made within. Antibiotics highly target a relatively small region of the exit tunnel within the large subunit. In fact, over 25% of the antibiotics prescribed in 2011 in the United States of America[1] were of classes that bind within a 15 Å window spanning the PTC down to a naturally existing choke point, discussed shortly. Throughout this 100 Å long and 20 Å wide tunnel, protein lines a rather small portion approximately 20 Å into the tunnel. The protrusion of ribosomal proteins L4 and L22 create a choke point, reducing the aperture to a tight 10 Å. The macrolide class, as well as streptogramin B types, exploit this by increasing steric bulk and creating congestion. The greater extent of the exit tunnel is lined by ribosomal RNA (rRNA) and with that, a strong negative charge from the nonbridging oxygens of the phosphate backbone. While it was once believed that the exit tunnel was more "Teflon"-like in nature, meaning allowing a passive route of travel for the nascent peptide, growing evidence is suggesting the contrary where situational interactions serve to modulate the rate of translation. Partial understanding has been achieved for these situational cases; however a more broad understanding of the interactions possible within the exit tunnel has remained elusive. Herein, I will discuss the approach to generate a series of probes capable of scanning varied windows of the exit tunnel through a convergent conjugation system.

## 2.2 Puromycin

In addressing how to present our probe peptides, we systematically approached the anchor design. Beginning in the peptidyl transferase center, a puromycin-like anchor was first explored. As stated previously, puromycin is a tRNA mimic that binds very well within the PTC, effectively performs the nucleophilic attack and encumbers the nascent peptide, however stalls translation after progressing to the P-site due to the nonhydrolyzable amide bond replacing the ester bond at the ribose 3'. With the tyrosine-like moiety of puromycin selectively projecting to the exit tunnel, we surmised that replacement of this moiety with a simple aniloamide group will furnish a puromycin mimic which could be easily functionalized with polypetides to arrive puromycin derived probes. Toward this end, we synthesized anchor compound **3** starting with puromycin aminonucleoside allowing for the incorporation of a synthetically accessible secondary

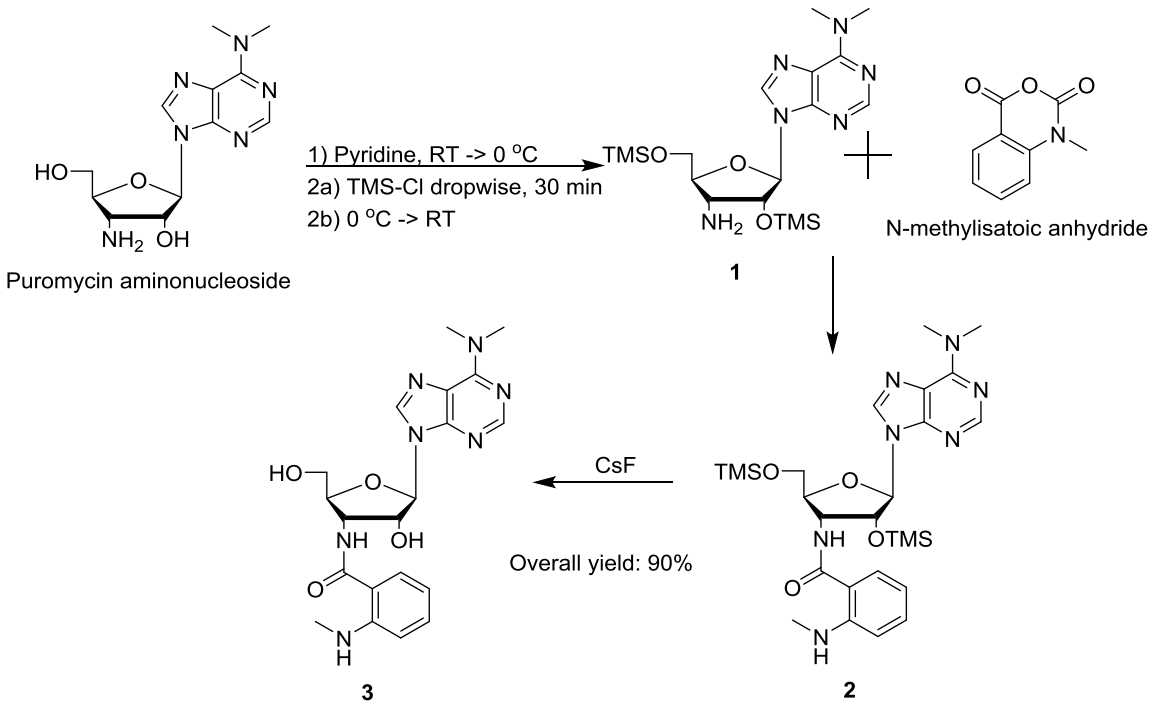


**Figure 16: Synthesis of puromycin-inspired anchor.**

amine (Fig 16).

### 2.2.1 Synthesis of Puromycin-NMIA Coupled Anchor (3)

To a solution of puromycin aminonucleoside (49.2 mg, 0.167 mmol) in 10 mL tetrahydrofuran was added pyridine (0.06 mL, 0.7 mmol). The reaction was stirred at room temperature for 30 min before bringing the temperature to 0 $^{o}$C. Upon cooling, chlorotrimethylsilane (0.13 mL, 1.0 mmol) was added dropwise over 30 min and continued to stir for an additional 30 min at 0 $^{o}$C. After warming to room temperature, N-methylisatoic anhydride (38.7 mg, 0.219 mmol) was added and allowed to stir for an additional hour. The reaction was diluted with 10% methanol in ethyl acetate (25 mL) and extraction was performed with saturated $NH_4Cl$ (3 x 30 mL). The organic layer was first treated with NaSO4 followed by rotary evaporation to afford 64.7mg (90%) of **3** as an off-white powder. $^{1}$H NMR (400 MHz, cdcl$_3$) δ 7.97 (d, *J* = 7.9 Hz, 3H), 7.42 (t, *J* = 7.8 Hz, 3H), 6.68 (d, *J* = 8.6 Hz, 3H), 6.62 (t, *J* = 7.5 Hz, 3H), 2.93 (s, 7H), 2.85 (d, *J* = 12.7 Hz, 1H), 1.26 (s, 3H); HRMS (MALDI) calc for $[C_{20}H_{25}N_7O_4 + H]^+$ 428.2024, found 428.2046. Structural characterization can be found in Appendix A.1.1.

Upon challenging compound **3** with the cell-free assay described below in 2.2.2, it was shown to have no activity up to a maximum tested dose of 10 μM. This anchor was not pursued further. We believe that the synthetic modification about the ribose sugar clashes with the neighboring region, thus preventing similar binding as seen with the inspiring parent.

### 2.2.2 Translation Inhibition

For all compounds tested within this document, this will be referred to as the "cell-free translation inhibition assay". This assay functions as an indirect measure of translation by determining the concentration of compound required to inhibit 50% of ribosomal activity ($IC_{50}$). Initial incubation of positive controls or conjugates with *Escherichia coli* (*E. coli* S30 Extract System for Circular DNA, L1020, Promega) or

rabbit reticulocyte (Rabbit Reticulocyte Lysate System, Nuclease Treated, L4960, Promega) cellular extracts follow by addition of a plasmid encoding luciferase provides varied levels of the final protein as a result of the compound's ability to inhibit translation. The inclusion of the eukaryotic assay is to ensure that the conjugate probes maintain prokaryotic activity. The prokaryotic assay was used as an initial screen to determine whether or not the extensive chemical modification of the parent anchors disrupt their ability to target and bind to the ribosome. If substantial deviation from the parent or abolishment of activity was observed, the conjugates were not pursued further.

## 2.3 Linezolid

The infeasibility of the puromycin analog encouraged the exploration of an alternate anchor. Staying within the PTC, linezolid was seen as a viable possibility. With the morpholino and oxazolidinone rings fundamental to binding and the acetamide projecting toward the tunnel[2,3], this latter functionality was selected as the synthetic handle.

### 2.3.1 Design and Evaluation of Linezolid Classes

Starting with a linezolid precursor **4**, the primary alcohol was first activated through mesylation followed by nucleophilic displacement using sodium azide to afford compound **6** in 86% yield (Figure 17). A portion of **6** was selectively reduced using ammonium chloride and zinc powder in ethanol/water under reflux conditions in a pressure tube. Amine **7** was obtained as an off-white powder in 34% yield.

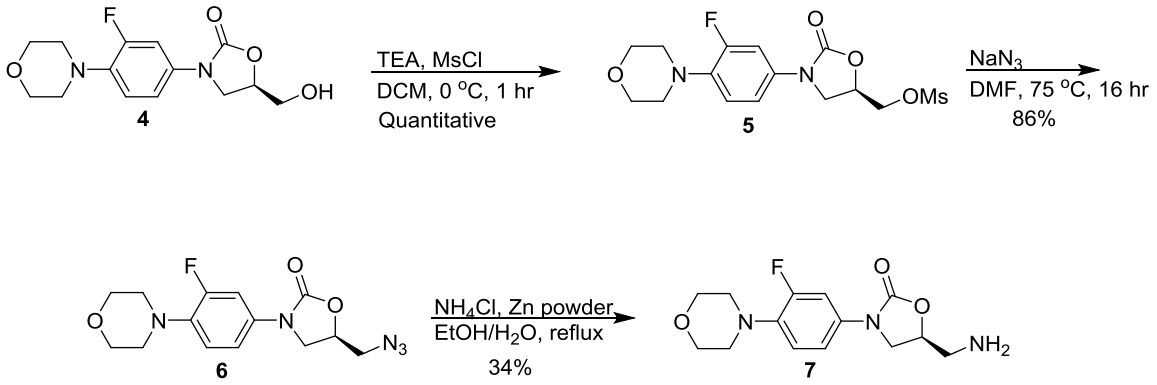


**Figure 17: Synthesis of linezolid-inspired anchor.**

Azide **6** was subjected to copper-mediated cycloaddition with a series of alkyne-decorated peptides.[4] The first peptide sequences selected for this "click" reaction were highly cationic in nature. Recalling that the exit tunnel and walls of the PTC itself are lined heavily with rRNA, the belief was that greater cationic character would be better

suited to engage with the phosphate backbone, thus providing greater opportunity for interaction. The resulting probes **9a** and **9b** (coupling and deprotection performed by Eric Raftery) are seen in Figure 18. An additional note regarding these probes, they contain the identical sequence; however directionality is reversed in **9b** from the biologically relevant N terminus to C terminus. It was expected that probe **9a** would have the ability to bind within the PTC, facilitated by the oxazolidinone anchor, while threading the protein portion down the tunnel mimicking a nascent peptide. Conversely, **9b** would be unable to bind as the exit tunnel would possibly reject the reversed sequence.

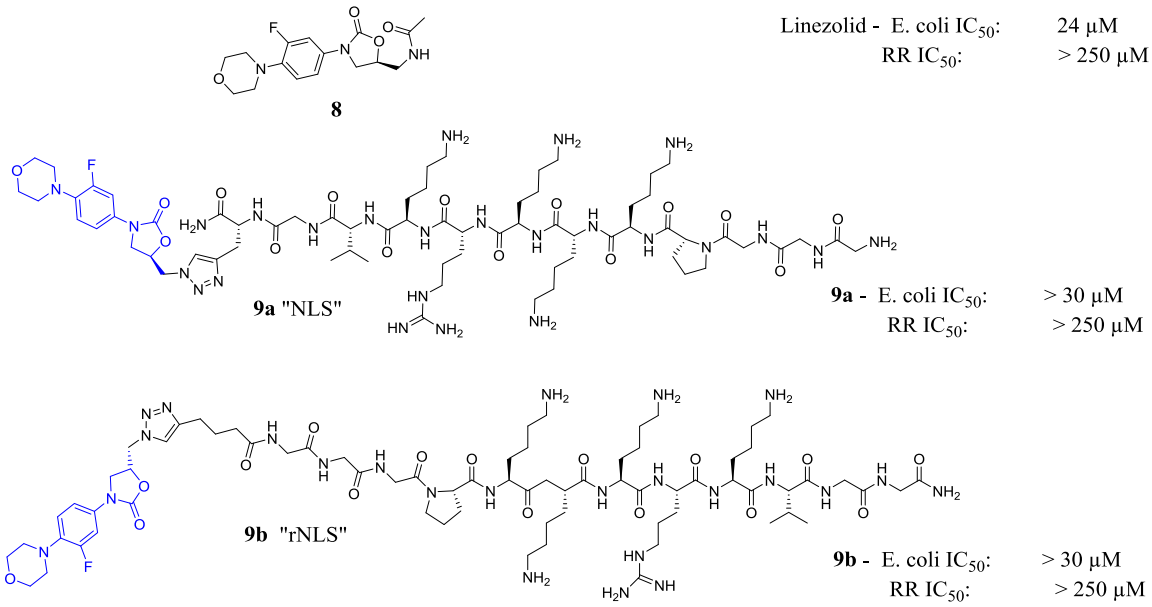


**Figure 18: Linezolid probes. Cell free translation inhibition assays for the parent linezolid as well as the two conjugate probes. Final "click" and deprotection performed by Eric Raftery.**

Upon successful synthesis and characterization, probes **9a** and 9**b** were subjected to initial assay screening to evaluate probe binding. Unfortunately, both probes were unable

to inhibit translation up to a maximum tested dose of 30 µM suggesting the covalent modification was too much to overcome.

To determine if the sequence and/or length of the appended peptide influence binding, another sequence **10**, that was substantially shorter, was selected. Cycloaddition reaction between **6** and **10** followed by deprotection afforded probe **11** in high yield (Figure 19).

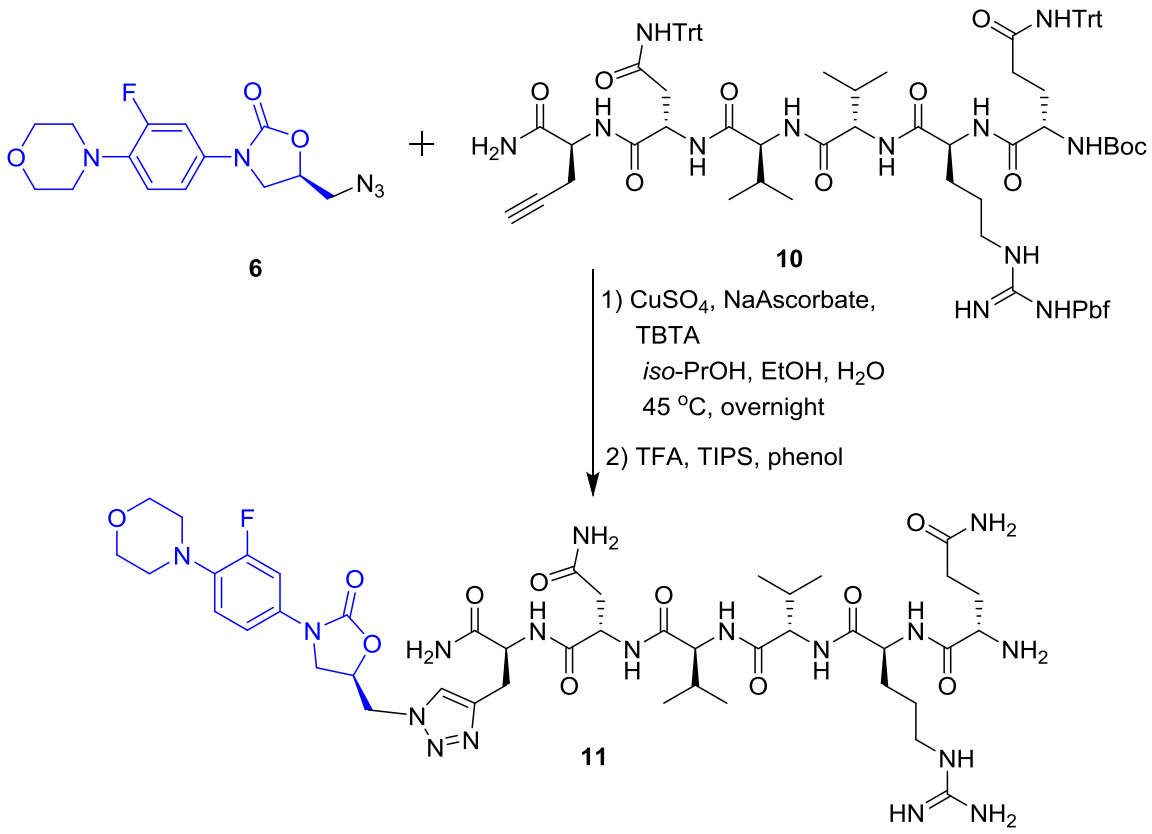


**Figure 19: Synthesis of Probe 11.**

Moreover, to parse out the overall contribution of the triazole, the same sequence was coupled via an amide bond in probe **13** (Figure 20). The synthesis of **13** was accomplished in high yield using hydroxybenzotriazole (HOBT) and *N*-(3-dimethylaminopropyl)-*N'*-ethylcarbodiimide (EDCI) promoted coupling reaction between amine **7** and peptide **12** followed by TFA deprotection agents.

Subjecting this redesigned series to the same prokaryotic cell-free analysis resulted in no translation inhibition for either **11** or **13** up to a maximum tested dose of 25 µM. This data continues to reinforce the notion that the linezolid anchor may not be tolerant of this level of covalent modification.

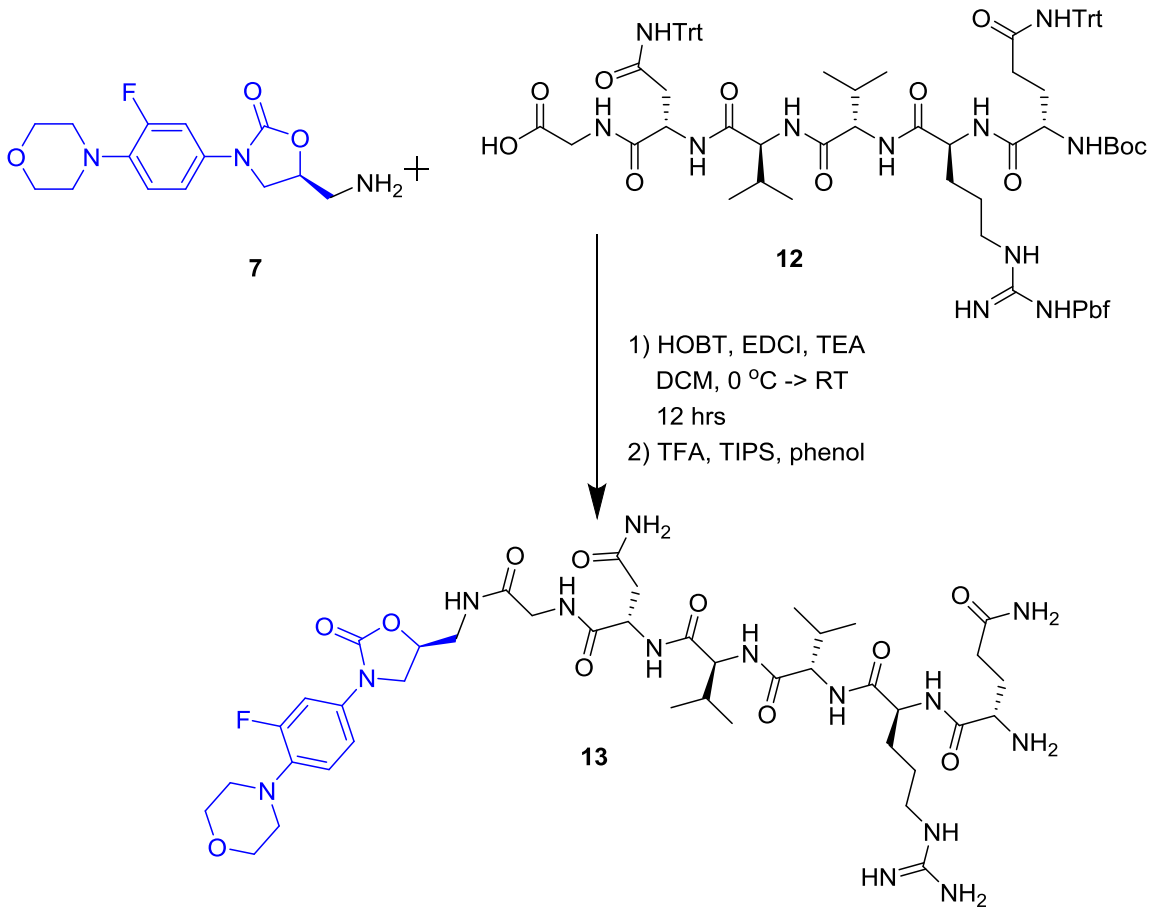


**Figure 20: Synthesis of Probe 13.**

### 2.3.2 Synthesis of Linezolid Class Anchors and Probes 11 and 13

**(R)-3-(3-fluoro-4-morpholinophenyl)-5-(((trimethylsilyl)oxy)methyl)oxazolidin-2-one (5)**

A solution of (R)-3-(3-fluoro-4-morpholinophenyl)-5-(hydroxymethyl)oxazolidin-2-one (3.49 mg, 1.179 mmol) and triethylamine (3.3 mL, 0.024 mmol) in 65 mL dichloromethane was held at 0 $^{o}$C and allowed to stir. To this was added methanesulfonyl chloride (1.38 mL, 1.77 mmol) dropwise over 15 min followed by an additional 20 min of stirring. The crude product was filtered and washed with water (3 x 20 mL) and dried further in a vacuum oven. The filtrate was moved to a separatory funnel and the aqueous layer was washed with dichloromethane ( 3 x 20 mL). The organic fraction was dried with $NaSO_4$ followed by rotary evaporation. A total of 4.71 g (98%) of activated alcohol **5** was combined.

**(R)-5-(azidomethyl)-3-(3-fluoro-4-morpholinophenyl)oxazolidin-2-one (6)**

To a solution of activated alcohol **5** (3.71 g, 9.92 mmol) in 70 mL of dimethylformamide was added $NaN_3$ (2.58 g, 40.0 mmol) and was allowed to stir overnight at 75 $^{o}$C. After returning to room temperature, the reaction was diluted by addition of 150 mL water and 50 mL ethyl acetate. Extraction was performed with ethyl acetate (3 x 30 mL) and the combined organic fractions were dried with $NaSO_4$ followed by rotary evaporation resulting in 2.75 g (86%) of azide **6**.

**(S)-5-(aminomethyl)-3-(3-fluoro-4-morpholinophenyl)oxazolidin-2-one (7)**

To a solution of azide **6** (107.7 mg, 0.335 mmol) in 2 mL ethyl acetate and 0.67 mL water was added $NH_4Cl$ (45.4 mg, 0.85 mmol) and zinc powder (28.4 mg). The solution stirred under reflux for 6 hrs and allowed to cool. The solution was filtered over Celite and the filtrate was acidified by the addition of 1N HCl (10 mL). Extraction was performed with

dichloromethane (3 x 10 mL). Confirming removal of azide **6** through TLC (20 DCM: 1 MeOH: 0.1 $NH_4OH$), the aqueous layer was basified and extracted with dichloromethane (3 x 10 mL) to extract out amine **7**. Rotary evaporation of the amine extraction layers resulted in 33.6 mg (34%) of amine **7**.

**Linezolid-QRVVNG triazole conjugate (11)**

To a solution of azide **6** (3.21 mg, 0.010 mmol) and $QRVVNG_{pNH2}$ protected peptide alkyne **11** (14.70 mg, 0.0095 mmol) in 1 mL of *tert*-butanol and 1 mL of ethanol was added tris[(1-benzyl-1H-1,2,3,-triazol-4-yl)methyl]amine (0.63 mg, 0.0012 mmol). Next added was $CuSO_4 \cdot 5H_20$ (0.2 mg, 0.00097 mmol) sonicated in 0.2 mL $H_2O$ followed by sodium ascorbate (0.8 mg, 0.004 mmol) sonicated in 0.2 mL $H_2O$. The reaction stirred overnight at 45 $^oC$. The reaction was allowed to cool, diluted by addition of 50 mL ethyl acetate and transferred to a separatory funnel. Extraction was performed with a 4 $NH_4Cl$ : 1 $NH_4OH$ solution (2 x 10 mL). The organic layer was dried with $NaSO_4$. Solvent was removed by rotary evaporation. The white solid obtained above was dissolved in TFA/TIPS/phenol (90:5:5, 2 mL) and stirred at room temperature for 2 h. Rotary evaporation followed by addition of diethyl ether (1 mL) lead to a white precipitate. The solution was vortexed for 1 min before pelleting through centrifugation (13,200 rpm, 5 min) followed by removal of the supernatant. The final pellet was dissolved in acetonitrile (0.75 mL) and deionized water (0.25 mL) was added, and the mixture was shaken. The final aqueous layer was flash frozen in dry ice/acetone and lyophilized overnight to give **11** as fluffy, white solid (6.96 mg, 71%). $^1H$ NMR (400 MHz, $d_2o$) δ 7.86 (s, 1H), 7.05 (dd, *J* = 44.2, 33.6 Hz, 1H), 4.36 (s, 1H), 4.28 (s, 1H), 4.02 (s, 1H), 4.00 (s, 1H), 3.92 (s, 1H), 3.79 (s, 1H), 3.08 (s, 2H), 2.98 (s, 1H), 2.75 (s, 1H), 2.72 (s, 1H), 2.62 (d, *J* = 2.6 Hz, 3H), 2.30 (s, 3H), 2.02 (s, 2H), 1.92 (s, 2H), 1.67 (s, 2H), 1.48 (s, 2H), 0.92 (s, 1H), 0.81 (d, *J* = 20.9 Hz, 12H); HRMS (ESI) calc for [$C_{44}H_{68}FN_{17}O_{11}$ +

$2H]^{2+}$ 515.7701, found 515.7707. Structural characterization can be found in Appendix A.1.1.

**Linezolid-QRVVNG amide conjugate (13)**

A solution of QRVVNG protected carboxylic acid peptide **12** (14.8 mg, 0.0098 mmol) in 3 mL of dichloromethane was cooled to 0 $^{o}$C. To this was added hydroxybenotriazole (1.9 mg, 0.014 mmol) and this was allowed to stir for 5 min. Next was added 1-ethyl-3-(3-dimethylaminopropyl)carbodiimide (2.3 mg, 0.012 mmol) followed by another 10 min stirring at 0 $^{o}$C. Finally, a solution of amine **7** (6.9 mg, 0.023 mmol) in Hunig's base (0.0069 mL) and 2 mL dichloromethane was added to the peptide solution. This was allowed to warm to room temperature and react overnight. The reaction was stopped by quenching with water and transferred to a separatory funnel. Dichloromethane (20 mL) was added and the organic layer was extracted with alternate washings of saturated $NaHCO_3$ and water (2 x 20 mL). The organic layer was dried with $NaSO_4$. Solvent was removed by rotary evaporation. The white solid obtained above was dissolved in TFA/TIPS/phenol (90:5:5, 2 mL) and stirred at room temperature for 2 h. Rotary evaporation followed by addition of diethyl ether (1 mL) lead to a white precipitate. The solution was vortexed for 1 min before pelleting through centrifugation (13,200 rpm, 5 min) followed by removal of the supernatant. The final pellet was dissolved in acetonitrile (0.75 mL) and deionized water (0.25 mL) was added, and the mixture was shaken. The final aqueous layer was flash frozen in dry ice/acetone and lyophilized overnight to give **13** as fluffy, white solid (8.00 mg, 86%). $^{1}$H NMR (400 MHz, $d_2o$) δ 7.27 (d, *J* = 13.2 Hz, 1H), 7.03 (s, 1H), 4.36 (s, 1H), 4.19 (s, 1H), 3.99 (s, 1H), 3.94 – 3.84 (m, 2H), 3.71 (d, *J* = 12.2 Hz, 5H), 3.50 (s, 2H), 2.95 (d, *J* = 28.0 Hz, 5H), 2.49 (s, 2H), 2.21 (s, 2H), 1.91 (s, 4H), 1.58 (s, 2H), 1.48 – 1.28 (m, 2H), 0.81 – 0.58 (m, 12H); HRMS (ESI) calc for $[C_{41}H_{65}FN_{14}O_{11} + H]^{+}$ 949.5009, found 949.5014. Structural characterization can be found in Appendix A.1.1.

## 2.4 Telithromycin

This work was published with multiple contributors. Their contributions will be pointed out when appropriate.

Washington, A. Z., Benicewicz, D. B., Canzoneri, J. C., Fagan, C. E., Mwakwari, S. C., Maehigashi, T., Dunham, C. M. and Oyelere, A. K. (2014) Macrolide-peptide conjugates as probes of the path of travel of the nascent peptides through the ribosome. *ACS Chem Biol 9*, 2621-2631

As discussed in 1.2.1, telithromycin displays species-dependent orientation of its alkyl-aryl arm in response to the presence or absence to the Watson-Crick interaction of U2609-A752 of the 23S rRNA. In each of the structures, the alkyl-aryl arm is engaged in different stabilizing interactions (Figure 21). In *E. coli* and *T. thermophilus*, the arm is stabilized by stacking against the rRNA A752:U2609 base pair. In *H. marismortui*, which lacks the A752:U2609 base pair, the arm is stabilized by a hydrogen bond with the O2' of U2609 while in *D. radiodurans*, the arm extends down the exit tunnel and is potentially engaged in van der Waals interactions with the rRNA.[6] This dynamic flexibility of the alkyl-aryl portion can be exploited as a means of potentially doubling the intended probing window. By using the same peptide sequences as those in **9a** and **9b**, the reversed sequence could conceivably self-align and project back toward the PTC, thus providing a platform to probe in both directions.

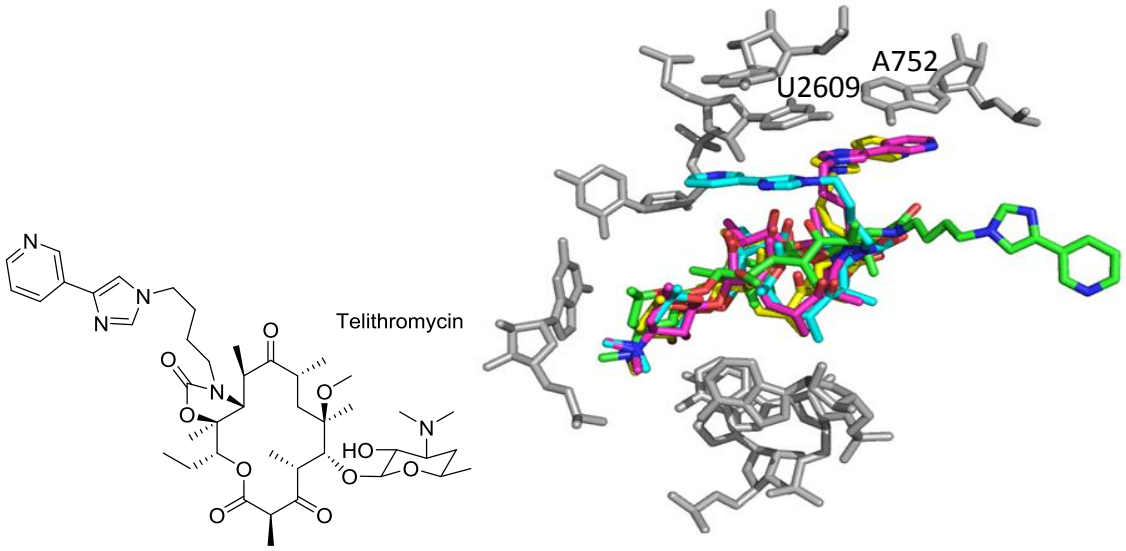


**Figure 21: Telithromycin. Structure of Telithromycin (left). Path of alkyl-aryl arm changes based on response to U2609-A752 base pair of the 23S rRNA (right). Yellow: *T. thermophilus* (PDB 3OI3)[8]; Green: *D. radiodurans* (PDB 1P9X)[9]; Cyan: *H. marismortui* (PDB 1YIJ)[10]; Magenta: *E. coli* (PDB 3OAT)[11]. All images containing PDB structures are generated using the PyMol Molecular Graphics System.[23]**

### 2.4.1 Design and Probe Synthesis

We designed a series of telithromycin-derived peptide-ketolide (or peptolide) probes which have the phenyl and the imidazolyl groups substituted by peptides and 1,2,3-triazole ring, respectively. The synthesis of these peptodies was accomplished through the Cu(I) promoted cycloaddition reaction of azido-ketolide intermediates and appropriately protected terminal alkyne modified peptides (full synthesis performed by Derek Benicewicz).[12,13] Of these azido-ketolides, there is variation about the alkyl region spanning the carbamate and the azide: a butyl group used to most closely mimic the parent telithromycin, and a propyl variant to offer a slightly shifted probing window. The peptide portions differ in the (1) direction of attachment (amino or carboxy terminus), (2) number of the amino acids in the peptide moiety, and (3) composition of amino acid of

the peptide moiety. These variations are incorporated into the design in order to investigate the influence of both the nature of individual amino acids, and the orientation of the peptide chain within the exit tunnel on the affinity of the peptolides for the ribosome. The combination of the four peptide probes and two linker lengths resulted in a series of eight total probes as shown in Figure 22.

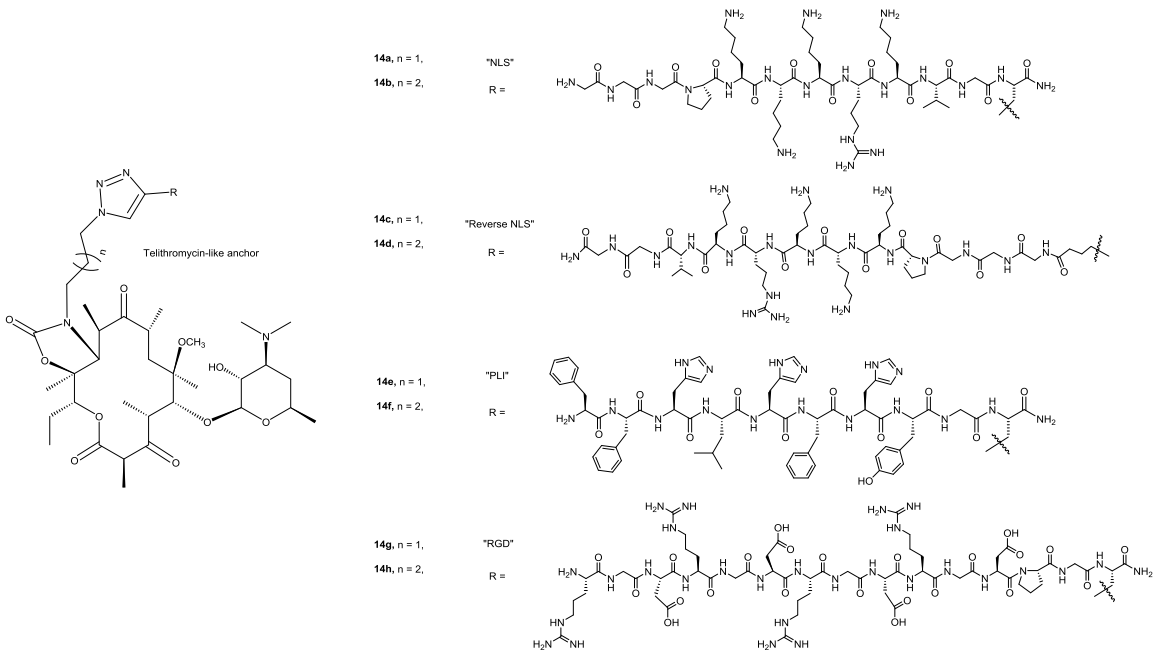


**Figure 22: Peptolide final structures.**

The NLS and rNLS are the same reversed pair used within the linezolid series where they are highly cationic carrying a +5 charge at physiological pH. The second level of modification is that the rNLS sequence is reversed such that the attachment to the ketolide base is near the N terminus. This sequence reversal as well as the flexibility of the alkyl-aryl arm of telithromycin discussed above is intended to provide the opportunity for the peptide to self-align to adopt the correct N term → C term projection by flipping over the macrolactone ring and projecting the C terminus back to the PTC.

The other sequences were designed primarily to evaluate the charge effect where the highly aromatic plicatamide (PLI) sequence holds a +3 charge and the Arg-Gly-Asp tetramer repeat (RGD) is Zwitterionic neutral overall while at physiological pH.

### 2.4.2 Peptolide Cell-Free Assay Evaluation

Similar to previous series', the cell-free luciferase reporter assay was employed to validate the probes' ability to maintain translation inhibition activity. Additionally, by independently measuring the effects of the deprotected, uncoupled peptides on luciferase activity, we were able to evaluate the effect of the coupled probe as well as the potential contribution of the peptide alone on translation inhibition.

It was observed that all coupled peptolides not only retained potent translation inhibition capability, but the best performer of the series, **14b**, performed on par with both macrolide positive controls. This inhibition was shown to be exclusive to the full probe and not an inherent effect of the peptide portion alone as displayed by no inhibition activity up to the maximum tested dose of either 250 or 1000 μM.

A remarkable difference in the inhibition profile can be seen when put in context of both the linker length as well as the overall charge of the peptide portion. Collectively, the butyl linker performed better. This is not unexpected as the $C_4$ linker is the nearest mimic to telithromycin. In looking at the effect of the amino acid composition, and thus the overall charge, there is a strong correlation between the higher cationic character of the probe and the increased inhibition. This observation suggests that the positively charged peptides such as **15** and **16** have an enhanced affinity for the phosphate backbone of the rRNA which lines the exit tunnel. Since the peptide tails alone did not cause significant translation inhibition, it is believed that the ketolide macrocyclic ring of the peptolide acts as an anchor whose affinity for the ribosome is in turn modulated by the extent of accommodation of the peptide moieties within the ribosome. The impact of directionality of the peptide could not be determined from this assay. When comparing

the matched pairs of **14a**/**14c** and **14b**/**14d** there is virtually no deviation in the inhibition values. However, based on these data alone, it cannot be determined whether the peptides are adopting reversed directions.

In expanding the analysis to those probes with a +3 overall charge (**14e**/**f**) and the zwitterions (**14g**/**h**), the charge clearly dominates the major influencing factor. Reducing charge by two results in a 3- to 4-fold reduction in inhibition activity. Amazingly, those of the zwitterion class are not just the worst within the series, but the propyl linker zwitterion **14g** displays nearly a 50-fold reduction in inhibition activity over **14a**.

The peptolides were evaluated in a eukaryotic translation system to assess their selectivity for prokaryotic ribosomes over eukaryotic ribosomes. As anticipated, the control TE-802 and clarithromycin are inactive at 250 μM. The majority of the peptolides and the analogous deprotected peptides were unable to inhibit eukaryotic translation at the same maximum tested dose. However, the unattached deprotected peptide **17** showed slight translation inhibition with an $IC_{50}$ of 205μM, resulting in only a ~ 4-fold selectivity over the prokaryotic ribosome. When coupled to the butyl linked ketolide, the resulting peptolide **14f** showed significant inhibition of eukaryotic translation with an $IC_{50}$ of 38μM. This suggests there are subtle architectural differences between the eukaryotic and prokaryote exit tunnels which allow for more favorable interactions with peptide **17** and its analogous peptolide **14f** within the context of the eukaryotic ribosome.

**Table 1: $IC_{50}$ cell free assays translation inhibition activity of peptolides against prokaryotic and eukaryotic ribosomal preparations. Luciferase activity was used as a reporter of translation inhibition in both systems. $IC_{50}$ values were obtained from an average of three independent experiments. * No inhibition at maximum tested concentration (250 µM). ** Maximum tested concentration increased 4-fold to obtain information about the extent of selectivity over RRL. # Values determined by Dr. Joshua Canzoneri.**

| Compounds | *E. coli* $IC_{50}$ (µM) | Rabbit Retic. $IC_{50}$ (µM) [#] |
|---|---|---|
| **14a** | 1.32 ± 0.08 | > 250 |
| **14b** | 0.67 ± 0.28 | > 250 |
| **15** | > 250*[#] | > 250 |
| **14c** | 1.86 ± 0.35 | > 250 |
| **14d** | 1.10 ± 0.22 | > 250 |
| **16** | > 250*[#] | > 250 |
| **14e** | 4.32 ± 0.25 | 140 |
| **14f** | 2.73 ± 0.82 | 38 |
| **17** | > 1000**[#] | 205 |
| **14g** | 56.00 ± 9.60 | > 250 |
| **14h** | 7.41 ± 1.20 | > 250 |
| **18** | > 250*[#] | > 250 |
| **TE-802** | 0.52 ± 0.05 | > 250 |
| Clarithromycin **1** | 0.32 ± 0.12 | > 250 |

### 2.4.3 Chemical Footprinting of *E. coli* 23S rRNA

Chemical footprinting of the *E. coli* 23S rRNA was performed with dimethyl sulfate (DMS) and 1-cyclohexyl-(2-morpholinoethyl)carbodiimide metho-p-toluenesulfonate (CMCT) according to the following protocol:

2.4.3.1 Probe binding

All probes and the synthetic precursor were incubated at a final concentration of 150 μM with 100 pmol *E. coli* 70S ribosomes (New England Biolabs), whereas clarithromycin was incubated at a concentration of 50 μM. Binding was performed in binding buffer (10 mM HEPES, 10 mM $MgCl_2$, 60mM $NH_4Cl$) at 37°C for 30 min.

2.4.3.2 DMS Chemical Modification

DMS chemical modification was performed on intact 70S *E. coli* ribosomes in the absence and presence of bound drug. Approximately 50 μg of intact ribosome, or ribosome-probe complex, in 25 μM DMS buffer (80 mM K-HEPES, 10 mM $MgCl_2$, 100 mM $NH_4Cl$) was aliquoted and to this was added 1 μL DMS Stock (880 mM DMS in abs. EtOH) and the mixture was then incubated for 10 min at 37°C. The reaction was terminated by the addition of 12.5 μL of DMS stop buffer (1 M Tris-HCl, 0.1 M EDTA, 1 M β-mercaptoethanol, pH7.5). Ethanol precipitation was followed by RNA extraction. The RNA pellet was resuspended in 400 μL extraction buffer (0.3 M NaOAc (pH 6.5), 0.5% SDS, 5 mM EDTA (pH 8.0)) at room temperature. This was subsequently extracted three times via addition of 400 μL of acid phenol chloroform (pH 4.5, Invitrogen). The final RNA fraction was ethanol precipitated and the pellet was resuspended in $H_2O$ (final concentration: 0.4 μM). Aliquots were stored at -80$^{o}$C.

2.4.3.3 CMCT Chemical Modification

CMCT chemical modification was performed on intact 70S *E. coli* ribosomes in the absence and presence of bound drug. Approximately 50 μg of intact ribosome, or

ribosome-probe complex, in 25 μM CMCT buffer (50 mM potassium borate pH 8.0, 10 mM $MgCl_2$, 100 mM $NH_4Cl$) was aliquoted and to this was added 12.5 μL CMCT Stock (100 mM CMCT in CMCT buffer) and the mixture was then incubated for 10 min at 37°C. The reaction was terminated by the addition of 2.5 volumes of -20°C 95% EtOH. Subsequent ethanol precipitation was followed by RNA extraction as described above.

2.4.3.4 Reverse Transcription

A list of primer sequences was generously provided by Dr. Alexander Mankin. DNA primers were purchased from Keck Biotechnology (New Haven, CT). An array of primers was initially purchased with the intent of covering as much of the 23S rRNA strand as possible. After footprinting analysis of all primers, the primer yielding the most useful data, named primer 2180, has the following sequence: 5`-GGGTGGTATTTCAAGGTCGG-3`. Primer 2180 is named as such because the 5` G of the primer anneals to position 2180 (*E. coli* numbering) of the 23S rRNA. Primer concentration was determined by UV-vis spectroscopy in 1 cm path length quartz cuvettes using molar extinction coefficients determined by OligoAnalyzer (IDT).

A working primer stock (2.0 μM) in $H_2O$ was made fresh for each reaction. A hybridization buffer (225 mM K-Hepes (pH 7.0), 450 mM KCl) was used to bring primer concentration to 1.0 μM. This primer mix (2 μL) was added to tubes containing RNA (0.8 μmol). Annealing proceeded by placing tubes in a water bath at 90$^{o}$C for 1 min, and allowed to cool to room temperature. While cooling, a master mix was prepared using 20 μL 5x First Strand Buffer (supplied with RT enzyme, Invitrogen), 150 μCi dATP$\alpha^{35}$S (PerkinElmer), 6.6 μL dNTP mix (110 μL 1mM d(T, G, C)TP, 6 μL 1 mM dATP, 664 μL $H_2O$), and 1 μL each of RNasin Plus (Promega) and 100 mM dithiothreitol (DTT).

Upon completion of annealing, samples were briefly centrifuged at room temperature. Each tube received 2 μL master mix and the sequencing tubes received the appropriate ddNTP (1 μL, 9 μM). Added last to each tube was 200U SuperScript II reverse transcripase (Invitrogen). Tubes were gently mixed and centrifuged before being placed in a heating block at 55$^{o}$C for 30 min. Chase was initiated by addition of 1 μL dNTP (100 mM) to each tube and 1 μL appropriate ddNTP (402 mM) to sequencing tubes. Tubes were placed back in the heating block at 55$^{o}$C for 15 min. The reaction was terminated by the addition of precipitation buffer (75 μL, 95% ethanol, 0.3 M NaOAc pH 6.5, 4$^{o}$C) and centrifuged for 90 min (13,200 rpm, 4$^{o}$C). The supernatant was removed and the pellets were dried and resuspended in 10 μL loading buffer (95% formamide, 10 mM EDTA, 0.1% xylene cyanol, 0.1% bromophenol blue, pH 11).

2.4.3.5 Analysis of Footprinting by Gel Electrophoresis

Samples were analyzed by running on a 5% polyacrylamide gel in a Sequi-Gen GT system (Bio Rad). The gel and 1x TBE buffer (100 mM Tris, 90 mM boric acid, and 1 mM EDTA) were brought to temperature by pre-running at 55 W to 50$^{o}$C. Lanes were thoroughly flushed with buffer and loaded with 1 μL of sample each. Migration occurred from 45 to 90 min at 55W and 50°C. Gels were transferred to Whatman paper and were fixed in 20% EtOH for 20 min. They were then dried under vacuum for 90 min at 80$^{o}$C. Once dry, gels were exposed onto a phosphor screen (GE Healthcare) overnight. Screens were scanned on a Typhoon Trio+ (GE Healthcare) and digital images were analyzed with Multi Gauge (FujiFilm).

### 2.4.4 Peptolide Cell-Free Assay Evaluation

The above translation inhibition data does not suggest that the mode of inhibition is the same as the unadorned ketolide parent. To elucidate the binding location, small

molecule probing was utilized. This probing was performed on the *E. coli* 23S rRNA of intact 70S. Dimethylsulfate (DMS) and N-cyclohexyl-N′-(2-morpholinoethyl)carbodiimide (CMCT) were employed as the nucleic acid modifying agents.[14,15] DMS footprinting gel in Figure 23 shows a clear peptolide footprint at the residue A2058 of the *E. coli* 23S rRNA. In lanes 5 and 6 are unmodified and DMS-modified rRNAs respectively in the absence of probes. Any differences between these lanes highlight residues that are available for DMS modification, ie solvent exposed adenines. Similarly, any differences between lane 6 and lanes 7-16, lanes containing rRNAs that are DMS-modified after drug or probe binding, will highlight sites of probe-dependent interactions either through protection or enhancement of alkylation by DMS. The reduction in intensity seen at nucleotide A2058 in the presence of each peptolide is clear evidence of a drug binding footprint. This is an expected site of drug interaction as A2058 is known to interact with the macrolide ring upon binding to the well-defined macrolide binding pocket of the ribosome.[16-19] This footprint confirms that the binding target of the macrocycle moieties of the peptolide probes is indeed the same as the parent ketolide drug.

For nearly all peptolides, the A2058 band is barely visible except for **14g**, the peptolide derived from the propyl-linked ketolide and the zwitterionic peptide **18**, which has a relatively more pronounced A2058 band (lane 15). The reduction seen in peptolide-induced protection from DMS modification at nucleotide A2058 by peptolide **14g**, in comparison to the other peptolides, suggests a decreased binding affinity of peptolide **14g**

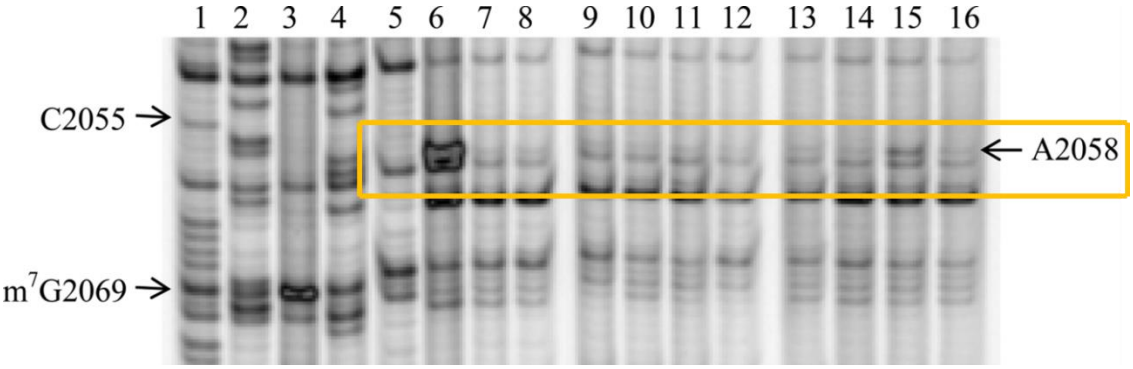


**Figure 23: DMS small molecule probing (A2058). DMS footprinting of the whole 70S *E. coli* ribosome. Primer regions contained within the 23S rRNA. Dideoxy sequencing lanes G, C, A and T (lanes 1-4) followed by unmodified rRNA (lane 5), DMS modified 23S rRNA (lane 6), DMS modified 23S rRNA in presence of clarithromycin and butyl azido ketolide intermediate (lanes 7-8, respectively), 23S rRNA DMS modified in the presence of 14a-h (lanes 9-16, respectively). (Work performed by Dr. Joshua Canzoneri)**

in the macrolide binding pocket. This decreased binding affinity corroborates the *E. coli* translation inhibition study which showed peptolide **14g** has the weakest translation inhibition activity ($IC_{50}$ value of 60 μM, Table 1). DMS probing of the other key residues within the large subunit did not reveal strong peptolide-induced protection (data not shown). Importantly, A752 is protected by TEL presumably due to the placement of the alkyl-aryl arm into this section of the tunnel.[20] However, A752 is not protected by any of the peptolides (Figure 24) indicating that the peptide moiety of the peptolides is not oriented toward the A752:U2609 base pair and projecting further down the exit tunnel. In light of this A752 data, we probed the PTC side of the exit tunnel scanning for additional interactions. In doing so, we observed a peptolide-dependent protection at

U1963 using CMCT. In looking at lanes 6-8 (Figure 25), there is no change in the amount of CMCT modification in

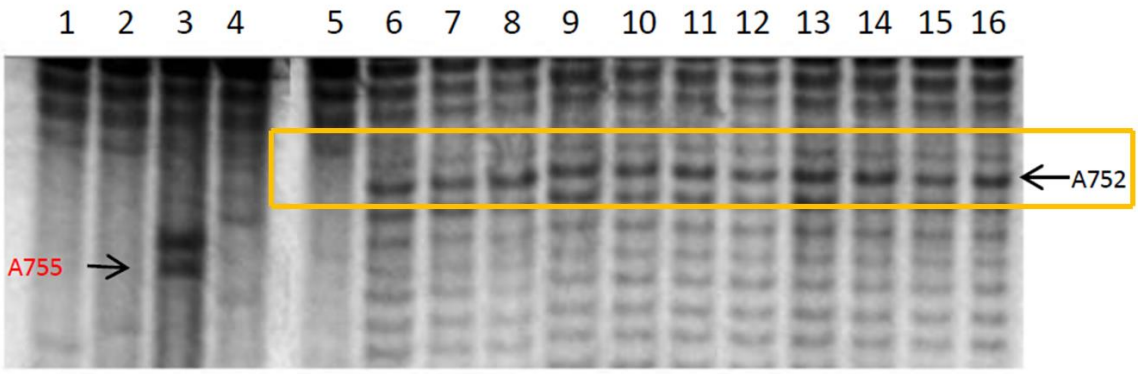


**Figure 24: DMS small molecule probing (A752). DMS footprinting of the whole 70S *E. coli* ribosome. Primer regions contained within the 23S rRNA. Dideoxy sequencing lanes G,C,A and T (lanes 1-4) followed by unmodified rRNA (lane 5), DMS modified 23S rRNA (lane 6), DMS modified 23S rRNA in presence of clarithromycin and butyl azido ketolide intermediate (lanes 7-8, respectively), 23S rRNA DMS modified in the presence of 14a-h (lanes 9-16, respectively).**

the presence or absence of macrolide binding. This tells us that the selective protection observed in lanes 9-16 are a result of the peptide portion. U1963 is part of Helix 71 (H71) located within domain IV of the 23S which forms part of the front rim of the peptidyl transferase active site cleft.[4] The CMCT protection seen here suggests that these peptolides all adopt a similar binding orientation such that their peptide moieties mimic the path a nascent peptide would travel extending from the PTC to the proximity of the entrance to the exit tunnel. Ribosomal rRNA U1963 is a crucial residue within the overlapping binding sites of RRF, EF-G, and the P-site tRNA[23] suggesting a plausible

mechanism of translation inhibition by inhibiting the binding of these critical translation components. Both the N- and C-linked peptolides **14a-d** cause indistinguishable

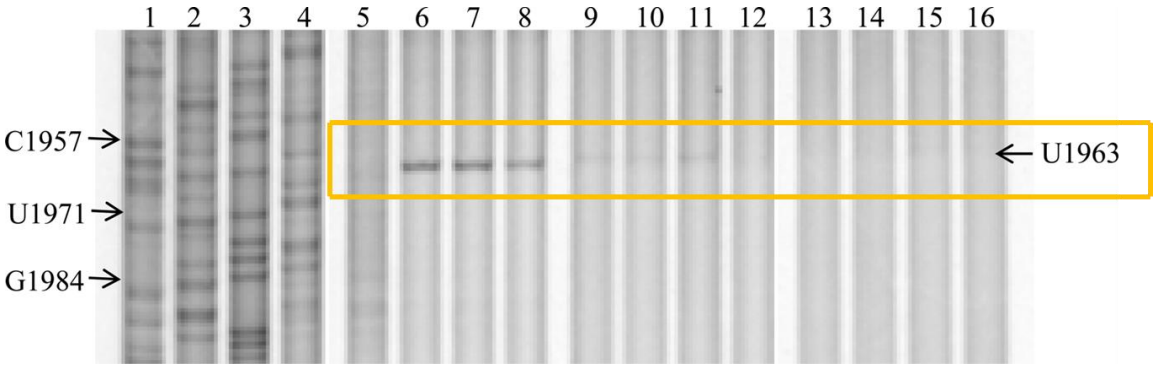


**Figure 25: CMCT small molecule probing (U1963). CMCT footprinting of the whole 70S *E. coli* ribosome. Primer regions contained within the 23S rRNA. Dideoxy sequencing lanes G,C,A and T (lanes 1-4) followed by unmodified rRNA (lane 5), CMCT modified 23S rRNA (lane 6), CMCT modified 23S rRNA in presence of clarithromycin and butyl azido ketolide intermediate (lanes 7 and 8, respectively), 23S rRNA CMCT modified in the presence of 14a-h (lanes 9-16, respectively).**

protection of U1963, indicating the tolerance of the exit tunnel for either the biological N → C or the abiological C → N orientation of nascent peptide.

### 2.4.5 Biochemical Validation Through Crystallography

In collaboration with Professor Christine Dunham of Emory University, we were able to crystalize peptolide **14c**, the propyl linker ketolide coupled with the reversed NLS sequence, to 3.6 Å. The 70S-peptolide **14c** structure shows the ketolide macrocyclic ring adopts a similar orientation within the 50S subunit as observed in previous structures.[16-18] Specifically, the desosamine sugar of the ketolide hydrogen bonds with the 23S rRNA

A2058 and the surface of this ring forms hydrophobic packing interactions with the bases of U2611, A2058, and A2059. These results show that the addition of the peptide tail does not alter the binding profile of our ketolide anchor when compared to that within other crystal structures.

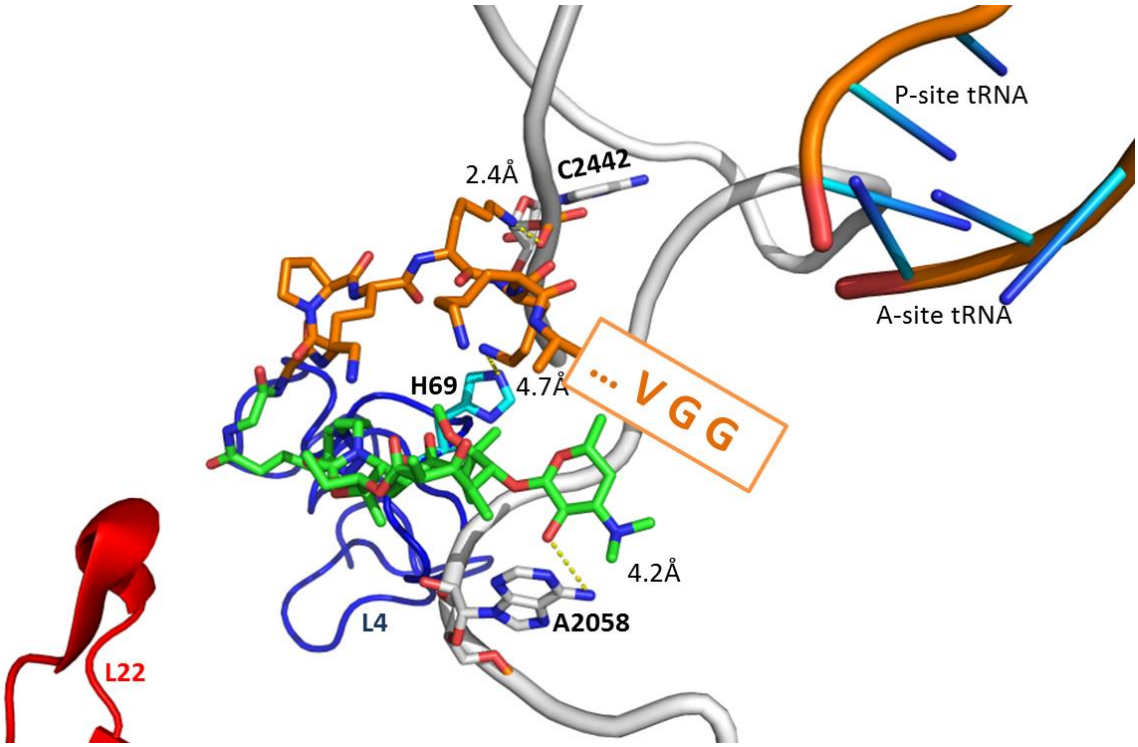


**Figure 26: Crystal Structure of peptolide 14c. Crystallographic evidence of peptolide binding and orientation. Hydrogen bonds highlighted by distance measurements. The disordered region is shown by the box filled with the missing residues. Lys9 is shown as Ala due to disorder. Crystal structure solved by Dr. Christine Dunham (Emory University).**

Continuing the investigation of the more complete binding profile, it was observed that the alkyl linker continues to travel down the tunnel, adopting an orientation akin to that observed of the alkyl aryl arm of telithromycin in *D. radiodurans*. However, the peptide portion seems to reverse direction and project back over the macrolactone

ring, potentially as a means of reorienting to the proper C term → N term alignment. This realignment is believed to be stabilized by two hydrogen bonds. The peptolide Lys6 hydrogen bonds to a phosphate oxygen of 23S rRNA C2442 while Lys7 hydrogen bonds with the side chain of His69 of ribosomal protein L4 (Figure 26). The peptide tail continues to adopt this orientation as it traverses the path back to the PTC, however the electron density of the peptolide tail is disordered beyond the seventh amino acid resulting in an inability to build the remainder of the tail.

Despite the region associated with the tail being disordered, there is still clarity about the 23S residues. As a result, an overlay of multiple *T. thermophilus* 50S ribosomal subunits provided an opportunity to see drug- or probe-dependent shifts within the region. PDB 3UXR was used as a "naked" ribosome to provide a natural state of 23S residues, PDB 3OI3 was used to view residue states as a result of telithromycin binding, and PDB 4W2B was used to view residue states with **14c** bound. We first analyzed any potential deviation in U1963 that may account for the footprint observed. The protection shown biochemically must have been the result of downstream effects since the distance was too far to be due to direct peptolide protection. By overlaying the three ribosomal structures and isolating residues of interest, we are afforded the opportunity to visualize the rationale for the biochemical data. In looking at U1963, we are able to see that the positioning within the naked or telithromycin-containing ribosomes is highly similar. More so, it is understandable why they show such a strong footprint seeing as how it is extremely solvent exposed. However, in the presence of our **14c** probe, we see that U1963 is clearly shifting out of its natural position (Figure 27). Toward exploring the cause for this structural change, we scanned the local region and identified a likely Watson-Crick interaction formed between U1963 and A1936 at a distance of 3.1 Å. The overlay of A1936 from all three PDBs does not show a significant shift when compared to the natural state (cyan, Figure 27) however we could find no deviation within the phosphate backbone surrounding either residue. With crystallographic data supporting

our footprinting, it is clear that a downstream effect is responsible for this migration of U1963 that allows it to adopt a favorable Watson-Crick interaction. Once engaged in this, CMCT modification would become disallowed. This shifting of U1963 and resulting Watson-Crick interaction is clearly visible in Figures 27 and 28.

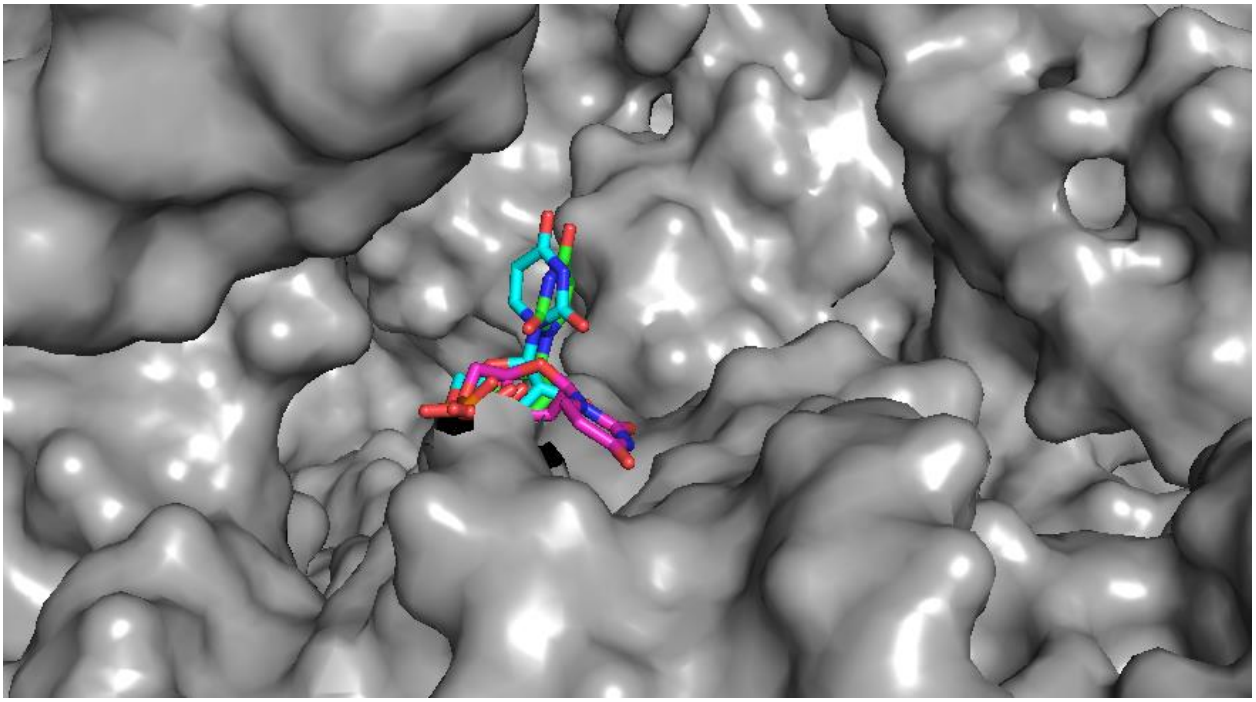

**Figure 27: U1963 movement. Space fill model showing region around U1963. Blue: PDB 3UXR[32], representing the natural state when no macrolide is bound. Green: 3OI3[7], representing the shifting of nucleotides as an effect of telithromycin binding. Magenta: 4W2B[5], representing the shifting of nucleotides in the presence of probe 14c.**

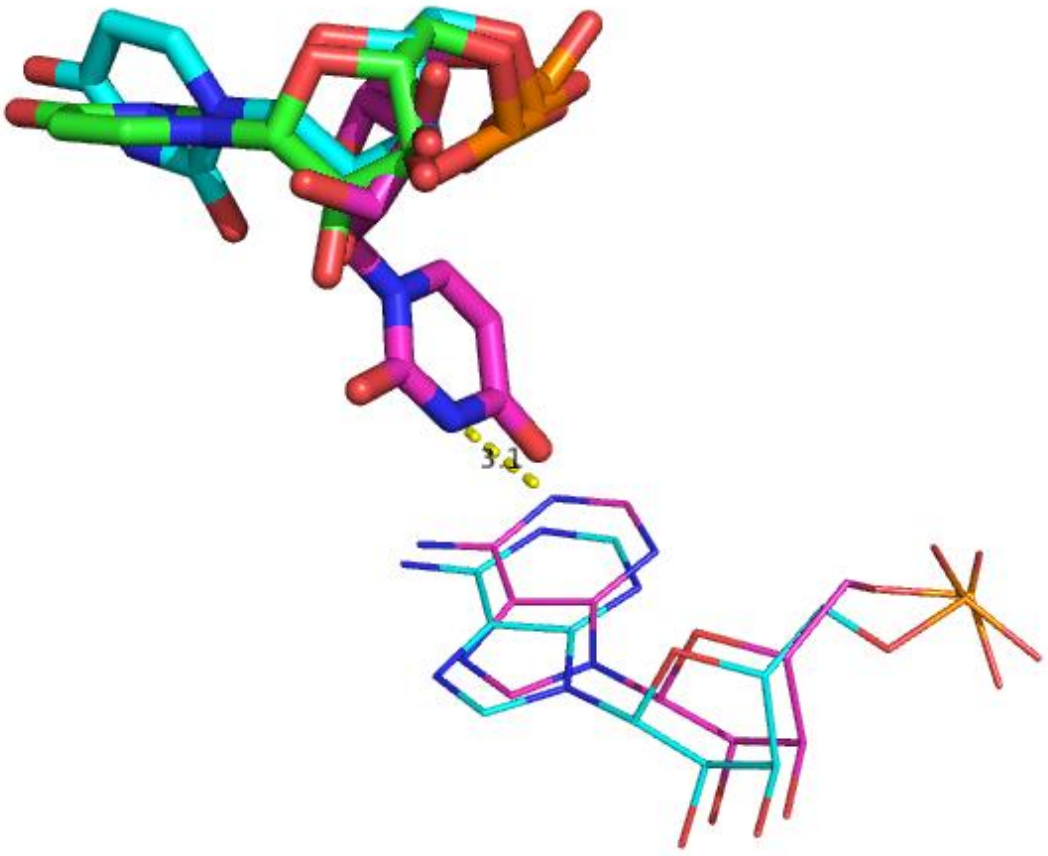


**Figure 28: U1963 Adopted Base Pair. Coloring is the same as in Figure 26. New base pair between U1963 and A1936 can be seen at a distance of 3.1 Å. No major movement shown in A1936, however U1963 realigns upon 14c binding to sequester and base pair.**

### 2.4.6 Further Analyses of Peptolide-Induced Conformational Changes within the Exit Tunnel

Encouraged by this overlay, we sought out other possible sites of interaction supported by crystallography but perhaps unobserved by footprinting. By starting at residues closest to the peptolide **14c** and moving outward, we identified three additional sites of shifted bases. The first, C790, becomes displaced upon probe binding (Figure 29). Expanding past this, we observed an additional interaction at U2506 where the residue seemingly projects inward toward the probe (Figure 30). This suggests an additional hydrogen bond previously not identified. Lastly, we observed a deviation of U2585 pitching inward, again toward the probe (Figure 31). These last two interactions involving U2506 and U2585 are very interesting as the portion of the probe responsible for the interaction is held within the disordered region. Collectively, these data show an extensive network of interactions spanning the region of the PTC to the macrolide binding site.

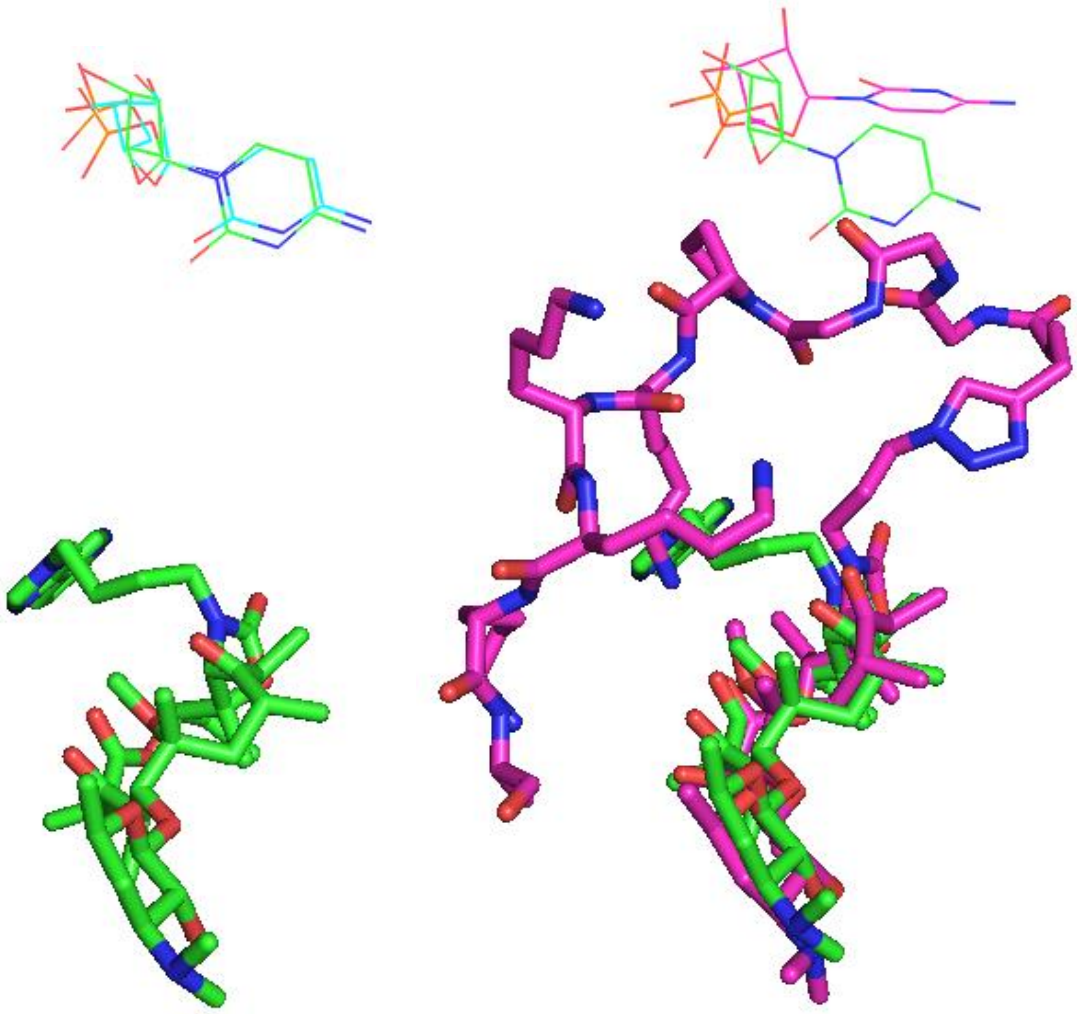

**Figure 29: C790 Migration. Coloring is the same as in Figure 26. C790 clearly is forced out of position through a steric interaction as a result of 14c probe binding.**

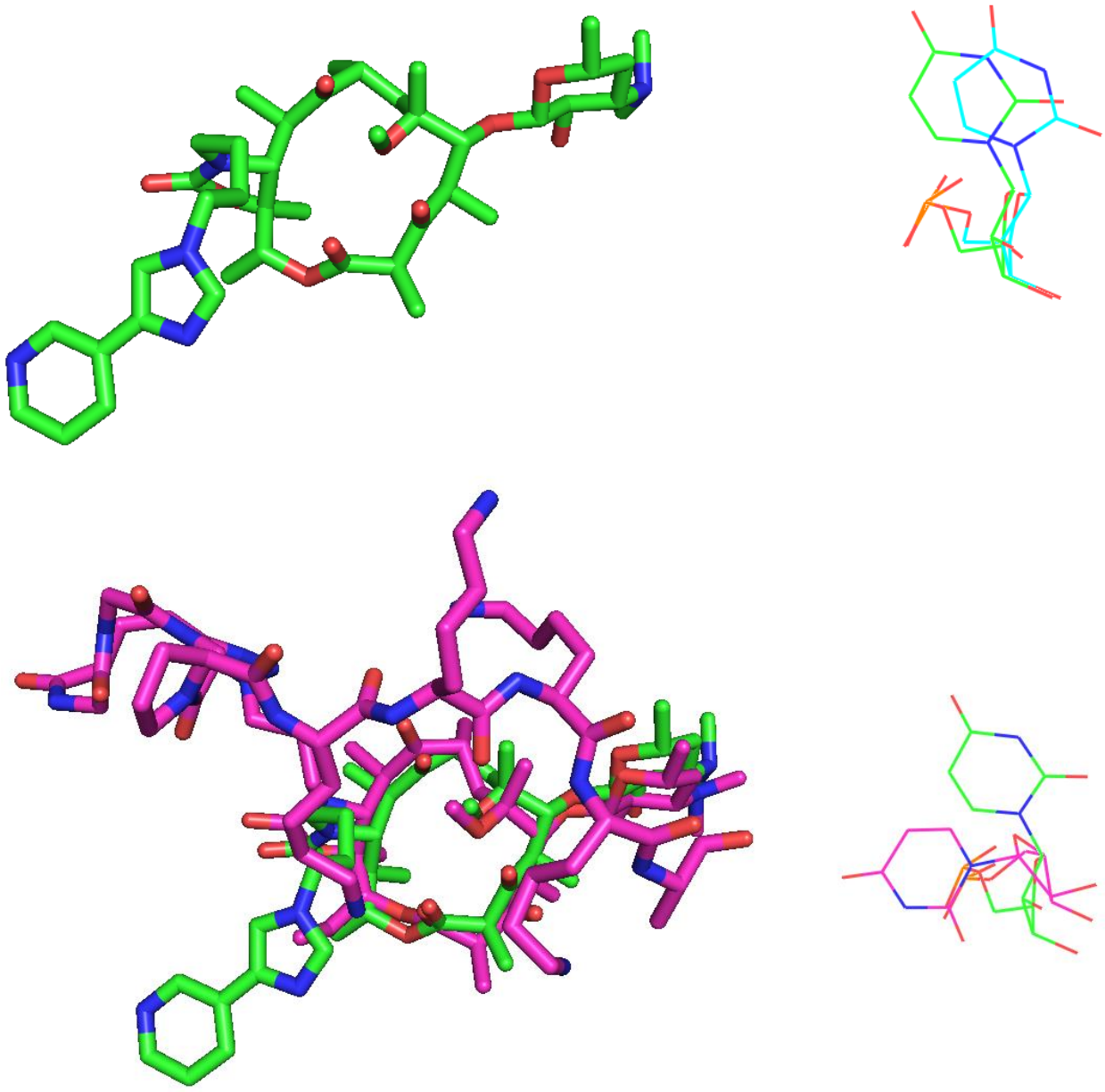

**Figure 30: U2506 Migration. Coloring is the same as in Figure 26. U2506 is shifting inward to engage in a suspected hydrogen bond with the peptide portion of 14c.**

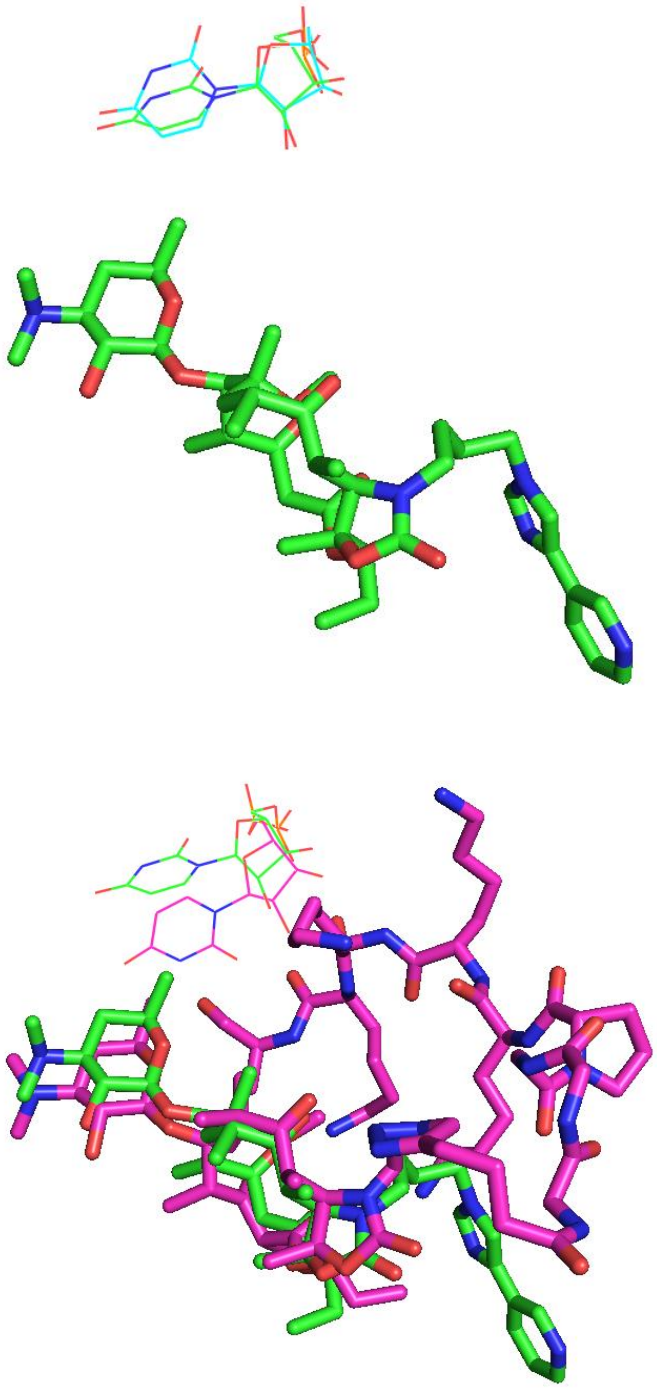

**Figure 31: U2585 Migration. Coloring is the same as in Figure 26. U2506 is shifting inward to engage in a suspected hydrogen bond with the peptide portion of 14c.**

## 2.5 Discussion

By progressing systematically through potential anchors starting with the PTC and moving down the exit tunnel, we have successfully developed a set of probes, proven not only to be a potent inhibitor of translation, but more importantly, capable of delivering a broad range of peptide sequences to a known location within the exit tunnel. These sequences were shown to not be travelling continually down the tunnel, but were in fact reversing orientation and aligning to the PTC regardless of the directionality engineered within the design. Further evidence of this reversed orientation was shown with additional footprinting data showing a probe dependent protection at U1963, a residue shown to be engaged in a new Watson-Crick interaction with A1936. X-ray crystallography corroborated these data. Crystal structure of **14c** bound to the 70S bacterial ribosome revealed that the macrolide ring of the peptolide binds in the same position as other macrolides while the peptide tail adopted an orientation which is an exact mimic of the orientation of the nascent peptide during elongation. Further analyses of this crystal structure revealed an extensive network of 23S nucleotides shifting out of normal alignment in response to the probe. These exit tunnel nucleotide conformation changes were still visible despite density mapping for the probe itself becoming too disordered to predict. This study marks the first time that a molecular probe of this nature not only was shown to bind successfully through rRNA footprinting as well as crystallography, but also establish a series of probe-dependent interactions within a discrete window of the exit tunnel. Improvements upon this design will focus on the probe's ability to project further down the exit tunnel to complement the probes which align back to the PTC as seen within this series.

## 2.6 References


1. Hicks, L., Bartoces, M. G., Roberts, R. M., Suda, K. J., Hunkler, R. J., Taylor, T. H. Jr. and Schrag, S. J. (2015) US outpatient antibiotic prescribing variation according to geography, patient population, and provider specialty in 2011. *Clinical Infect Dis, 60*, 1308-1316.
2. Eyai, Z., Matzov, D., Krupkin, M., Wekselman, I., Paukner, S., Zimmerman, E., Rozenberg, H., Bashan, A. and Yonath, A. (2015) Structural insights into species-specific features of the ribosome from the pathogen *Staphylococcus aureus*. *Proc Natl Acad Sci USA 112*, E5805-E5814.
3. Wilson, D. N., Schluenzen, F., Harms, J. H., Starosta, A. L., Connell, S. R. and Fucini, P. (2008) The ozazolidinone antibiotics perturb the ribosomal peptidyl-transferase center and effect tRNA positioning. *Proc Natl Acad Sci USA 105*, 13339-13344.
4. Numerous examples of Cu(I) catalyzed Huigsen cycloaddition reaction have appeared in the literature (a comprehensive list is available at www.scripps.edu/chem/sharpless/click.html). Cited here are three examples: (a) Rostovtsev, V.-V., Green, L.-G., Fokin, V.-V., Sharpless, K.-B. (2002) A stepwise huigsen cycloaddition process: copper (I)-catalyzed regioselective "ligation" of azides and terminal alkynes. *Angew Chem, Int Ed 41*, 2596–2599. (b) Tornoe, C.-W., Christensen, C., Meldal, M. (2002) Peptidotriazoles on solid phase: [1,2,3]- triazoles by regiospecific copper(I)-catalyzed 1,3-dipolar cycloadditions of terminal alkynes to azides. *J Org Chem 67*, 3057–3064. (c)

Kolb, H.-C., Finn, M.-G., Sharpless, K.-B. (2001) Click Chemistry: Diverse chemical function from a few good reactions. *Angew Chem, Int Ed*. *40*, 2004-2021.

5. Washington, A. Z., Benicewicz, D. B., Canzoneri, J. C., Fagan, C. E., Mwakwari, S. C., Maehigashi, T., Dunham, C. M. and Oyelere, A. K. (2014) Macrolide-peptide conjugates as probes of the path of travel of the nascent peptides through the ribosome. *ACS Chem Biol 9*, 2621-2631.
6. Merryman, C. & H. F. Noller. (1998). Footprinting and modification-interference analysis of binding sites on RNA, p. 237-253. In C. W. J. Smith (ed.), RNA:protein interactions, a practical approach. Oxford University Press, Oxford, United Kingdom.
7. Schluenzen, F., Tocilj, A., Zarivach, R., Harms, J., Gluehmann, M., Janell, D., Bashan, A., Bartels, H., Agmon. I., Franceschi, F., Yonath, A. (2000) Structure of functionally activated small ribosomal subunit at 3.3 angstroms resolution. *Cell.102*, 615-23.
8. Bulkley, D., Innis, C.-A., Blaha, G., Steitz, T.-A. (2010) Revisiting the structures of several antibiotics bound to the bacterial ribosome. *Proc Natl Acad Sci U S A. 107*, 17158-17163.
9. Berisio, R., Harms, J., Schluenzen, F., Zarivach, R., Hansen, H.-A., Fucini, P., Yonath, A. (2003) Structural insight into the antibiotic action of telithromycin against resistant mutants. *J Bacteriol 185*¸4276-4279.

10. Tu, D., Blaha, G., Moore, P.-B., Steitz, T.-A. (2005) Structures of MLSBK antibiotics bound to mutated large ribosomal subunits provide a structural explanation for resistance. *Cell 121*, 257-270.
11. Dunkle, J.-A., Xiong, L., Mankin, A.-S., Cate, J.-H. (2010) Structures of the Escherichia coli ribosome with antibiotics bound near the peptidyl transferase center explain spectra of drug action. *Proc Natl Acad Sci USA. 107*, 17152-17157.
12. Mwakwari, S.-C., Guerrant, W., Patil, V., Khan, S.-I., Tekwani, B.-L., Gurard-Levin, Z.-A., Mrksich, M., Oyelere, A.-K. (2010) Non-Peptide Macrocyclic Histone Deacetylase Inhibitors Derived from Tricyclic Ketolide Skeleton. *J Med Chem 53*, 6100-6111.
13. Oyelere, A.-K., Chen, P.-C., Guerrant, W., Mwakwari, S.-C., Hood, R., Zhang, Y., Fan, Y. (2009) Non-peptide macrocyclic histone deacetylase inhibitors. *J Med Chem 52*, 456–468.
14. Tijerina, P., Mohr, S., Russell, R. (2010) DMS footprinting of structured RNAs and RNA-protein complexes. *Nat Protoc 2*, 2608-23.
15. Shaw, L.-C., Lewin, A.-S. (1995) Protein-induced folding of a group I intron in cytochrome b pre-mRNA. *J Biol Chem*. *270*, 21552-62.
16. Bulkley, D., Innis, C.-A., Blaha, G., Steitz, T.-A. (2010) Revisiting the structures of several antibiotics bound to the bacterial ribosome. *Proc Natl Acad Sci U S A. 107*, 17158-17163.
17. Berisio, R., Harms, J., Schluenzen, F., Zarivach, R., Hansen, H.-A., Fucini, P., Yonath, A. (2003) Structural insight into the antibiotic action of telithromycin against resistant mutants. *J Bacteriol 185*¸4276-4279.

18. Tu, D., Blaha, G., Moore, P.-B., Steitz, T.-A. (2005) Structures of MLSBK antibiotics bound to mutated large ribosomal subunits provide a structural explanation for resistance. *Cell 121*, 257-270.
19. Dunkle, J.-A., Xiong, L., Mankin, A.-S., Cate, J.-H. (2010) Structures of the Escherichia coli ribosome with antibiotics bound near the peptidyl transferase center explain spectra of drug action. *Proc Natl Acad Sci USA. 107*, 17152-17157.
20. Xiong, L., Korkhin, Y., Mankin, A.-S. (2005) Binding site of the bridged macrolides in the *Escherichia coli* ribosome. *Antimicrob Agents Ch 49*, 281-288.
21. Ban, N., Nissen, P., Hansen, J., Moore, P.-B., Steitz, T.-A. (2000) The complete atomic structure of the large ribosomal subunit at 2.4 A resolution. *Science 289*, 905-920.
22. Bulkley, D., Johnson, F., Steitz, T.A. (2012) The antibiotic thermorubin inhibits protein synthesis by binding to intersubunit bridge b2a of the ribosome. *J Mol Biol 416*, 571-578.
23. Agrawal, R.-K., Sharma, M.-R., Kiel, M.-C., Hirokawa, G., Booth, T.-M., Spahn, C.-M.-T., Grassucci, R.-A., Kaji, A., Frank, J. (2004) Visualization of ribosome-recycling factor on the Escherichia coli 70S ribosome: Functional implications. *Proc Natl Acad Sci U S A 101*, 8900-8905.
24. The PyMOL Molecular Graphics System, Version 1.5.0.4 Schrödinger, LLC.

# CHAPTER 3 Design Approach Toward Peptolide Probes with Affinity for the L4/L22 Constriction Section to the Egress Point at the Back of the 50S Subunit

This work was published under the following reference:

Washington, A. Z., Tapadar, S., George, A. and Oyelere, A. K. (2015) Exploiting translational stalling peptides in an effort to extend azithromycin interactions within the prokaryotic ribosome nascent peptide exit tunnel. *Bioorg Med Chem 23,* 5198-5209.

Portions of the manuscript are presented here without modification.

## 3.1 Introduction

Efforts aimed at elucidating the nascent peptide-tunnel interaction have been hampered by a dearth of molecular probes. As discussed in Chapter 2, a class of oligopeptide telithromycin-like (peptolides) probes were capable of furnishing atomic level information about specific interactions between the ribosomal exit tunnel and models of nascent peptides.[1] However, these were all shown to interact between the peptidyl transferase center and the L4/L22 constriction section regardless of the inherent directionality incorporated into the peptide sequence. Both probes mimicking the biologically N term → C term and the reversed C term → N term, intended to self-align by reversing direction, were biochemically demonstrated to adopt an orientation pointing exclusively toward the PTC. Earlier studies with translation stalling peptide sequences, including SecM, ErmBL and TnaC, have provided evidence of direct interaction of the nascent peptide with the components of the exit tunnel.[2-4] Toward an alternative structure-guided optimization of macrolides, the X-ray structures of azithromycin bound to the ribosomes from various prokaryotes was analyzed[5,6] as well as the simulated

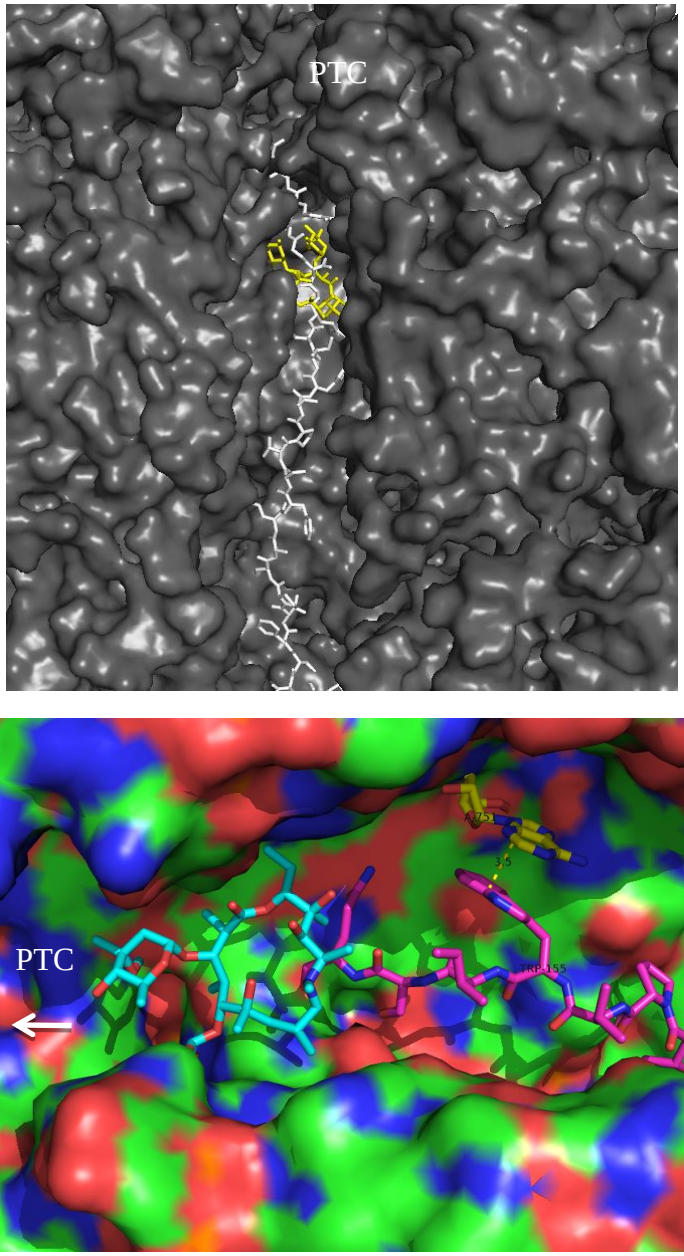


**Figure 32: SecM Design. PBD 3OI1[5] showing the overlay of ribosome-bound azithromycin and modeled SecM. *Top* Cross section of the exit tunnel. 50S shown in grey, SecM model in white, azithromycin in yellow. PTC is at the top of the image. *Bottom* View atop the exit tunnel where W155 and A751 are shown with 3.5 Å separation. Images generated using PyMOL.[9]**

structure of SecM bound to *E.coli* ribosome.[2] As discussed in Chapter 1.2.2 of this thesis, the minimum sequence of SecM required for ribosomal stalling has been identified as $^{150}$FXXXXWIXXXXGIRAGP$^{166}$, and mutational studies have shown that W155A led to the abolishment of translational stalling.[7,8] Simulations performed by Gumbart *et al.*[2] suggested that the stacking of W155 with A751 of the 23S rRNA is vital to stalling.[2,7,8] Our analyses of the X-ray structures of azithromycin bound to the ribosomes and the simulated structure of SecM suggested that the crucial SecM W155 residue could be incorporated into the azithromycin endocyclic amine (N-10, adopting the azithromycin ring numbering by Hansen *et al*)[5], possibly resulting in N-10 functionalized azithromycin analogs with enhanced affinity for the prokaryotic 50S ribosomal subunit. This rational designed was informed by an overlay of both SecM simulations and azithromycin crystal structures (Figure 32) showing the peptide backbone virtually passes right through the N-10 of azithromycin.

## 3.2 Azith-Trp Conjugate Design and Synthesis

To confirm this deduction, we designed a series of azithromycin analogs modified at the N-10 with indoles. These compounds were designed such that their indole moiety will mimic the 23S A751/SecM W155 stacking. Beginning with commercially available azathromycin, we synthesized two distinct alkynl azithromycin intermediates (synthesis performed by Dr. Subhasish Tapadar). We chose these two distinct moieties – alkyl and alkyl aryl – as linkers to connect the indole analogs to the azithromycin ring. The alkyl linker is flexible and was inspired by a similar group in the ketolide antibiotic telithromycin. In contrast, the alkyl aryl group is more rigid and was designed to test the effect of such constraint on compound ribosome binding affinity. Additionally, the substitutions on the indole ring were chosen to test the reliance of the interaction of the compounds with the ribosome on the A751/W155 $\pi$ stacking. The requisite azithromycin-indole derivatives were obtained via copper (I) catalyzed azide-alkyne cycloaddition.[14] Expanding upon the observation of the previous peptolide class, the incorporation of this selective interaction moiety into N-10 modified, azithromycin-derived peptolides will furnish a new class of probes which are expected to bind the exit tunnel within the L4/L22 constriction section to the egress point at the back of the 50S subunit. We showed that derivatization of the N-10 endocyclic amine of azithromycin with moieties which mimicked the SecM W155 side-chain resulted in a sub-set of analogs with enhanced translation inhibition activities against *E.coli* ribosome.

### *3.3* *In Vitro* Translation Inhibition Assay

To characterize the effects of azithromycin N-10 functionalization on ribosome function, we analyzed the ability of the all the synthesized compounds to inhibit prokaryotic and eukaryotic translation. The prokaryotic ribosome functional assay we used is based on the whole cell extract from *E. coli*, while the eukaryotic assay is derived from rabbit reticulocyte lysate (RRL) extract. Both assays utilize a luciferase based reporter, which measures the amount of luciferase protein produced, to indirectly quantify ribosome function.[11,12] We determined the $IC_{50}$s for all the target compounds in addition to that of azithromycin which we used as a positive (Table 2).

We observed that all N-10 functionalized azithromycin compounds retained the prokaryotic translation inhibition preference of the parent azithromycin skeleton as none inhibits eukaryotic ribosome function up to the maximum tested concentration of 250 μM (Table 2). All compounds potently inhibit the prokaryotic ribosome function with a sub-set having enhanced translation inhibition activities relative to the azithromycin positive control. For the alkyl-linked series, the attachment of the indole moiety through the C-3 (compound **19a**) weakens translation inhibition activity by 2-fold relative to azithromycin. Chloro- and fluoro-substitution at C-5 (compound **20a** and **21a** respectively) further weakens activity with fluorination resulting in the weakest activity (9-fold less than azithromycin). Interestingly, N-1 methylation of the unsubstituted indole ring (compound **22a**) restores translation inhibition to a level slightly better than azithromycin. Connection of the indole to the azithromycin ring through the N-1 position further enhanced translation inhibition as the resulting compound **23a** is 2.3-fold more potent then azithromycin. Although the subsequent C-5 halogenation compromised

**Table 2: $IC_{50}$ and $MIC_{50}$ data for compounds 19a-28a and 19b-28b. All indole modifications studied are as shown. S30 = *E. coli* cell free; RRL = rabbit reticulocyte cell free. SA29213 = *S. sureus* ATCC 29213 (with serum as indicated). Enhancement is calculated as the ratio of $MIC_{50}$ without serum over that with serum. ErmMRSA33591 = $Erm^+$ MRSA ATCC 33591. EC27856 = *E. coli* ATCC 27856. nt = not tested.**

| | | Cmpd ID | | $IC_{50}$ (μM) | | $MIC_{50}$ (μg/mL) | | | | |
|---|---|---|---|---|---|---|---|---|---|---|
| | | | R= | S30 | RRL | SA29213 | SA29213 w/ serum | Enhancement | ErmMRSA33591 | EC27856 |
| 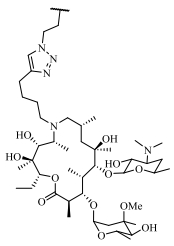 |  | **19a** | H | 0.540 ± 0.056 | >250 | 0.78 | 0.078 | 10 | NI | 16 |
| | | **20a** | Cl | 0.88 ± 0.020 | >250 | 0.78 | 0.16 | 5 | NI | 32 |
| | | **21a** | F | 2.6 ± 0.29 | >250 | 0.78 | 0.16 | 5 | NI | 32 |
| |  | **22a** | | 0.227 ± 0.048 | >250 | 1.56 | 0.16 | 10 | NI | 128 |
| | | **23a** | H | 0.128 ± 0.032 | >250 | 1.56 | 0.16 | 10 | NI | 64 |
| | | **24a** | Cl | 0.490 ± 0.070 | >250 | 0.78 | 0.16 | 5 | NI | 64 |
| |  | **25a** | F | 0.646 ± 0.27 | >250 | 1.56 | 0.31 | 5 | NI | 16 |
| | | **26a** | $NO_2$ | 0.811 ± 0.24 | >250 | 1.56 | 0.63 | 2.5 | NI | 16 |
| | | **27a** | OMe | 0.238 ± 0.046 | >250 | 1.56 | 0.16 | 10 | NI | 16 |
| |  | **28a** | | 0.147 ± 0.013 | >250 | 1.56 | 0.16 | 10 | NI | 4 |
| 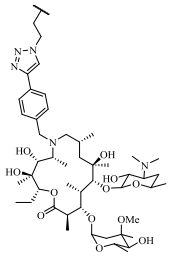 |  | **19b** | H | 0.12 ± 0.11 | >250 | 3.13 | 1.56 | 2 | NI | NI |
| | | **20b** | Cl | 0.586 ± 0.065 | >250 | 1.56 | 1.56 | 1 | NI | NI |
| | | **21b** | F | 2.03 ± 0.29 | >250 | 3.13 | 1.56 | 2 | NI | NI |
| |  | **22b** | | 0.641 ± 0.19 | >250 | 6.25 | 1.56 | 4 | NI | 128 |
| | | **23b** | H | 0.197 ± 0.026 | >250 | 1.56 | 0.63 | 2.5 | NI | 64 |
| | | **24b** | Cl | 1.25 ± 0.41 | >250 | 3.13 | 1.56 | 2 | NI | NI |
| |  | **25b** | F | 0.463 ± 0.16 | >250 | 1.56 | 0.78 | 2 | NI | 64 |
| | | **26b** | $NO_2$ | 0.442 ± 0.16 | >250 | 1.56 | 0.39 | 4 | NI | 128 |
| | | **27b** | OMe | 0.504 ± 0.0051 | >250 | 1.56 | 0.78 | 2 | NI | NI |
| |  | **28b** | | 0.555 ± 0.045 | >250 | 1.56 | 0.78 | 2 | NI | 64 |
| 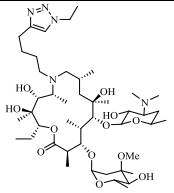 | | **29** | | 1.22 ± 0.063 | >250 | 3.13 | 0.31 | 10 | NI | 32 |
| **Azithromycin** | | | | 0.292 ± 0.12 | >250 | 0.78 | 0.13 | 6 | NI | 4 |
| **Chloramphenicol** | | | | nt | nt | nt | nt | | nt | 4 |
| **Vancomycin** | | | | nt | nt | 1.56 | 1.56 | 1 | 4 | nt |

translation inhibition, fluorination at this position did not result in a glaring deleterious effect on potency as seen in the C-3 linked series (Table 2, comparing **20a**/**21a** with **24a**/**25a**). Introduction of nitro group into the C-5 position further weakens compound potency while methoxy group in the same position is less deleterious but the resulting compound **27a** is about 2-fold less active than the unsubstituted compound **23a**. Reduction of the indole group to indoline has only a modest effect on compound translation inhibition activity (Table 2, comparing **23a** and **28a**). Compound **29**, alkyl-linked analog lacking the indole moiety, is about 2- to 10-fold weaker translation inhibitor than the unsubstituted C-3 and N-1 compounds **19a** and **23a** respectively. This data is suggestive of the essential role the interaction of the indole group with the ribosome components, possibly A751, plays in the potency of these N-10 functionalized azithromycin compounds.

The trend of translation inhibition activities among the more rigid alkylaryl-linked compounds **19b**-**28b** is somewhat different from the trend within the flexible alkyl-linked compounds **19a**-**28a**. Specifically, the alkylaryl-linked compounds are more tolerant of the points of linkage of the indole to the azithromycin as the translation inhibition activities of the C-3 and N-1 linked compounds **19b** and **23b** are virtually indistinguishable. Similar to the alkyl-linked compounds, halogenation at C-5 proved not to be beneficial. Nevertheless, we noticed an interesting switch of preference for either fluoro or chloro-substitution within the N-1 and C-3 linked compounds (Table 2, comparing **20b**/**21b** vs **24b**/**25b**). In contrast to what we observed in the alkyl-linked compounds, N-1 methylation of the unsubstituted indole ring worsens translation inhibition by more than 5-fold (Table 2, comparing **19b** and **22b**). Introduction of nitro (**26b**) or methoxy (**27b**) group into the C-5 position of the N-1 linked analogs has no added benefit to potency while reduction of the indole group to indoline surprisingly

weakens compound potency by about 3-fold (Table 2, comparing **23b** and **28b**). Collectively, this translation inhibition study revealed that N-1 linked compounds **23a** and **28a**, C-3 linked compounds **19b** and **23b** are more potent prokaryotic translation inhibitors than azithromycin.

## 3.4 Antibacterial Activity

### 3.4.1 Protocol

Minimum inhibitory concentrations ($MIC_{50}$) of all compounds was determined using liquid microdilution methods.[13] Briefly, *E. coli* (ATCC 27856, LB liquid medium), *S. aureus* (ATCC 29213, TSB broth), and methicillin-resistant *S. aureus* (ATCC 33591, Nutrient broth) were grown overnight at 37 $^{o}$C. These cultures were diluted 1:1000 with their respective growth media prior to plating onto TPP 96-well tissue culture plates (Sigma, TPP 92096). Positive controls were as follows: chloramphenicol for *E.* coli, whereas azithromycin and vancomycin for *S. aureus* and MRSA, respectively. Cell growth was determined by a comparison of OD600 values using a Molecular Devices SpectraMax M2 both before and after incubation (18 hrs, 37 $^{o}$C). All compounds were done in triplicate and standardized against an internal vehicle control.

Bovine serum (Life Technologies, 16170-086) trials with *S. aureus* ATCC 29213 were prepared and analyzed in a similar manner with the only variation being that the 1:1000 dilution was done with 50% of serum and broth.

### 3.4.2 Antibacterial Activity Results

To test if these N-10 functionalized azithromycin compounds possess bacterial growth inhibition activity, we challenged them with a wild type, macrolide susceptible *S. aureus* (ATCC 29213), macrolide resistant *S. aureus* (ErmMRSA, ATCC 33591) and gram negative (*E. coli*, EC 27856) bacterial strains. Against *E. coli*, most of these N-10 functionalized compounds are weakly active with only **28a** performing at a comparative level as azithromycin. Against macrolide susceptible *S. aureus*, we observed that despite their enhanced cell-free activities, compounds **19b, 23a, 23b** and **28a** are no better than azithromycin (Table 2). This discrepancy may be due to impairment of cell penetration of

the N-10 functionalized compounds. However, the compounds within the alkyl-linked series (**19a-28a**) are slightly more potent than their alkylaryl-linked counterparts (**19b-28b**). Relative to **29**, the antibacterial activity of compounds **19a** and **23a** is about 2-fold enhanced, further supporting the role of the indole moiety in the interaction of these azithromycin analogs with the ribosome.

Interestingly, inclusion of 50% bovine serum into the culture media resulted in moderate (**24b, 25b**) to 10-fold (**19a, 22a, 27a, 28a**) enhancement of the antibacterial activities of these N-10 functionalized azithromycin compounds. In comparison, azithromycin displayed a 6-fold potency enhancement in 50% bovine serum media. A similar serum-induced potency enhancement has been observed with azithromycin and other macrolides. This has been shown to be immune response independent, however pH and cell wall morphology disruption could play a role.[10] Neither azithromycin nor any of these N-10 modified compounds are active against *S. aureus* with constitutively active *ermA* ($Erm^{+}$MRSA, ATCC33591), a macrolide resistant mechanism which targets the desosamine sugar common to this class of macrolides.

## 3.5 Discussion

The ribosomal peptide exit tunnel is an inviting site for drug design. We have disclosed a set of functionalized azithromycin analogs incorporating an indole moiety at the N-10 position of the macrolactone ring. The indole moiety of these compounds is designed to mimic the translation stalling π-stack interaction of SecM W155 side-chain with the prokaryotic ribosome A751 residue. Our data revealed that many of these N-10 functionalized compounds have enhanced translation inhibition activities against *E.coli* ribosome relative to azithromycin, possibly due to proper presentation of the indole moiety for stacking interaction with A751. However, despite their enhanced cell-free activities, a subset of these compounds inhibited the growth of representative susceptible bacteria strains to about the same extent as azithromycin. Additionally, none of these compounds was able to overcome *ermA*-mediated macrolide resistance. This suggests that the extra indole-A751 π-stacking isn't sufficient to overcome resistance. While they were unable to overcome this resistance, the indole-A751 π-stacking could pre-set the orientations of peptolides bearing this moiety such that they bind the exit tunnel within the L4/L22 constriction section to the egress point at the back of the 50S subunit.

## 3.6 References


1. Washington, A. Z.; Benicewicz, D. B.; Canzoneri, J. C.; Fagan, C. F.; Mwakwari, S. C.; Maehigashi, T.; Dunham, C. M.; Oyelere, A. K. (2014) Macrolide-peptide conjugates as probes of the path of travel of the nascent peptides through the ribosome. *ACS Chem Biol 9*, 2621-2631.
2. Gumbart, J.; Schreiner, E.; Wilson, D. N.; Beckmann, R.; Schulten, K. (2012) Mechanisms of SecM-mediated stalling in the ribosome. *Biophys J 103*, 331-341.
3. Seidelt, B.; Innis, C. A.; Wilson, D. N.; Gartmann, M.; Armache, J.-P.; Villa, E.; Trabuco, L. G.; Becker, T.; Mielke, T.; Schulten, K.; Steitz, T. A.; Beckmann, R. (2009) Structural insight into nascent polypeptide chain-mediated translational stalling. *Science 326*, 1412-1415.
4. Arenz, S.; Ramu, H.; Gupta, P.; Berninghausen, O.; Beckmann, R.; Vasquez-Laslop, N.; Mankin, A. S.; Wilson, D. N. (2014) Molecular basis for erythromycin-dependent ribosome stalling during translation of the ErmBL leader peptide. *Nature Comm 5*, 3501, DOI 10.138/ncomms4501
5. Hansen, J. F.; Ippolito, J. A.; Ban, N.; Nissen, P.; Moore, P. B.; Steitz, T. A. (2002) The structures of four macrolide antibiotics bound to the large ribosomal subunit. *Mol Cell 10*, 117-128.
6. Bulkley, D.; Innis, C.A.; Blaha, G.; Steitz, T.A. (2010) Revisiting the structures of several antibiotics bound to the bacterial ribosome. *Proc Natl Acad USA 107*, 17158-17163.
7. Nakatogawa, H.; Ito, K. (2002) The ribosomal exit tunnel functions as a discriminating gate. *Cell 108*, 629-636.

8. Muto, H.; Nakatogawa, H.; Ito, K. (2006) Genetically encoded but nonpolypeptide prolyl-tRNA functions in the A Site for SecM-mediated ribosomal stalling. *Mol Cell22*, 545-552.
9. *The PyMOL Molecular Graphics System*, Ver. 1.5.0.4 Schrödinger, LLC: New York.
10. Pruul, H.; McDonald, P. J. (1992) Potentiation of antibacterial activity of azithromycin and other macrolides by normal human serum. *Antimicrob Agents Ch 36, 10-16.*
11. Pratt, S. D.; David, C. A.; Black-Schaefer, C.; Dandliker, P. J.; Xuei, X.; Warrior, U.; Burns, D. J.; Zhong, P.; Cao, Z.; Saiki, A. Y.; Lerner, C. G.; Chovan, L. E.; Soni, N.B.; Nilius, A. M.; Wagenaar, F. L.; Merta, P. J.; Traphagen, L. M.; Beutel, B. A. (2004) A strategy for discovery of novel broad-spectrum antibacterials using a high-throughput Streptococcus pneumoniae transcription/translation screen. *J Biomol Screen 9*, 3-11.
12. Thorne, C. A.; Lafleur, B.; Lewis, M.; Hanson, A. J.; Jernigan, K. K.; Weaver, D. C.; Huppert, K. A.; Chen, T. W.; Wichaidit, C.; Cselenyi, C. S.; Tahinci, E.; Meyers, K. C.; Waskow, E.; Orton, D.; Salic, A.; Lee, L. A.; Robbins, D. J.; Huppert, S. S.; Lee, E. (2011) A biochemical screen for identification of small-molecule regulators of the Wnt pathway using Xenopus egg extracts. *J Biomol Scr 16*, 995-1006.
13. LeTourneau, N.; Vimal, P.; Klepacki, D.; Mankin, A. S.; Melman, A. (2012) Synthesis and antibacterial activity of desosamine-modified macrolide derivatives. *Bioorgan Med Chem Lett 22*, 4575-4578.

14. Numerous examples of Cu(I) catalyzed Huigsen cycloaddition reaction have appeared in the literature (a comprehensive list is available at www.scripps.edu/chem/sharpless/click.html). Cited here are three examples: (a) Rostovtsev, V.-V., Green, L.-G., Fokin, V.-V., Sharpless, K.-B. (2002) A stepwise huigsen cycloaddition process: copper (I)-catalyzed regioselective "ligation" of azides and terminal alkynes. *Angew Chem, Int Ed 41*, 2596–2599. (b) Tornoe, C.-W., Christensen, C., Meldal, M. (2002) Peptidotriazoles on solid phase: [1,2,3]- triazoles by regiospecific copper(I)-catalyzed 1,3-dipolar cycloadditions of terminal alkynes to azides. *J Org Chem 67*, 3057–3064. (c) Kolb, H.-C., Finn, M.-G., Sharpless, K.-B. (2001) Click Chemistry: Diverse chemical function from a few good reactions. *Angew Chem, Int Ed 40*, 2004-2021.

# CHAPTER 4 Redesign of Conjugate Probes to Improve Cell Membrane Activity

## 4.1 Introduction

While working to incorporate a means of directing a peptide probe through the A751-W155 pi stack discussed within Chapter 3 of this document, an interesting question came about. Should the pi stack interaction be successfully engaged, would this added interaction provide enough stability to counteract the lost interaction brought about by *erm* methylation? While evaluation of whole cell viability of probes **19**-**28** showed that none within the series were active against a cell line with this resistance, we could not discount the possibility of other resistance phenotypes contributing to the loss of activity. This observation served as a start for a larger evaluation of how our full array of conjugate probes performs against whole cells. The telithromycin and azithromycin series certainly showed potent cell-free translation inhibition activity with the overall best in the respective series showing activity as good as, if not better, than the parent compounds. With the successful inhibition of whole cell growth in a quality control *S. aureus* line (ATCC 29213) by the azithromycin-tryptophan conjugates, we decided to revisit a more broad range of probes within various anchor classes to investigate their performance as inhibitors of cell growth.

## 4.2 Whole Cell Activity of Linezolid-Inspired Anchors

The linezolid probes discussed within Chapter 2.3 were challenged in the same quality control *S. aureus* (ATCC 29213) used in Chapter 3. All within this series displayed no inhibition up to a maximum tested dose of 64 µg/mL (Figure 33) even though the parent linezolid, trade name Zyvox, displayed activity within the Clinical and Laboratory Standards Institute (CLSI) accepted experimental range. As a result of no activity within the QC line, they were not carried through to the methicillin resistant *S. aureus* (MRSA, ATCC 33591) cell line.

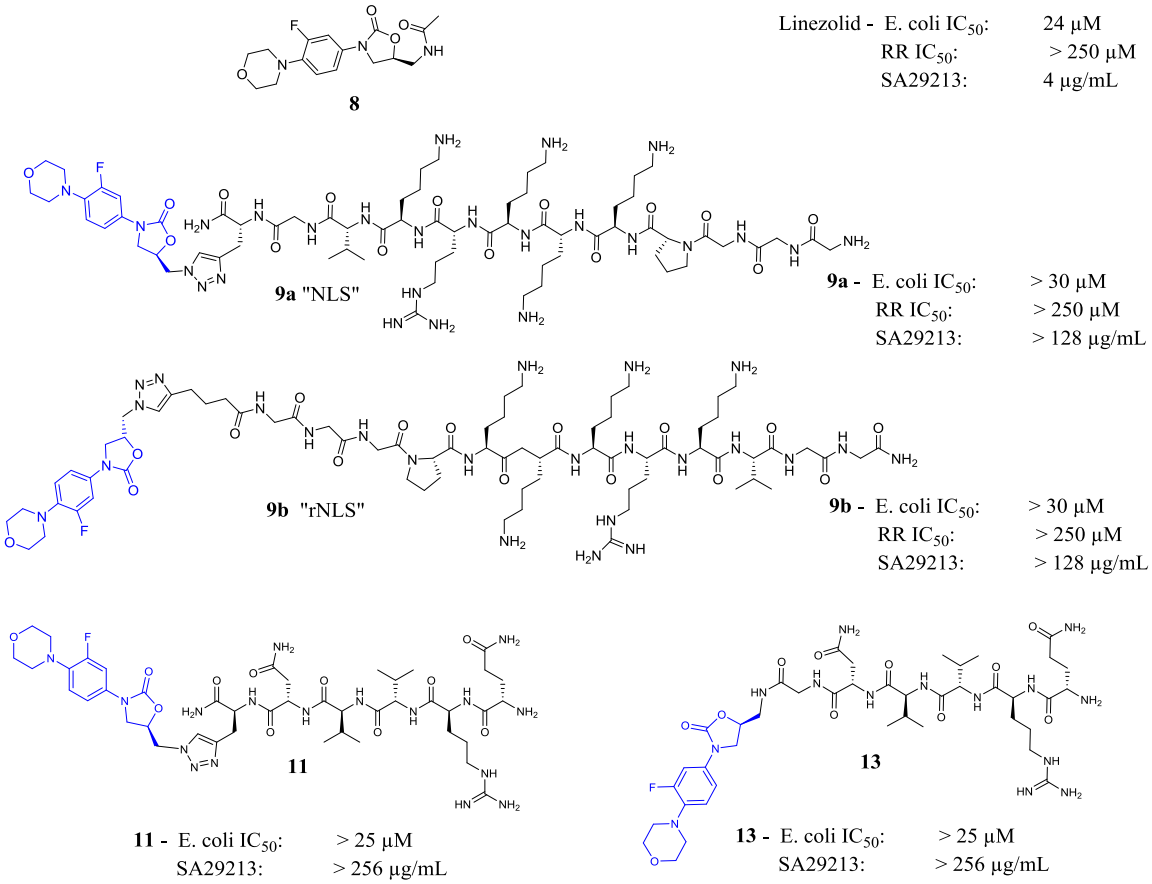


**Figure 33: Structures and $MIC_{50}$s of linezolid-inspired conjugates. Values determined in *S. aureus* QC cell line (ATCC 29213).**

## 4.3 Whole Cell Activity of Azithromycin-Inspired Anchors

Concurrent with the synthesis of the azithromycin-tryptophan conjugates, azithromycin-peptide probes were developed and synthesized. The rational design was borne of the same thinking as the tryptophan series: modification about azithromycin's N10 of the macrolactone would project the probe of interest more exclusively down the tunnel by restricting the opportunity to align back toward the PTC. These conjugates (synthesized by Dr. Subhasish Tapadar) contained a peptide sequence very similar to the central aromatic core of peptolides **12e/f**. While these all possessed rather potent cell-free translation inhibition, none within the series displayed any whole cell inhibition activity (Figure 34).

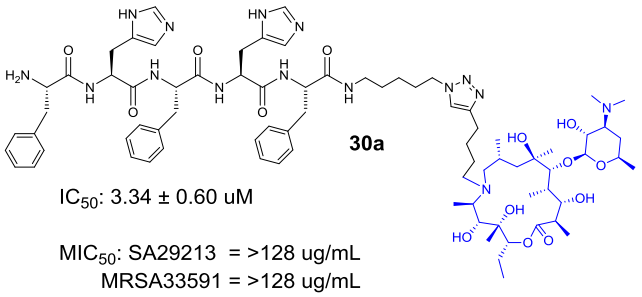

**30a**

$IC_{50}$: 3.34 ± 0.60 uM

$MIC_{50}$: SA29213 = >128 ug/mL
MRSA33591 = >128 ug/mL

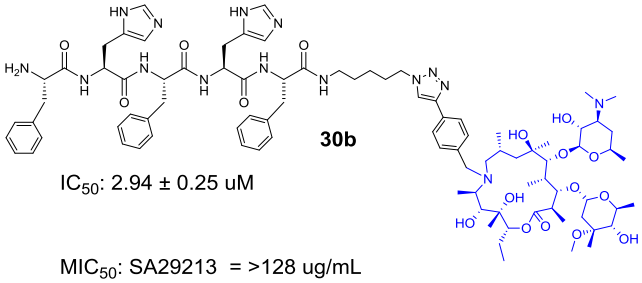

**30b**

$IC_{50}$: 2.94 ± 0.25 uM

$MIC_{50}$: SA29213 = >128 ug/mL
MRSA33591 = >128 ug/mL

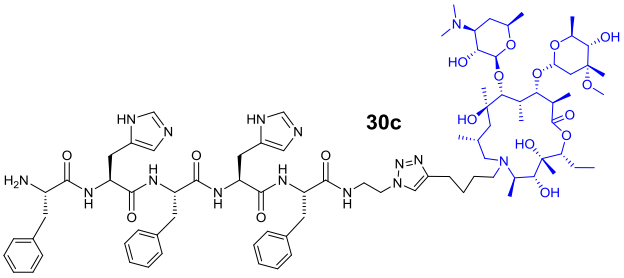

**30c**

$IC_{50}$: 0.587 ± 0.25 uM

$MIC_{50}$: SA29213 = >128 ug/mL
MRSA33591 = >128 ug/mL

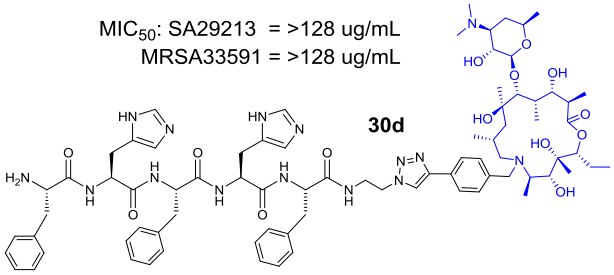

**30d**

$IC_{50}$: 11.84 ± 2.15 uM

$MIC_{50}$: SA29213 = >128 ug/mL
MRSA33591 = >128 ug/mL

**Figure 34: Structures and $MIC_{50}$s of azithromycin-inspired conjugates. Values determined in *S. aureus* QC cell line (ATCC 29213) and MRSA resistance strain (ATCC 33591).**

### 4.4 Whole Cell Activity of Telithromycin-Inspired Anchors

The original peptolide series, as described in Chapter 2.4, was also analyzed for whole cell activity. It had also expanded to include additional peptide sequences, all containing the butyl linker. This linker, as opposed to the propyl linker also used, is more directly comparable to the telithromycin parent as well as showing consistently better translation inhibition in a cell-free system. This newest subset of conjugates, while even showing improved activity over telithromycin in cell-free trials, displayed no activity against *S. aureus* 29213 (Figure 35)

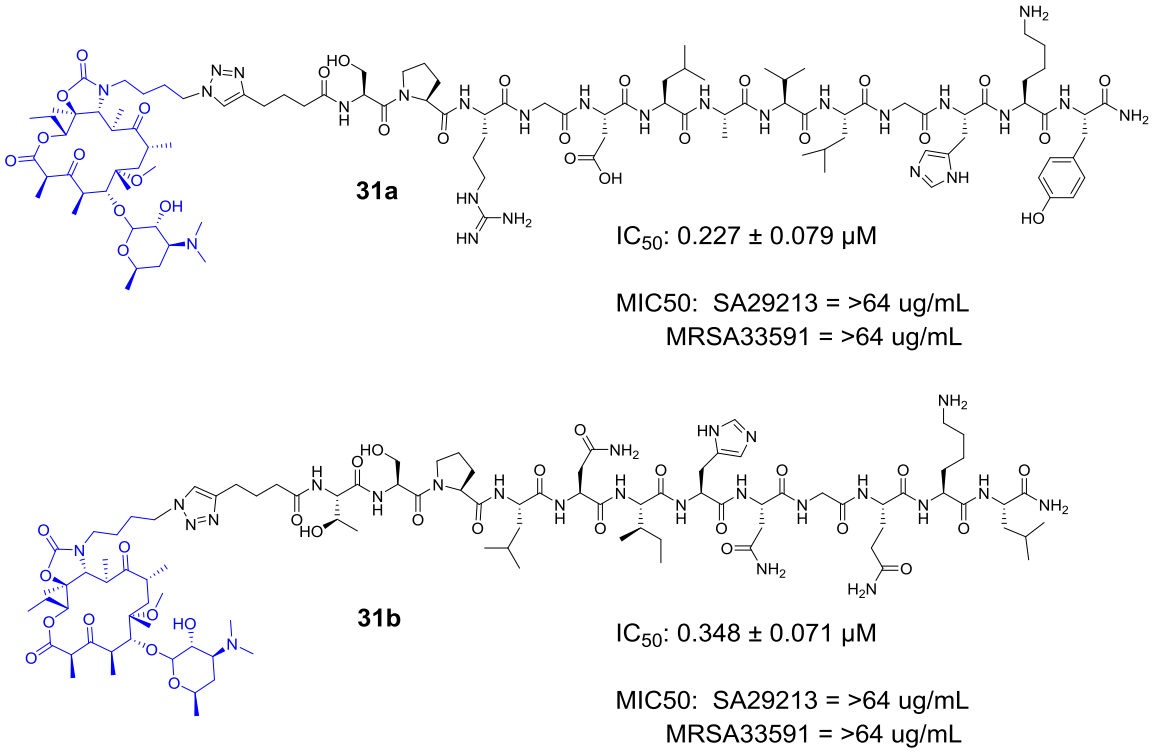


**Figure 35: Structures and $MIC_{50}$s of second generation telithromycin-inspired conjugates. Values determined in *S. aureus* QC cell line (ATCC 29213) and MRSA resistance strain (ATCC 33591).**

Within the original peptolide series, a similar trend was seen where there was no activity for most. The peptolide **12b** of biologically appropriate peptide backbone with the greatest cationic nature and butyl linker displayed activity at 149.00 ± 3.65 µg/mL.

While this value suggests very weak antibacterial activity, it provided a direction and possibility. In analyzing the potential cause for activity, cell permeability seemed the best starting approach, however alternative possibilities for low activity were believed to be resistance mechanisms such as active efflux or enzymatic degradation of the conjugate. With data showing that the parent compounds and, in some cases, the synthetic intermediates retained whole cell growth inhibition, we focused out attention on improving the profile of our peptide.

## 4.5 Replacement of the Peptide Moiety for Peptidiomimetic Peptoids

We first considered the use of naturally occurring antimicrobial peptides. These are translated by an organism as a defense peptide, are relatively short (less than 100 amino acids), and highly cationic and amphipathic.[1] This last inclusion greatly bolsters the ability of these small peptides to penetrate the cell wall by aligning the R-groups of the amino acids in such a way that all hydrophobic moieties are able to bore into the cell wall while hydrophilic ones can maintain a favorable interaction with the surrounding solvent. These peptides, however, tend to be very short-lived and highly susceptible to enzymatic hydrolysis. This can be mitigated by shifting the R-group identity off of the α-carbon and onto the amide nitrogen (Figure 36). This peptidomimetic structure, dubbed peptoid, have been used extensively as antimicrobials, molecular transporters, anticancer agents, and even nanostructured materials.[1-4]

Dr. Jainfend Cai of University of South Florida has extensive experience with membrane active peptides and peptoids. In seeking sequences to explore, a collaboration was established. As an initial trial and potential proof of concept, we were provided with an alkynyl version of a peptoid. This peptoid, seen in Figure 4.5, was derived from a sequence with very weak bacterial membrane penetration activity.[5] In agreement with their findings and our experience with testing uncoupled peptide sequences, it displayed no activity when tested in either our cell-free translation inhibition ( > 250 μM) or the whole cell growth inhibition ( > 256 μg/mL) assays. While not identical sequences, this newly obtained peptiod (Figure 37, **33**) is very similar to the sequence found on the peptolide that displayed whole cell activity inasmuch as maintaining a central core that is highly cationic; +5 for both sequences.

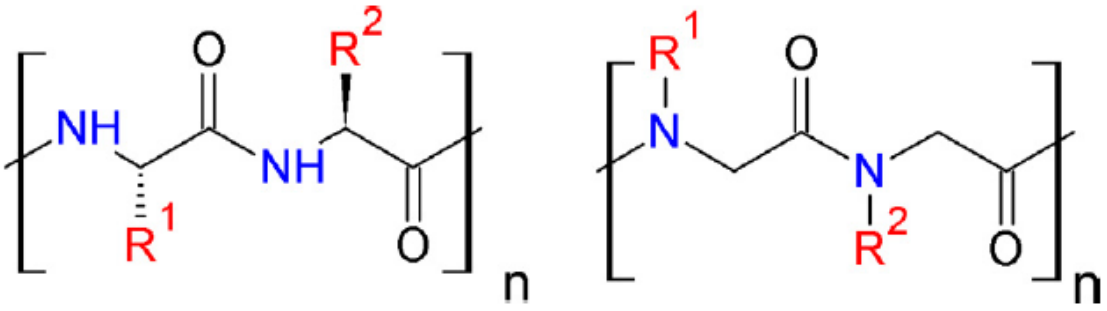


**Figure 36: Standard Peptides and Peptoids.** ***Left*** **Peptide formed from natural L-form amino acids where the amino acid identifiers, denoted as $R^n$, are bound to the α-carbon.** ***Right*** **Characteristic peptoid backbone where the side group has been shifted from the α-carbon onto the amide nitrogen. Figure adapted from [14].**

We proceeded to couple the peptoid sequence to the same telithromycin-azide anchor (synthesis performed by Dr. Subhasish Tapadar). In cell free translation inhibition, peptoid peptolide **32** inhibits prokaryotic translation with potency that is approximately five-fold weaker than the corresponding peptide ketolide **14b** (Figure 37).

This suggests that there is a possibility that the subtle structural changes about the peptide may result in a varied state of interaction with the ribosomal exit tunnel.

**Table 3: Peptoid conjugate activity. Peptide-ketolide ("peptolide") conjugate 14b was the only peptide conjugate to display whole cell activity. Peptoid-ketolide conjugate retained similar cell free IC50 values, however improved whole cell activity by 3-fold compared to peptolide 14b. Unconjugated peptoid 21 displays no activity.**

| | E. coli $IC_{50}$ (μM) | Rabbit Retic. $IC_{50}$ (μM) | S. aureus $MIC_{50}$ (μg/mL) |
|---|---|---|---|
| **14b** | 0.67 ± 0.28 | >250 | 149.00 ± 3.65 |
| **32** | 3.34 ± 0.54 | >250 | 47.08 ± 4.81 |
| **33** | >250 | >250 | >256 |

With validation that the peptoid conjugate retains translation inhibition activity, we compared the effect of the peptoid conjugate on whole cell activity against that of the peptolide probe. Despite the reduced cell free performance of **32**, we observed a potent enhancement of whole cell activity relative to **14b**. We believe that the replacement of the peptide for the peptoid results in additional membrane activity. This disruption contributes to a three-fold enhancement of whole cell activity over the peptide counterpart (Table 3). This is an incredibly exciting result as it suggests that the peptoid is capable of increased cell membrane penetration while ferrying in the ketolide antibiotic.

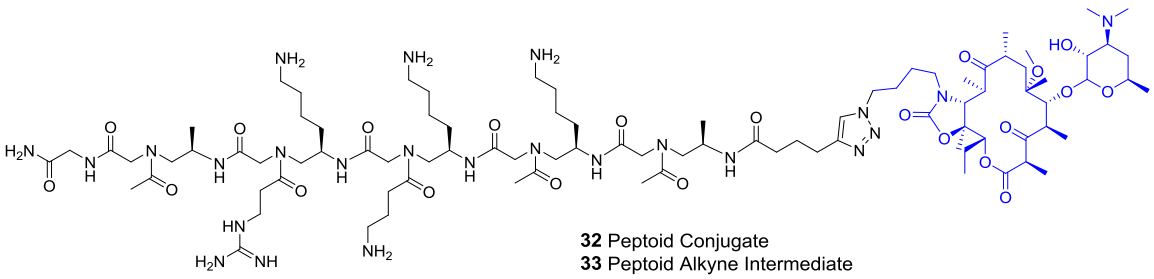


**Figure 37: Peptoid Conjugate. Alkyne peptoid provided by the Cai lab in University of South Florida.**

## 4.6 Discussion

The transition to a peptoid sequence is an interesting prospect. We observed that the peptoid conjugate **32** has prokaryotic cell free translation inhibition activity that is approximately five-fold less than the corresponding peptide conjugate **14b**, however displays improved whole cellactivity. As previously stated, it is believed at this point that this is due to enhanced cell membrane penetration activity afforded by the peptoid moiety while the tethered ketolide is responsible for maintaining translation inhibition activity. The collaboration with the Cai lab will continue as we explore the applications of this further. Additional conjugates will be made by first varying the peptoid in both R-groups as well as length, but also the anchor region may be altered to explore different possibilities of activity in both whole cell as well as cell free assays. As a probe, the varied backbone of the peptoid could provide an alternative window with perhaps more opportunity for variation about the R group identities. Collectively, this new avenue could offer a substantial opportunity for new exploration of therapeutic improvement as well as continuing to glean out exit tunnel interactions.

## 4.7 References


1. Smith, P. T., Huang, M. L., Kirshenbaum, K. (2015) Osmoprotective polymer additives attenuate the membrane pore-forming activity of antimicrobial peptoids. *Biopolymers*, *103*: 227–236.
2. Chongsiriwatana, N.P., Patch, J.A., Czyzewski, A.M., Dohm, M.T., Ivankin, A., Gidalevitz, D., Zuckermann, R.N., and Barron, A.E. (2008) Peptoids that mimic the structure, function, and mechanism of helical antimicrobial peptides. *Proc Natl Acad Sci USA 105:*2794–2799.
3. Niu, Y., Wu, H., Huang, R., Qiao, Q., Costanza, F., Wang, X.-S., Hu, Y., Amin, M. N., Nguyen, A.-M., Zhang, J., Haller, E., Ma, S., Li, X., and Cai, J. (2012) Nanorods formed from a new class of peptidomimetics. *Macromolecules, 45*, 7350-7355.
4. Niu, Y., Wu, Haifan, Li, Y., Hu, Y., Padhee, S., Li, Q., Cao, C. and Cai, J. (2013) AApeptides as a new class of antimicrobial agents.*Org Biomol Chem, 11*, 4283-4290.
5. Hu, Y., Amin, M. N., Padhee, S., Wang, R. E., Qiao, Q., Bai, G., Li, Y., Mathew, A., Cao, C., and Cai, J. (2012) Lipidated peptidomimetics with improved antimicrobial activity. *ACS Chem Biol 3*, 683-686.

# CHAPTER 5 CONCLUSIONS AND FUTURE DIRECTIONS

The study described in this thesis provides a foundation fundamental to the design of future probe conjugates capable of analyzing the nature and extent of interactions between a nascent peptide and the ribosomal exit tunnel. The possibility exists where sites of dynamic interaction within the tunnel may be used to design novel sets of compound classes capable of serving as antibiotics (prokaryotes) and anticancer agents (eukaryotes). We have demonstrated that the conjugate probe design is a viable approach affording the capability to biochemically evaluate retention of anchor function as well as crystallographically visualize atomic level interactions. Within the context of a synthetic probe not reliant on active translation, we are the first to show probe dependent conformational change of multiple residues lining the prokaryotic ribosomal exit tunnel. These changes are made up of both likely hydrogen bond interactions as well as steric repulsion. By taking a cue from nature, we have developed the approach to engage in the known critical interaction of 23S A751: SecM W155 to encourage a selective path of travel down the exit tunnel for future probe designs. Additionally, we are expanding our pool of peptide sequences to include peptidomimetics. The coupling of more cell membrane active peptoids to our antibiotic anchors is currently being pursued. Finally, by continuing to look at nature for peptide sequence inspiration, the Oyelere lab will work to incorporate newer models. One such class of peptide is the "proline-rich antimicrobial peptide" (PrAMPs). Many of these have a very high representation of not just proline, but also arginine. This inclusion of proline as well as basic residues is reminiscent of the peptide sequences of probes 14a-14d, probes responsible for very potent cell free translation inhibition and probe dependent interactions within the exit

tunnel shown by crystallography. While it had been previously shown that they have an ability to halt translation, recent crystal structures have shown their orientation within the PTC and exit tunnel. In overlaying crystal structures, an approach will be planned to utilize these PrAMPs as next generation of peptides to be explored for probe design.

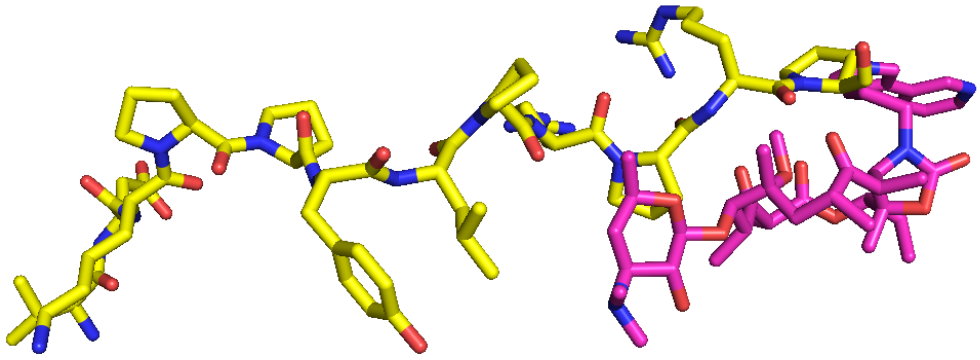

**Figure 38: PrAMP overlay. PrAMP "Onc112" (Yellow, PDB 4ZER) and telithromycin (Purple, PDB 3OI3). PTC lies to the left of the image. Final proline directly overlays with the butyl linker of telithromycin.**

Overlaying telithromycin (Figure 38) displays the alignment of the PrAMP to the alkyl-aryl arm. By modifying telithromycin in a manner similar to that of the peptolide probes discussed in Chapter 2.4, conjugation becomes achievable affording a series with peptide sequence specific stalling capability.

The variability in both the anchors and the peptides offers very exciting opportunities to truly explore the extent of nascent peptide-ribosomal exit tunnel interactions.

# APPENDIX

## A.1. Chapter 2 Supplemental

### A.1.1. Puromycin anchor characterization

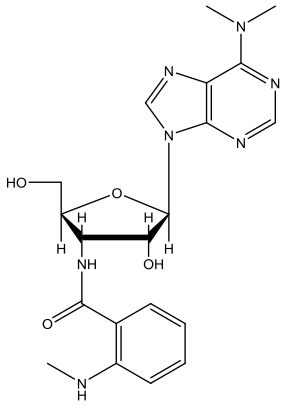

Puromycin-inspired anchor **3**

Chemical Formula: $C_{20}H_{25}N_7O_4$
Molecular Weight: 427.4570

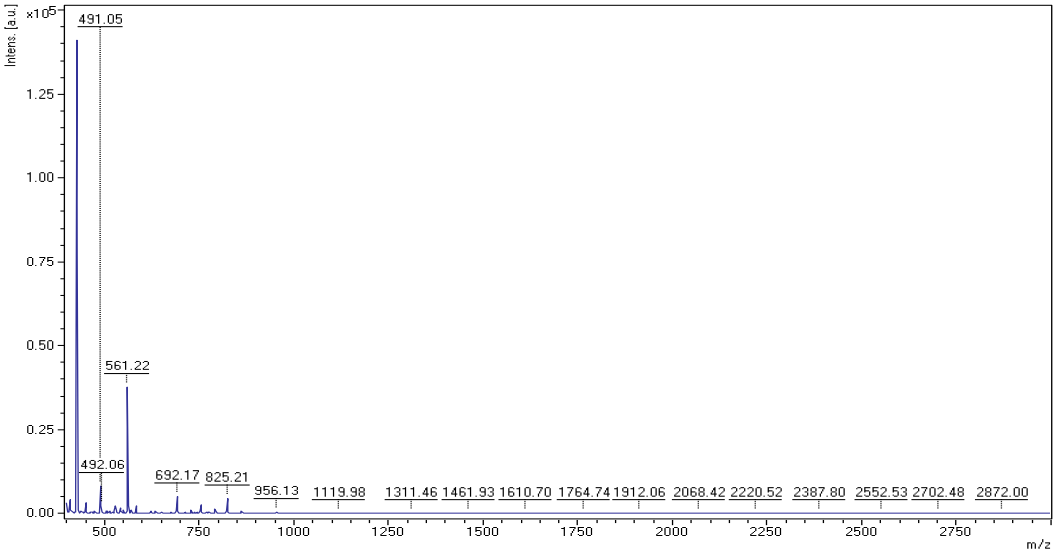

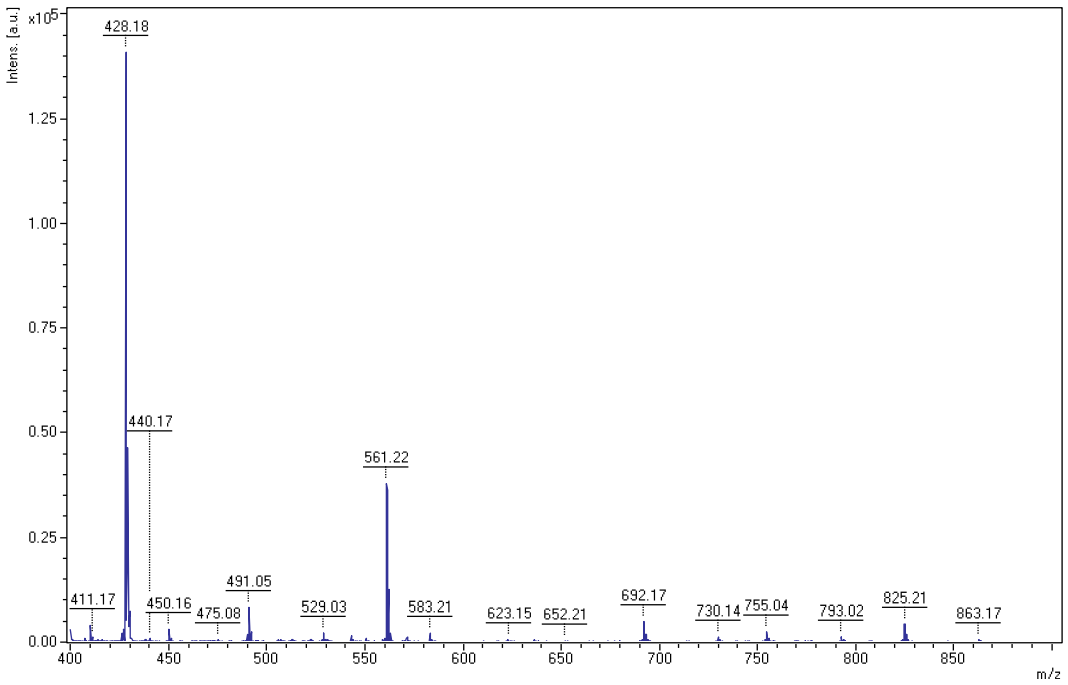
Intens. [a.u.]
x10^5
1.25
1.00
0.75
0.50
0.25
0.00
428.18
440.17
561.22
491.05
411.17
450.16
475.08
529.03
583.21
623.15
652.21
692.17
730.14
755.04
793.02
825.21
863.17
400
450
500
550
600
650
700
750
800
850
m/z

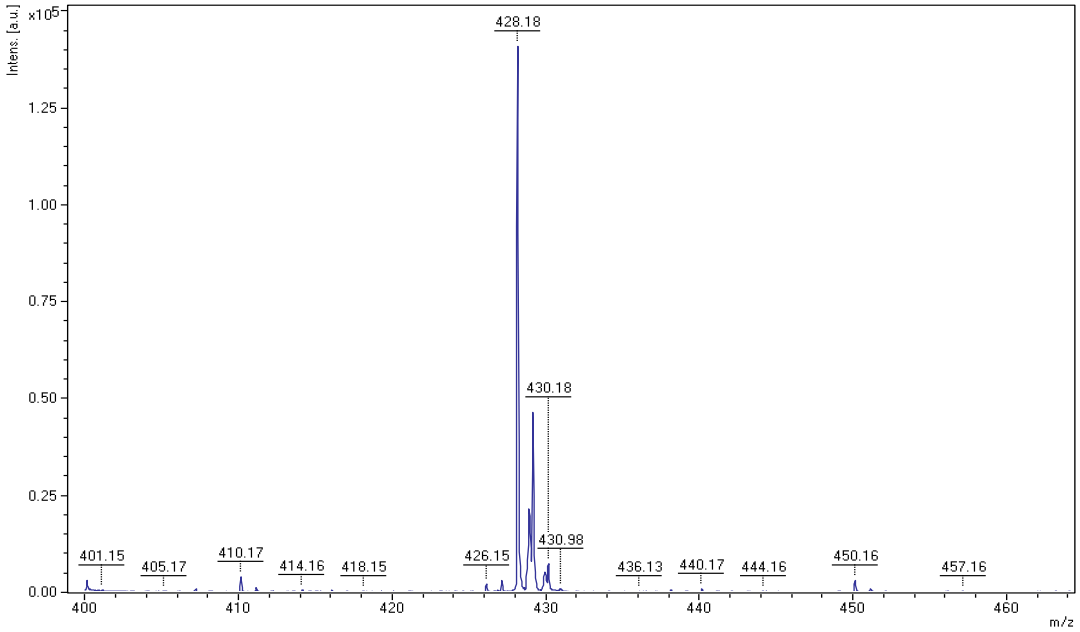
Intens. [a.u.]
x10^5
1.25
1.00
0.75
0.50
0.25
0.00
428.18
430.18
430.98
401.15
405.17
410.17
414.16
418.15
426.15
436.13
440.17
444.16
450.16
457.16
400
410
420
430
440
450
460
m/z

Elemental Composition Report

Single Mass Analysis (displaying only valid results)

Tolerance = 6.0 PPM / DBE: min = -1.5, max = 200.0

Selected filters: None

Monoisotopic Mass, Odd and Even Electron Ions

117 formula(e) evaluated with 2 results within limits (all results (up to 1000) for each mass)

Elements Used:

C: 0-500 H: 0-1000 N: 5-9 O: 2-6

| | | | | | |
|---|---|---|---|---|---|
| Minimum: | | | | -1.5 | |
| Maximum: | | 5.0 | 6.0 | 200.0 | |
| Mass | Calc. Mass | mDa | PPM | DBE | Formula |
| 428.2024 | 428.2046 | -2.2 | -5.1 | 11.5 | C20 H26 N7 O4 |
| | | 1.8 | 4.2 | 7.5 | C15 H26 N9 O6 |

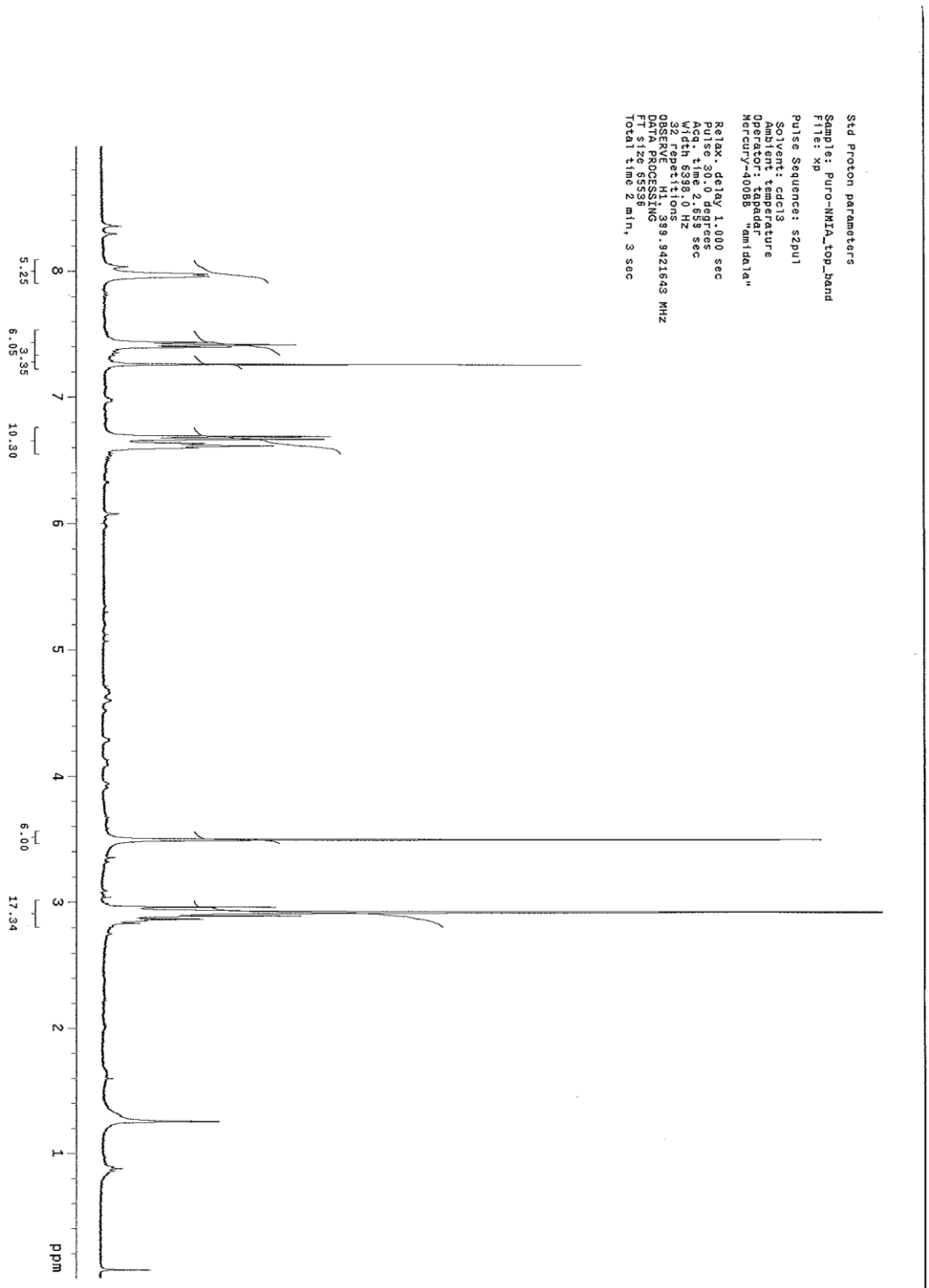
Std Proton parameters
Sample: Puro-NMIA_top_band
File: xp
Pulse Sequence: s2pul
Solvent: cdcl3
Ambient temperature
Operator: tapadar
Mercury-400BB "amidala"
Relax. delay 1.000 sec
Pulse 30.0 degrees
Acq. time 2.052 sec
Width 6398.0 Hz
32 repetitions
OBSERVE H1, 399.9421643 MHz
DATA PROCESSING
FT size 65536
Total time 2 min, 3 sec
5.25
3.35
6.05
10.30
6.00
17.34
8
7
6
5
4
3
2
1
ppm

## A.1.2. Linezolid anchor class characterization

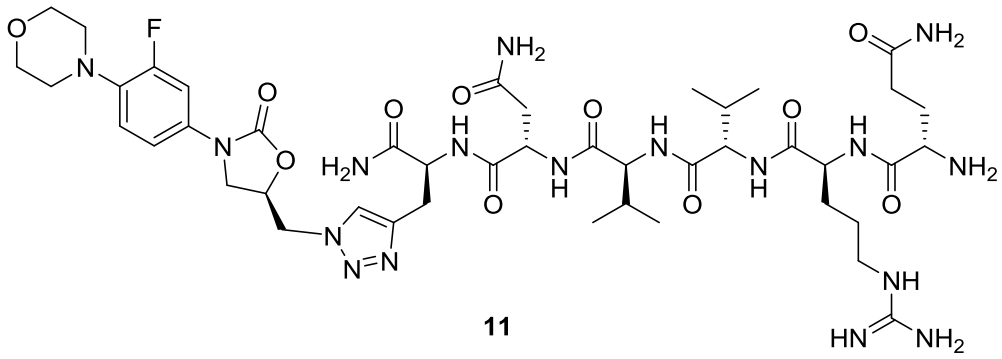

**11**

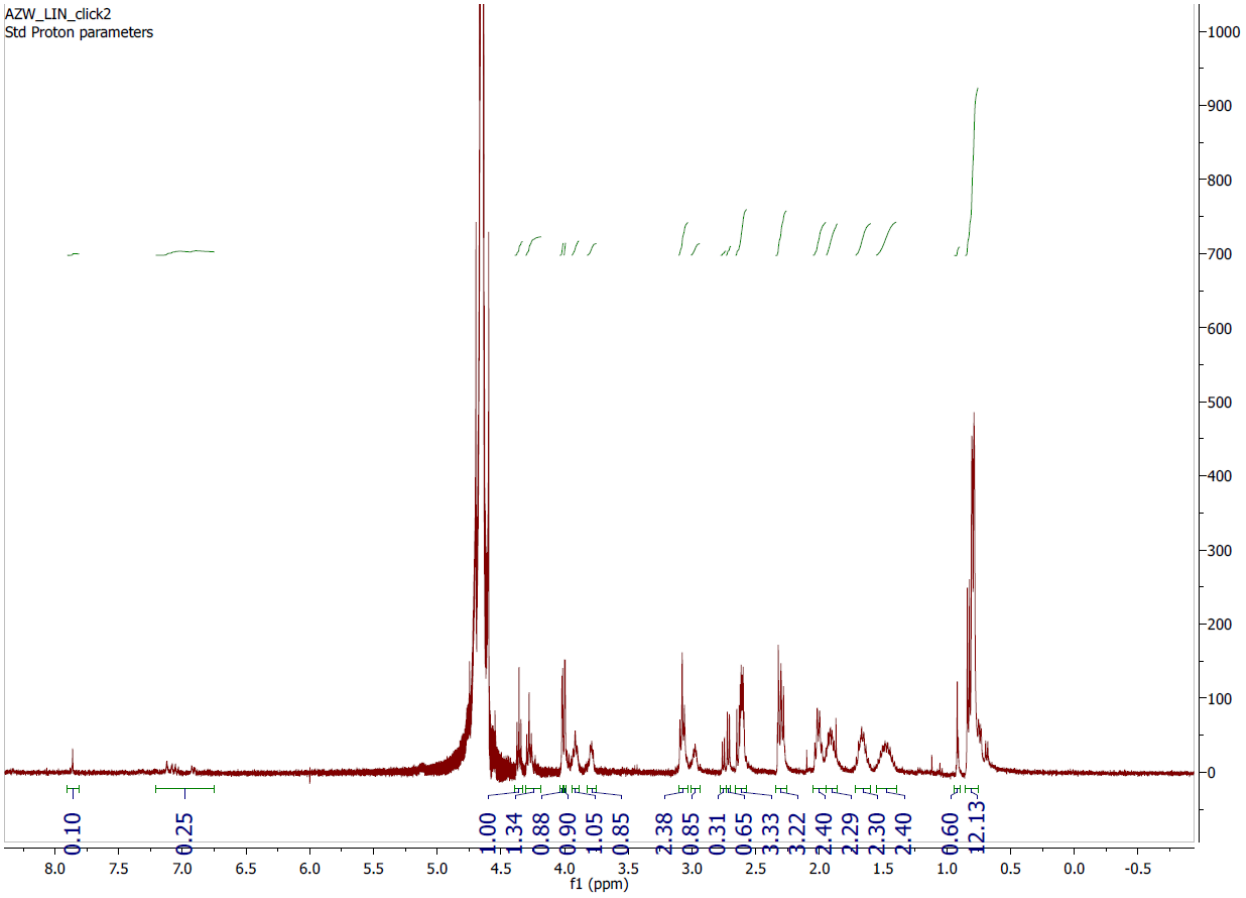

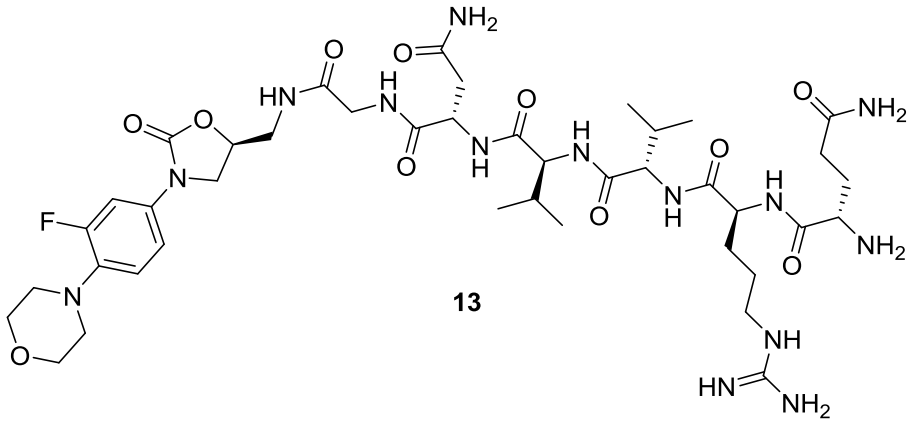

**13**

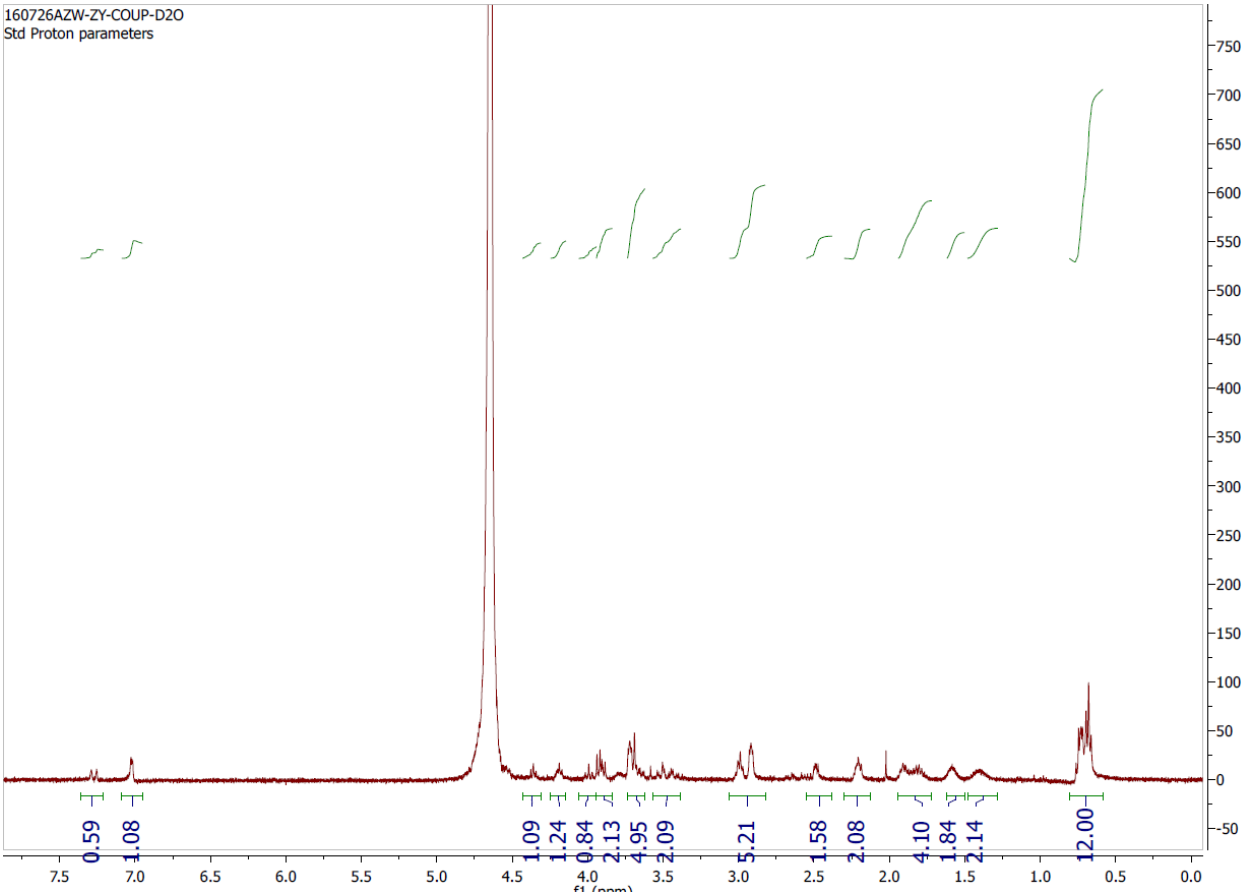
160726AZW-ZY-COUP-D2O
Std Proton parameters
0.59
1.08
1.09
1.24
0.84
2.13
4.95
2.09
5.21
1.58
2.08
4.10
1.84
2.14
12.00
f1 (ppm)

## A.2. Collaboration with Dr. Dev Arya of Clemson University

### A.2.1. Introduction

The following data was published as part of a collaboration with Clemson University and the lab of Dr. Dev Arya. My contribution to the manuscript was using the cell-free translation inhibition assay to validate a single-dose $IC_{50}$ determination of 12 neomycin-amino acid conjugates and 2 positive controls. Both eukaryotic and prokaryotic assays were utilized.

### A.2.2. Manuscript Citation

Jiang, L., Watkins, D., Jin, Y., Gong, C., King, A., Washington, A. Z., Green, K. D., Garneau-Tsodikova, S., Oyelere, A. K. and Arya, D. P. (2015) Rapid synthesis, RNA binding, and antibacterial screening of a peptidic-aminosugar (PA) library. *ACS Chem Biol 10*, 1278-1289.

## A.2.3. Full data contribution

### A.2.3.1. Prokaryotic Assay Results

| Abbreviation | Structures of free amine state. All compounds are available as TFA salts. | MW(Without TFA) | Translational Inhibition** ($IC_{50}$ in µM) |
|---|---|---|---|
| NeoAcid | | | 0.04438 ± 0.0120 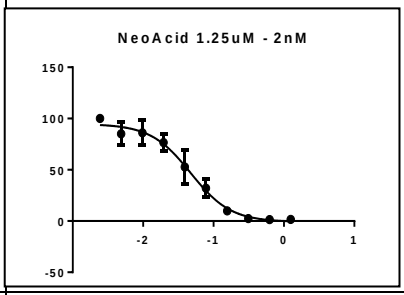  |
| NeoSul | | | 0.02390 ± 0.00922 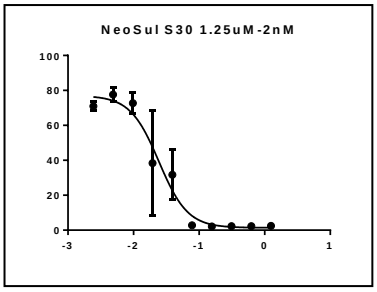  |
| NeoK | 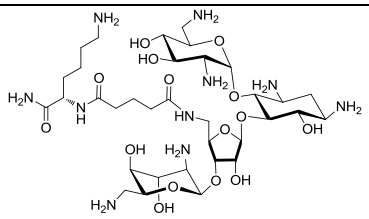 | 854.95 | 0.2625 ± 0.067 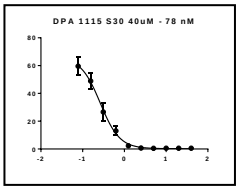  |
| NeoRW | 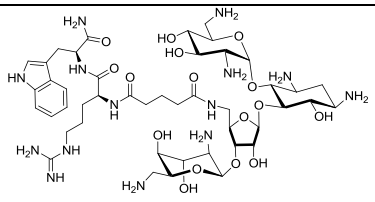 | 1069.17 | 0.05770 ± 0.00439 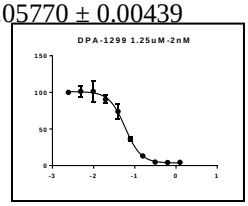  |
| NeoCR | 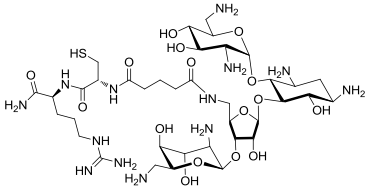 | 987.09 | 0.2457 ± 0.0550 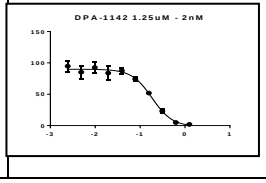  |

| | | | |
|---|---|---|---|
| NeoRH | 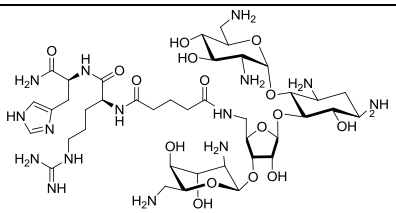 | 1020.10 | 0.2263 ± 0.0823<br> 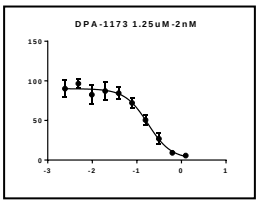 |
| NeoR | 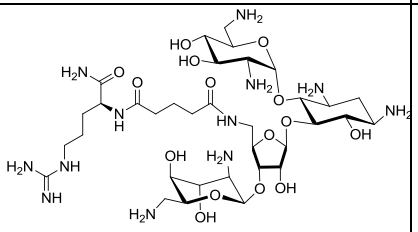 | 882.96 | 0.03399 ± 0.00348<br> 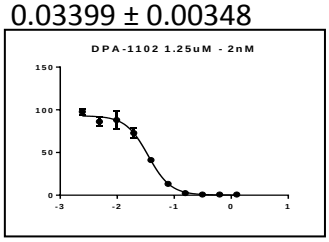 |
| NeoRC | 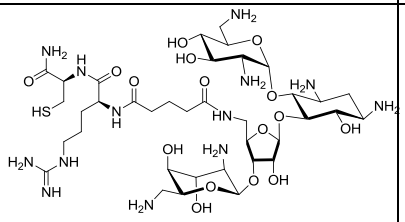 | 986.10 | 0.1040 ± 0.00125<br> 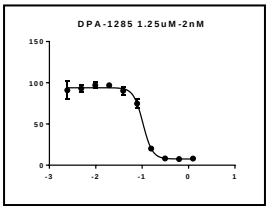 |
| NeoRY | 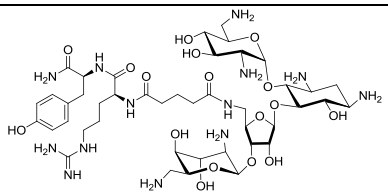 | 1046.13 | 0.05587 ± 0.00193<br> 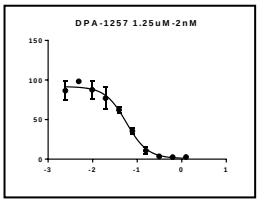 |
| NeoRV | 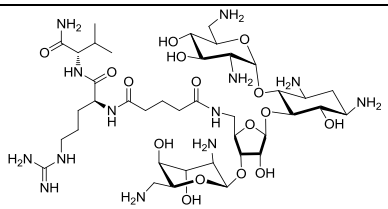 | 982.09 | 0.0732 ± 0.0166<br> 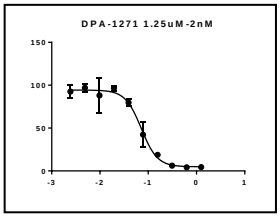 |
| NeoRT | 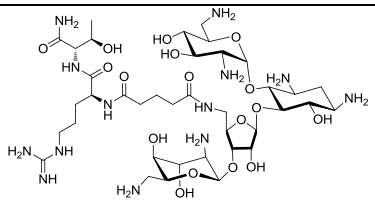 | 984.06 | 0.05621 ± 0.0105<br> 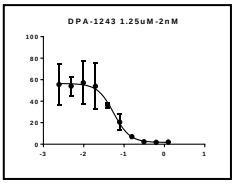 |

| | | | |
|---|---|---|---|
| NeoC | 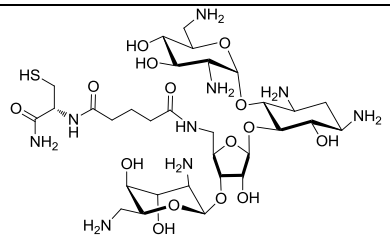 | 829.92 | 0.1180 ± 0.00985<br> 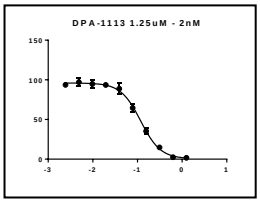 |
| NeoRS | 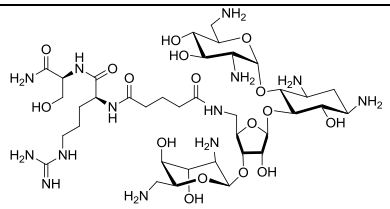 | 970.04 | 0.03362 ± 0.00222<br> 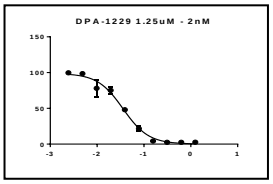 |

A.2.3.2. Eukaryotic Assay Results

| **Abbreviation** | **Structures of free amine state. All compounds are available as TFA salts.** | **MW(With out TFA)** | **Translational Inhibition** RRL $IC_{50}$ in µM [S30 $IC_{50}$ in () ]** |
|---|---|---|---|
| NeoAcid | | | 48.18 (0.04438 ± 0.0120) 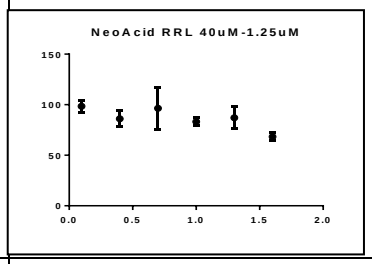  |
| NeoSul | | | 30.71 (0.02390 ± 0.00922) 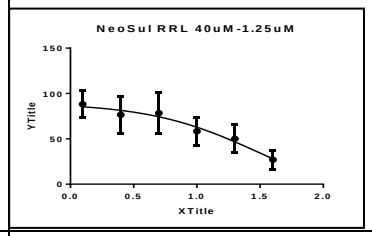  |
| NeoK | 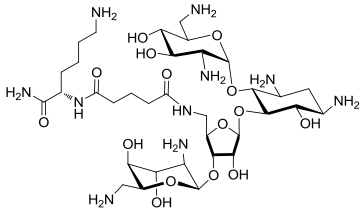 | 854.95 | 21.98 (0.2625 ± 0.067) 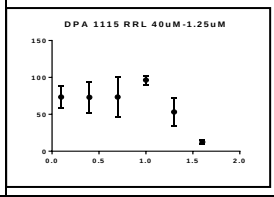  |
| NeoRW | 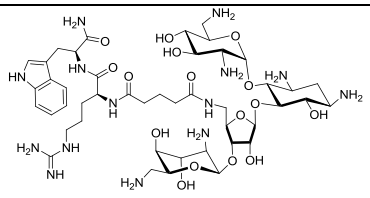 | 1069.17 | 6.56 (0.05770 ± 0.00439) 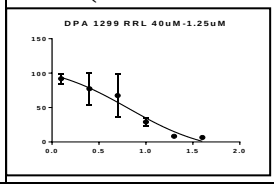  |
| NeoCR | 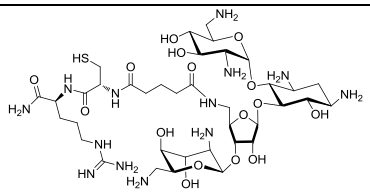 | 987.09 | 26.87 (0.2457 ± 0.0550) 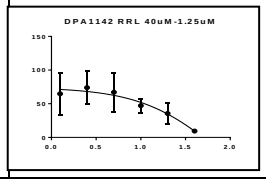  |

| | | | |
|---|---|---|---|
| NeoRH | 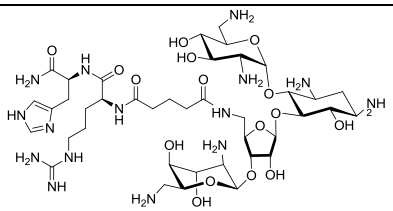 | 1020.10 | 32.32 (0.2263 ± 0.0823)<br> 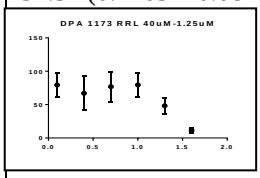 |
| NeoR | 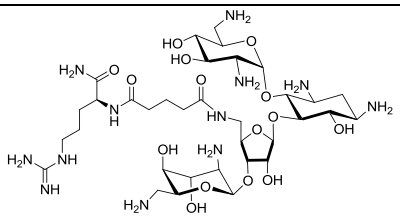 | 882.96 | 28.45 (0.03399 ± 0.00348)<br> 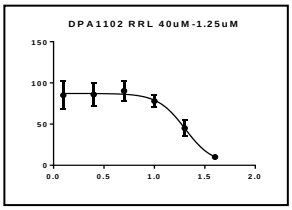 |
| NeoRC | 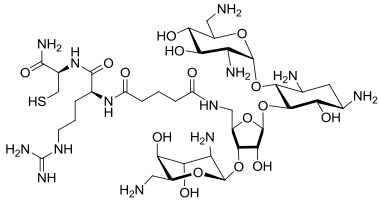 | 986.10 | 30.66 (0.1040 ± 0.00125)<br> 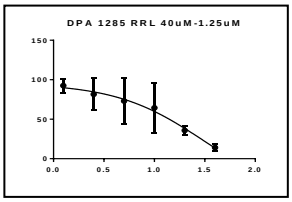 |
| NeoRY | 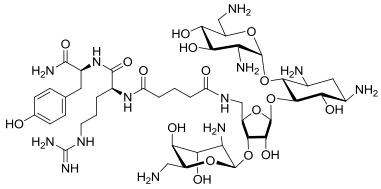 | 1046.13 | 10.97 (0.05587 ± 0.00193)<br> 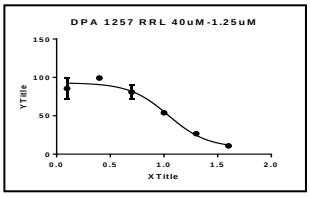 |
| NeoRV | 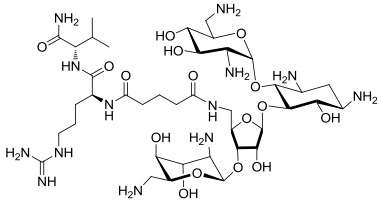 | 982.09 | 21.45 (0.0732 ± 0.0166)<br> 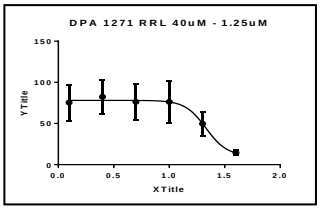 |
| NeoRT | 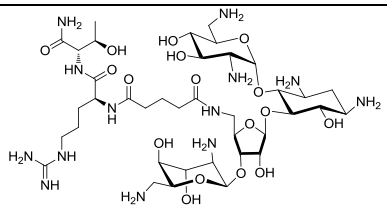 | 984.06 | 52.35 (0.05621 ± 0.0105)<br> 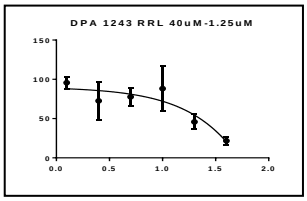 |

| | | | |
|---|---|---|---|
| NeoC | 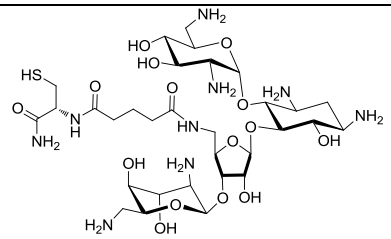 | 829.92 | 27.63 (0.1180 ± 0.00985)<br> 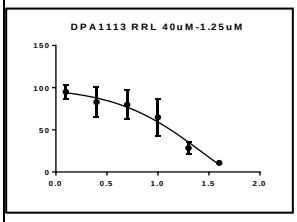 |
| NeoRS | 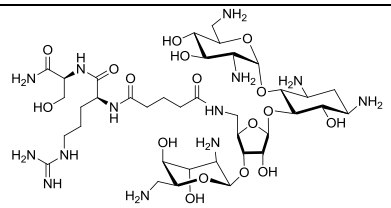 | 970.04 | 39.56 (0.03362 ± 0.00222)<br> 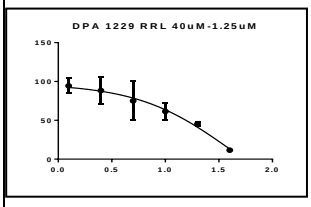 |
| NeoRN | 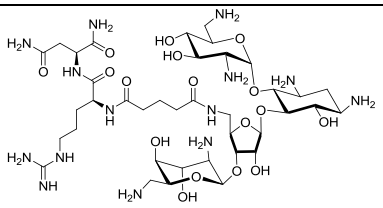 | 997.06 | DNC (0.07154 ± 0.0281)<br> 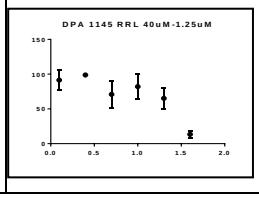 |